# Case Study of the Seismic Response of a Concrete Structure with Vertical Irregularity

**Supervisor:** 

Assoc. Prof. Dr. Iolanda-Gabriela Craifaleanu

**Presented by** 

PhD Student: Arif Weaam

# Contents

1	Int	troduction	3
2	De	escription of the studied buildings	4
	2.1	Structural design considerations	6
	2.2	Modeling of infill walls	8
	2.3	Design load combinations	9
	2.4	Vertical geometric irregularity	9
	2.5	Quantification of setback irregularity	10
3		mplified methodology used for investigating the behavior of the studied	frame
		res	
4		near analysis. Equivalent lateral forces procedure according to ISC 2016	
	4.1	General	
	4.2	Drift and P-Delta Effects	
5	No	on-linear analysis (static NSP and dynamic NDP)	21
	5.1	General	21
	5.2	Modeling nonlinearity of members	21
	5.3	Seismic performance levels	23
	5.4	Response limits and acceptability criteria	24
	5.5	Methodology for nonlinear analysis	24
	5.6	Results and discussion of structural behavior	26
	5.6	5.1 General	26
	5.6	Nonlinear static analysis procedure (NSP)	31
	5.6	J 1 1 1 1 1 1 1 1 1 1 1 1 1 1 1 1 1 1 1	
6		termining Performance Level and Vulnerability	
7	De	evelopment of fragility curves	45
8	Pe	rformance of the structural members	52
9	Co	onclusions	54
1(	) Bil	bliography	56
11	l Ap	ppendix –A	60
12	2 Ar	onendix –R	79

#### 1 INTRODUCTION

Depending on the design, the structural irregularities that affect the behavior or the resistance of buildings to static and dynamic actions differ widely. In the literature, the reference source in the definition of these irregularities in accordance to the geometric configuration and dynamic behavior are earthquake codes [1]. The provisions of Eurocode-8 [2] and ASCE/SEI 7-16 [3] are widely used. While the new Iraqi seismic code ISC 2016 [4] is used in Iraq, this is based mainly on the International Building Code, IBC 2012 [5] and on ASCE/SEI 7-10 [24]. Vertical structural irregularities occur due to various reasons, as, for instance, setbacks. According to the definitions in [3], setbacks occur when the horizontal dimension of the lateral-resisting system at one story is more than 130% of that for an adjacent story. According to Eurocode-8 [2] the setbacks occur, depending on setback type: a) if the setback at any floor is larger than 20% of the previous floor plan dimension in the direction of the setback; b) if the sum of the setbacks at all stories is more than 30% of the plan dimension of the first story, or c) if the setback represents more than 50% of the previous floor plan dimension (for a single setback within the lower 15% of the total height). According to P100-1/2013 [25], setbacks are considered to occur when the setback at any floor is more than 20% of the previous floor plan dimension in the direction of the setback.

Earlier research on mid-rise structures with setbacks [6-10] investigated whether dynamic analysis is important to design such buildings, although several design codes (i.e., [2], [3] and [11]) already recommend the dynamic method for the analysis of such irregular structures. At present, ASCE 7-16 [3], Section 12.2.3.2, allows the use of a two-stage equivalent lateral force analysis for structures that have a flexible upper portion over a rigid lower portion, provided that the following criteria are met:

- "a. The stiffness of the lower portion must be at least 10 times the stiffness of the upper portion.
- b. The period of the entire structure shall not be greater than 1.1 times the period of the upper portion considered as a separate structure supported at the transition from the upper to the lower portion.
- c., d. The lower and upper portions shall be designed as a separate structure using the appropriate values of R and  $\rho^1$ . The reactions from the upper portion shall be those obtained from the analysis of the upper portion increased by the ratio of the  $R/\rho$  of the upper portion over  $R/\rho$  of the lower portion. This ratio shall not be less than 1.0.
- e. The upper portion is analyzed with the equivalent lateral force or modal response spectrum procedure, and the lower portion is analyzed with the equivalent lateral force procedure."

To obtain a feasible story stiffness distribution for the upper and lower structures, a simplified seismic design approach, proposed in [13], was applied in the current study. This approach was adopted to avoid the dynamic-analysis-based trial-and-error procedure, such as that followed in the study [12], as this procedure is quite time-consuming. Taking into account the vertical irregularity in terms of mass and geometric irregularity (setback), design formulae for determining the story-stiffness distribution for both the upper and lower structures were developed by the cited authors. As mentioned in the study [13], the proposed method yields to an initial design that meets the story-drift restrictions and avoids the time-consuming trial-and-error process.

Unlike the two-stage analysis procedure required by ASCE 7-16 [3], the influences of the stiffness and mass interaction between the lower and upper structures on the seismic loads are taken into account. A shear-force-amplification factor,  $\alpha_U$ , is proposed to determine the shear

\_

 $<sup>^1</sup>$  R is a response modification coefficient and  $\rho$  is a redundancy factor based on the extent of structural redundancy present in a building

force influences induced by the lower structure to the upper one and to quantify the influences of this interaction on the base shear force of the upper structure, which is the main factor that affects the simplified design [13].

The aim of the following study is to assess the applicability of the above-mentioned two-stage equivalent lateral force analysis for structures that have a flexible upper portion over a rigid lower portion. In this study, the seismic behavior of various setback frames, derived based on a type of structural configuration located in Baghdad (Iraq) was studied based on the approach proposed in [13]. A verification of IDRa, the average inter-story drift ratio parameter obtained from this approach, was conducted and a comparison was made with the nonlinear static analysis (NSP) and nonlinear dynamic analysis (NDP) results. In addition, the shear ratio of the columns and the vulnerability index (VI) were assessed. The present study also is a contribution to the assessment of the seismic vulnerability of the studied buildings, in which the fragility curves developed based on nonlinear static analysis procedure (pushover) were determined in order to estimate the seismic damage probability in terms of spectral displacements. In addition, the setback ratios were studied to take into account their influence on the increase of damage hazard.

#### 2 DESCRIPTION OF THE STUDIED BUILDINGS

The studied RC frame structures shown in Fig. 2 are modified based on the archetypal building in Fig. 1, by introducing setbacks. The archetypal RC frame structures exists in Baghdad. The building has six stories above the ground level (the base). This is an office building, with uniform configuration over the height, constructed in 2015. The story height of the lower and upper structure is 3.0 m, the total building height is 18.0 m (GF+5S). The building has 8 bays in Y direction and 3 bays in X direction. The bay widths are 5.75 m and 6.0 m in X direction and 3.7 m, 3.05 m and 5.45 m in Y direction. The studied frame structures have the same plan layout as the archetypal building at the first two stories. It was assumed that there are masonry infill walls at these stories, as described in Section 2.2, and glass curtain walls for the upper stories, as shown in Fig. 2.

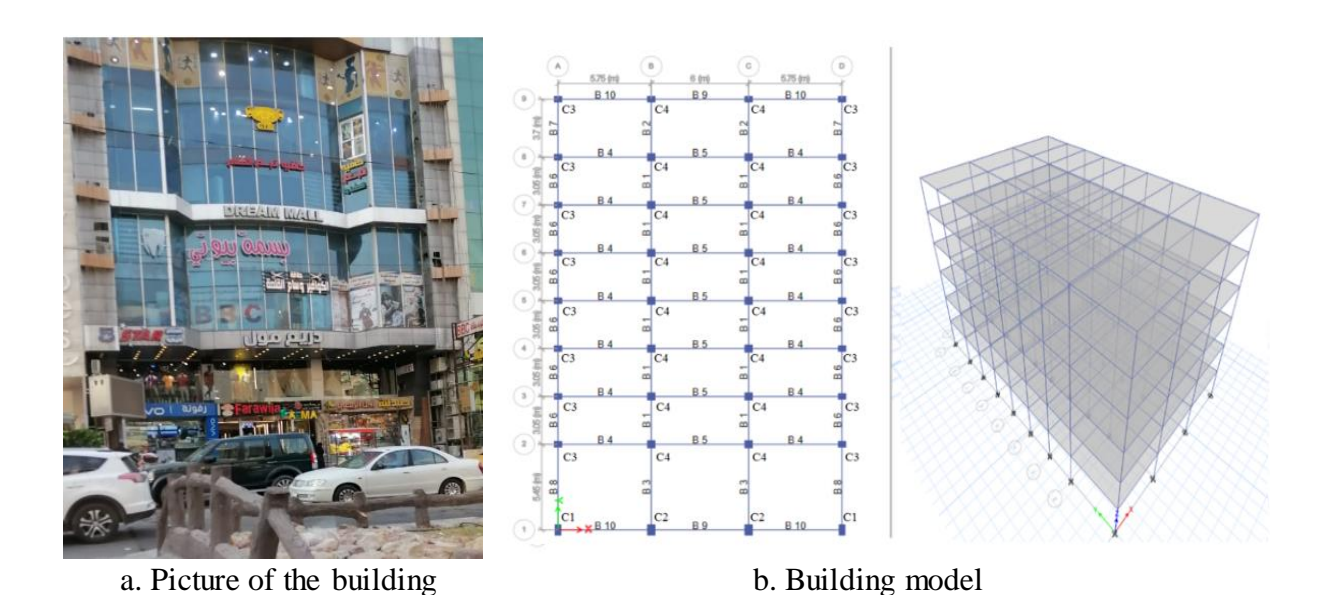


Figure 1: Archetypal building

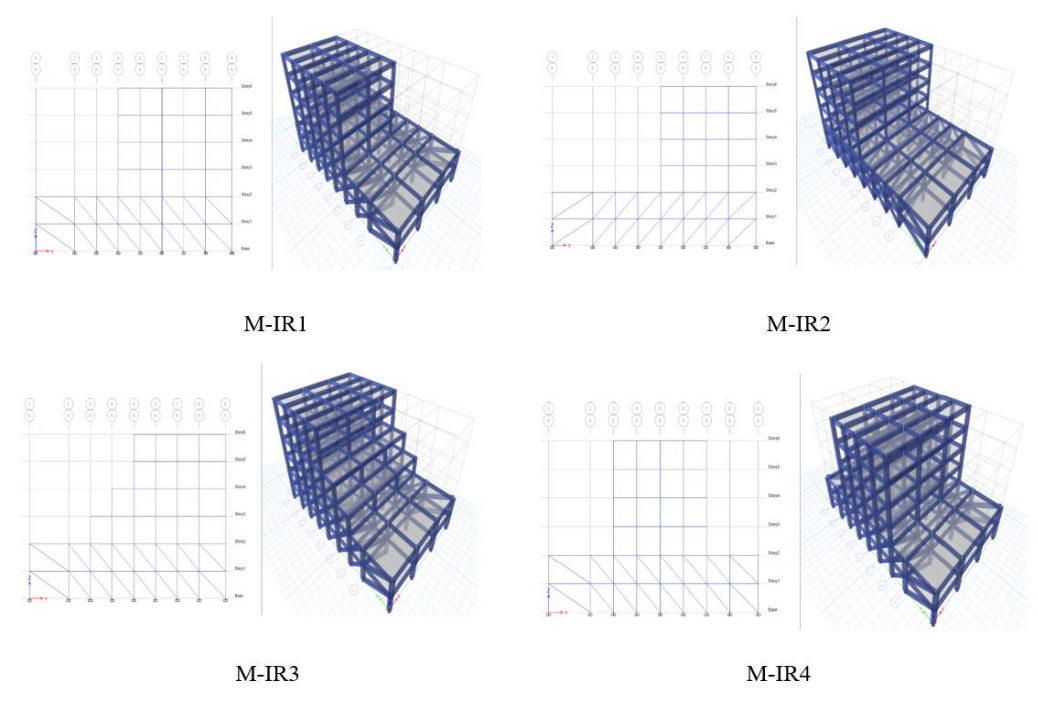


Figure 2. Geometries of the setback RC structures considered in this investigation

The material properties are chosen based on the specifications of ACI 318-19 [14], the standard code adopted for design in Iraq. The configuration of the frames is shown in Table 2-1 below.

Table 2-1: Building configuration data

Type of structure	Office building
Number of stories	6 (GF+5S)
Area of plan	(27.45 m, 17.5 m)
Story height	3 m
Diaphragms system	Rigid diaphragms are assumed
Column sizes*	
1) Perimeter columns C3	500mm x 400mm
2) Internal columns C4	500mm x 500mm
3) Axis 1 columns C1	700mm x 400mm
4) Axis 1 columns C2	700mm x 500mm
Beam size*	600mm x 300mm
Plan area	(17.5 m x 27.45 m)
Number of bays	3 on X, 8 on Y
Slab thickness	150 mm
Compressive strength of the concrete, $f'_c$	25 MPa
Modulus of elasticity of the concrete, $E_c$	23500 MPa
Minimum yield strength of the steel, $f_y$	414 MPa
Modulus of elasticity of the steel, $E_s$	200000 MPa
Masonry infill wall thickness (outer and inner, respectively)	240 mm, 120 mm
Masonry strength (assuming good condition), $f'_m$	6.2 MPa (FEMA 356, Table 7-1)
Masonry modulus of elasticity $E_m$ =550 x $f'_m$	3410 MPa (FEMA 356, Table 7-1)

<sup>\*</sup> All sections for columns and beams are illustrated in Appendix A

The design floor and roof live loads are 2.4 and  $1.0 \text{ kN/m}^2$ , respectively. The gravitational load combination includes the live load ratio according to ISC 2016 [4] (W = dead load, DL + 25 % of the floor live load, LL).

Table 2-2: Loading data according ASCE/SEI 7-16 and ISC 2016

Dead load (DL)	From structural and nonstructural elements
Live load (LL)	
1) typical floor	$2.4 \text{ kN/m}^2$
2) roof	$1 \text{ kN/m}^2$

For linear analysis, the cracked stiffness of the beams, columns and joints is considered. According to ACI 318-19 [14] (used for design in Iraq), Table 6.6.3.1.1(a), values for beams, columns and walls are as shown in Table 2-3.

Table 2-3: Effective stiffness values [14]

Member and condition	Moment of inertia	Cross-sectional area
Beams	$0.35 I_g$	$1.0A_g$
Columns	$0.70 I_{g}$	· ·
Walls (cracked)	$0.35 I_g$	

According to ACI 318, Section 18.7.3.2, it is allowed to model beam-column joints as rigid zones, where the flexural strengths of the columns shall satisfy this condition:

$$\Sigma M_{nc} / \Sigma M_{nb} > 1.2 \tag{1}$$

in which:

 $\Sigma M_{nc}$  is the sum of nominal flexural strengths of the columns framing into the joint;  $\Sigma M_{nb}$  is the sum of nominal flexural strengths of the beams framing into the joint.

Eurocode 8, clause 4.4.2.3, and P100-1/2013, clause 5.2.3.3.3(4), have similar provisions as well ( $\Sigma M_{nc} / \Sigma M_{nb} > 1.3$  for Eurocode 8 and  $\Sigma M_{nc} / \Sigma M_{nb} > 1.2$  for the medium ductility class (DCM) and 1.3 for the high ductility class (DCH) for P100-1/2013). All these clauses are meant to ensure a favorable energy dissipation mechanism (strong column, weak beam).

#### 2.1 Structural design considerations

According to the Iraqi seismic code ISC 2016, there are four categories for seismic design classification, i.e. A, B, C, and D. This differs from ASCE/SEI 7-16, which specifies six seismic design classes (A, B, C, D, E, and F). In both codes, each site's class is determined by the values of  $S_{D1}$  and  $S_{DS}$  (ASCE/SEI 7-16, Table 11.6-1, 2). The studied building (located in Baghdad) is considered to be of class C, regardless of the function or the building; however, the classification will be of class D if taking into account the structural system, with vertical geometric irregularity (ASCE/SEI 7-16, Table 12.3-2). The seismic factors for frames are shown in Table 2-4. According to ISC 2016 [4] and ASCE/SEI 7-16, all concrete frame

buildings in class D must be of the special type, as no ordinary or intermediate concrete frames are allowed.

Table 2-4: Seismic factors, according to ASCE/SEI 7-16 and ISC 2016

		CE/SEI /-10 and ISC 2010
Risk Category	II (offices)	ISC 2014 and Table (1.5-1) of
		ASCE/SEI 7-16
Occupancy Importance Factor $I_e$	1	ISC 2014 and Table (1.5-2) of
		ASCE/SEI 7-16
Seismic Design Category		
1) The archetypal frame	C *	Table (11.6-2) of ASCE/SEI 7-16
2) The setback frames*	D **	Table (12.3-2)/3 of ASCE/SEI 7-16
$S_{DS} = 2/3 \ S_{MS}$	0.312	
$S_{DI} = 2/3 S_{MI}$	0.160	
Site coefficient $F_a$	1.56	
Site coefficient $F_{\nu}$	2.4	
$S_I$	0.1	
$S_S$	0.3	ISC 2016
$S_{MS} = F_a S_s$	0.468	
$S_{MI} = F_{v} S_{I}$	0.24	
$T_0 = 0.2 \text{ S}_{DI}/S_{DS}$	0.103 s	
$T_S = S_{DI}/S_{DS}$	0.513 s	
Response reduction factor (R)	Special reinforced	Table (12.2-1) of ASCE/SEI 7-16
	concrete moment	
	frames (SMF) =8	
Damping	5 %	
Site class	D	ISC 2016
Overstrength Factor, $\Omega_0$	3	Table (12.2-1) of ASCE/SEI 7-16
Deflection Amplification Factor,	5.5	Table (12.2-1) of ASCE/SEI 7-16
$C_d$		
$PGA = S_a$		
At <i>T</i> =0 [ISC 2014, p. 4-12]:		
	=0.4*0.312	
$S_a = S_{DS} (0.4 + 0.6 (T/T_0))$ for	=0.125 g	
$T < T_0$		
Then, at $T=0 \rightarrow Sa = 0.4 S_{DS}$		

<sup>\*</sup> The Seismic Design Category is C, given that  $(0.133 \le S_{DI} < 0.20)$ 

#### where:

 $S_S$ : mapped MCE<sub>R</sub>, spectral response acceleration parameter at short periods (at a 0.2 speriod),

 $S_I$ : mapped MCE<sub>R</sub>, spectral response acceleration parameter at a long-period (at a 1.0 speriod),

 $S_{DS}$ : design spectral response acceleration parameter at short periods,

 $S_{DI}$ : design spectral response acceleration parameter at a period of 1.0 s,

 $S_{MS}$ : mapped MCE<sub>R</sub>, spectral response acceleration parameter at short periods (at a 0.2s-period), adjusted for site class effects,

 $S_{MI}$ : mapped MCE<sub>R</sub>, spectral response acceleration parameter at a long-period (at a 1.0 speriod), adjusted for site class effects,

<sup>\*\*</sup>The Seismic Design Category is D given that the structures have vertical geometric irregularity.

MCE<sub>R</sub>: Maximum Credible Earthquake spectral response acceleration

 $F_a$ : short-period site coefficient (at 0.2s-period),

 $F_{\nu}$ : long-period site coefficient (at 1.0s-period),

PGA: Peak Ground Acceleration,  $S_a$ : design spectral acceleration.

#### 2.2 Modeling of infill walls

The investigated structures were analyzed as frames with infill masonry walls. In the linear elastic range, the effect of an infill wall can be simulated using truss members. This type of "equivalent strut" [15, 16] is simply introduced along one diagonal. This diagonal strut is compressed for the chosen sense of application of the lateral load for linear or nonlinear static analysis. For nonlinear dynamic analysis, two diagonals should be introduced (X-shaped) to model each infill wall, taking into account that one diagonal is tensed and the other is compressed and then this situation inverts when the sense of the seismic load inverts. Details on the modeling of infill walls to account for nonlinear behavior under alternate loads are given in Section 6.2. The effective width, a, of similar equivalent struts for wall thickness  $t_{inf}$  and the effective diagonal length  $r_{inf}$  is determined according to the ASCE/SEI 41-06, Section C7.4.2 [18]. The diagonal strut (a) has similar modulus of elasticity and thickness with that of the masonry panel ( $t_{inf}$ ). The calculation of the equivalent width of a diagonal compressive strut is given by:

$$a = 0.175(\lambda_1 h_{col})^{-0.4} r_{inf} \tag{2}$$

where

$$\lambda_1 = \left[ \frac{E_{me} t_{inf} \sin 2\theta}{4E_{fe} I_{col} h_{inf}} \right]^{\frac{1}{4}}, \text{ in which } \theta = \tan^{-1} \left( \frac{h_{inf}}{L_{inf}} \right)$$
 (3)

and

 $E_{me}$ : expected modulus of elasticity of the infill wall.

 $E_{fe}$ : expected modulus of elasticity of the frame material (concrete).

 $h_{col}$  and  $I_{col}$ , respectively, stand for center-to-center height (m) and moment of inertia of the column (m<sup>4</sup>);

 $h_{inf}$  and  $L_{inf}$  represent the height and length of the infill wall, as shown in Fig. 3.

More details for the calculation of the equivalent width of the diagonal compressive strut are given in Appendix A.

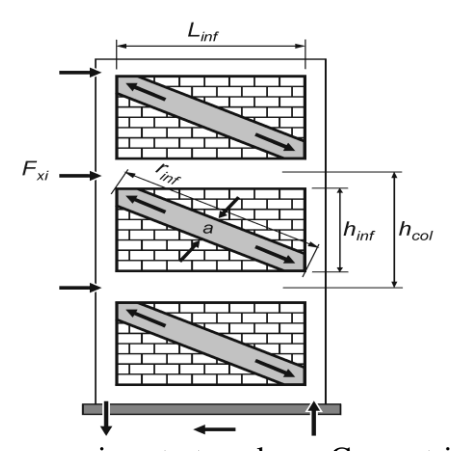


Figure 3: Compression strut analogy. Concentric struts [17]

#### 2.3 Design load combinations

The design load combinations that include earthquake effects, which should be used according to ACI 318-19, ASCE/SEI 7-16, and the Iraqi seismic code ISC 2016, are:

$$U_I = 1.2 DL + 1.6 LL \tag{4}$$

$$U_2 = 1.2 DL + 0.5 LL \pm 1.0 E$$
 (5)

$$U_3 = 0.9 DL \pm 1.0 E$$
 (6)

When the effects of seismic and gravity loads are additive:

$$E = \rho Q_E + 0.2 S_{DS} DL \tag{7}$$

In the case of seismic and gravity load counteracting effects:

$$E = \rho Q_E - 0.2 S_{DS} DL \tag{8}$$

Equations (6) and (7) will become:

$$U_4 = (1.2 + 0.2S_{DS})DL + 0.5LL \pm \rho Q_E \tag{9}$$

$$U_5 = (0.9 - 0.2S_{DS})DL \pm \rho Q_E \tag{10}$$

According to ASCE/SEI 7-16, the redundancy factor is  $\rho = 1.3$  for seismic design category D. The values of the design spectral accelerations at 0.2 and 1.0 seconds equal  $S_{DS} = 0.312$  s and  $S_{D1} = 0.160$  s, respectively, as shown in the Table 2-4, for Baghdad. Equations (9) and (10) will become:

$$U_6 = 1.262DL + 0.5LL \pm 1.3Q_E \tag{11}$$

$$U_7 = 0.838DL \pm 1.3Q_E \tag{12}$$

In the above relations:

DL =dead load,

LL = live load,

E = effect of horizontal and vertical earthquake induced forces,

 $Q_E$  = effect of horizontal seismic force,

 $U_{1...7}$  = load combinations.

# 2.4 Vertical geometric irregularity

As mentioned earlier, vertical geometric irregularity occurs when the horizontal dimension of the lateral-resisting system at one level is more than 130% of that at an adjacent story, according to the definition in ASCE/SEI 7-16. Based on this definition, all investigated frame structures illustrated in Fig. 2 have geometric irregularity. These geometric irregularities are described briefly in Table 2-5. The verification for vertical irregularity in terms of mass and stiffness is given in [Appendix A].

Table 2-5: Vertical geometric irregularity according to ASCE/SEI 7-16 and ISC 2016	Table 2-5: Vertical	geometric irregularity	v according to ASCE/SEI	7-16 and ISC 2016
--	---------------------	------------------------	-------------------------	-------------------

Model No.	Model Identification	1st and 2nd story	3 <sup>rd</sup> , 4 <sup>th</sup> , 5 <sup>th</sup> and 6 <sup>th</sup> story
1	M-IR1	3 bays in the X-direction 8 bays in the Y-direction	2 bays in the X- direction 5 bays in the Y-direction
2	M-IR2	3 bays in the X-direction 8 bays in the Y-direction	3 bays in the X-direction 4 bays in the Y-direction
3	M-IR3	3 bays in the X-direction 8 bays in the Y-direction	3 bays in the X-direction 6 bays on the 3 <sup>rd</sup> story 5 bays on the 4 <sup>th</sup> story 4 bays on the 5 <sup>th</sup> and 6 <sup>th</sup> stories in the Y-direction
4	M-IR4	3 bays in the X-direction 8 bays in the Y-direction	3 bays in the X-direction 4 bays in the Y-direction

# 2.5 Quantification of setback irregularity

To determine the gradual variation of setbacks along the height of the studied frame structures and to quantify the setback irregularity, the irregularity indices  $\phi_b$ , and  $\phi_s$ , proposed and used in [19, 20 and 21], are computed. The expressions of these parameters are according to Eqs. 13.

$$\phi_b = \frac{1}{n_b - 1} \sum_{1}^{n_b - 1} \frac{H_i}{H_{i+1}}, \qquad \phi_s = \frac{1}{n_s - 1} \sum_{1}^{n_s - 1} \frac{L_i}{L_{i+1}}$$
(13)

where:

 $n_b$  is the number of bays at the first story,

 $n_s$  is the number of stories,

 $H_i$  and  $L_i$  are the total height and the total width at/of the i<sup>th</sup> story, as illustrated in Fig. 4 [20].

A large value of the  $\phi_b$  index corresponds to a tower-like structure (with one single large setback, typically at the lower part), while a large value of the  $\phi_s$  index corresponds to a large reduction of the floor area. For a regular frame without setbacks, both indices are equal to unity [20].

The two indices are represented in Fig. 5 and Table 2- 6, as computed for the studied models shown in Fig. 2. The average is also computed, merely as an overall indication.

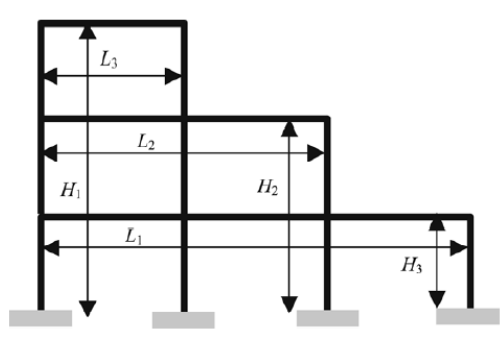


Figure 4: Frame geometry for the definition of irregularity indices, as proposed by Karavasilis *et al.* (2008) [19]

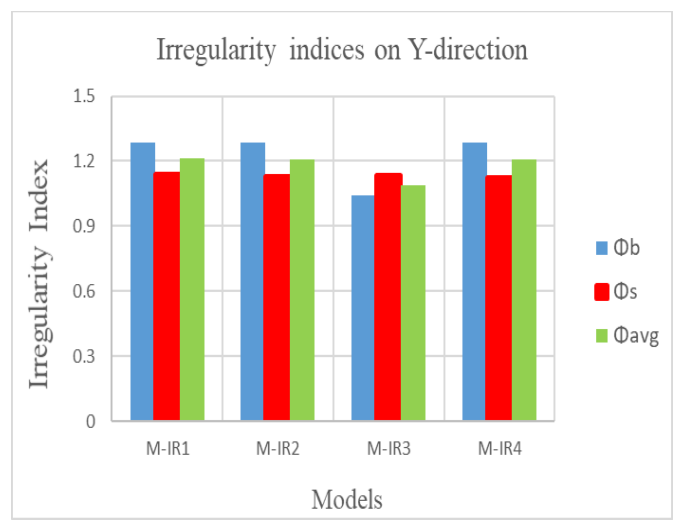


Figure 5: Variation of the irregularity index for the studied setback models (M-IR1, M-IR2, M-IR3, M-IR4) – Y direction

Table 2-6: Irregularity indices

G1			Y	-	2	X	
Sl. No.	Model Identification	фь	$\phi_s$	$\varphi_{avg}$	фь	φs	$\phi_{avg}$
1	M-IR1	1.286	1.139	1.212	4.500	1.116	2.808
2	M-IR2	1.286	1.128	1.207	-	-	-
3	M-IR3	1.040	1.135	1.088	-	-	-
4	M-IR4	1.286	1.125	1.206	-	-	-

# 3 SIMPLIFIED METHODOLOGY USED FOR INVESTIGATING THE BEHAVIOR OF THE STUDIED FRAME STRUCTURES

A simplified design approach was used to analyze the behavior of mid-rise multi-story structures with vertical irregularity given by the presence of setbacks along the building height, as described in [13]. The methodology of this approach is summarized in this section, with application to the setback models considered in the present study. More details on the equation derivation can be found in reference [13]. The solution obtained from the proposed procedure is verified by dynamic analysis after developing the nonlinear models.

Some assumptions were followed in the study [13], to simplify the proposed approach:

- 1. The analytical model is as shown in Fig. 6.
- 2. To evaluate the seismic response, the modal response spectrum analysis procedure was used, as prescribed by ASCE 7-16. For each vibration mode, a damping ratio of 5%, as in [3], was considered.

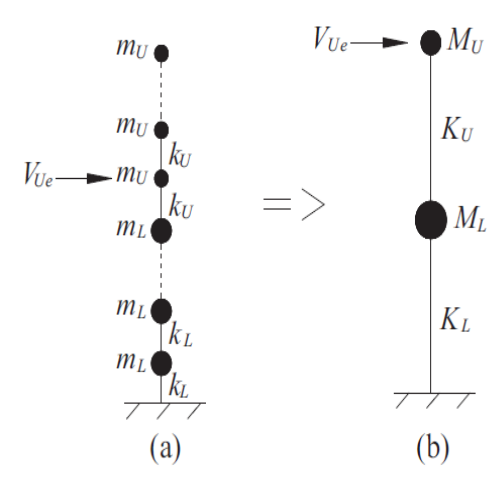


Figure 6: Analytical model of the mid-rise building: (a) MDOF and (b) 2DOF [13]

In the following, the procedure proposed in [13] is applied step-by-step, for the specific parameters of the M-IR1... M-IR4 models analyzed in the present study. The procedure was investigated by its authors for buildings that are subject to some limitations, as described in the cited article and mentioned below.

- 1. The total number of stories is limited to 10 i.e.  $(S_L + S_U) = 10$ , where  $S_U$  and  $S_L$  are the number of stories of the upper and lower structures, respectively. The M-IR1... M-IR4 models have 6 stories, thus they fall in the field of applicability of the procedure. Also, the lateral story stiffnesses and story masses of the lower and upper structures, denoted by  $(k_L \text{ and } k_U)$  and  $(m_L \text{ and } m_U)$ , respectively, should be distributed uniformly, as shown in Fig. 6. This is the case of the M-IR1... M-IR4 models as well.
- 2. For all models of this study, the single story-periods of the upper and lower structures, denoted by  $T_{singU}$  and  $T_{singL}$ , are limited to the range  $0.2T_S...,1.1T_S$ , where  $T_S$  is the period at the intersection of the horizontal and descending branches of the design spectrum. The value of Ts is shown in Fig. 7, for Baghdad, on the design spectrum adjusted for site coefficients. The single-story periods are computed using the approximate formula prescribed by ASCE 7-10 [3]. According to this formula, the period of a regular structure, T, for use in the computation of the seismic force coefficient in the equivalent lateral force procedure (ELF), should not exceed  $C_U T_a$ , where  $C_U$  is the upper limit coefficient and  $T_a$  is the approximative fundamental period, given by  $T_a = C_t(h_n)^x$  (ASCE 7, Section 12.8.2.1). Given that: (a) the story height  $h_n$  of the studied models is 3.0 m; (b) for concrete moment resisting frames,  $C_t = 0.0466$  and x = 0.9; (c) the maximum  $C_U$  (ASCE 7, Section 12.8.2.1) for high risk seismic zones is 1.58 (calculated by interpolation between two values (1.5 and 1.6), based on the value of the Design Spectral Response Acceleration Parameter at 1 s,  $S_{D1}$ , which is equal to 1.60), and (d) the minimum  $T_S$  can be assumed to be 0.513 s according to Iraqi Seismic Code, ISC 2016 [4], it results that the maximum  $T_{singL} = T_{singU} = 1.58 \times 0.0466 \times 3.0^{0.9}$ = 0.198 s. On the other side, 1.1  $T_S$  =1.1 x 0.513 s = 0.564 s. Consequently, both  $T_{singL}$ and  $T_{singU}$  do not exceed 1.1 $T_S$  for the models considered in the present study.

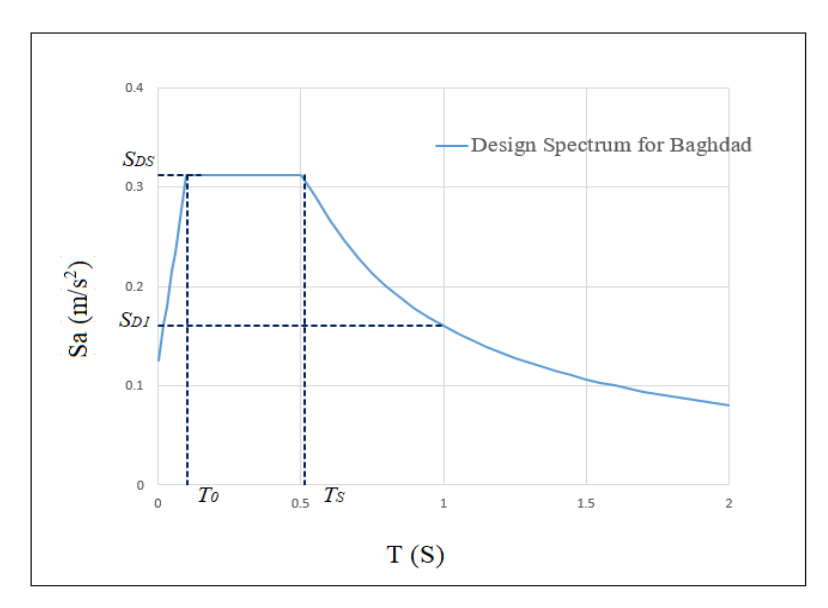


Figure 7: Design spectrum for Baghdad, for a return period of 2475 years and 5% damping, adjusted for site coefficients according to [4] and [24]

(3) For all the models in this study, the story-mass ratio,  $r_m = m_L/m_U$ , and the lateral story-stiffness ratio,  $r_k = k_L/k_U$ , of the upper and lower structures are within the following limits, which makes them compatible with the application of the cited method:  $1 <= r_m <= 3$  and  $\max(1; r_{kUI}) <= r_k <= 20$ . The ratio  $r_{kUI}$  was computed with relation (14) [13]:

$$r_{kU1} = \left[ \frac{r_m S_L(0.12S_L + S_U)}{(S_L + S_U)S_U} + \frac{0.12S_L + S_U}{0.88S_L} \right] \frac{S_U}{S_L} \left( \frac{\overline{\omega_{1U}}}{\overline{\omega_{1L}}} \right)^2$$
 (14)

in which  $\overline{\omega_{1L}}$  and  $\overline{\omega_{1U}}$  are the normalized first mode natural frequency of the structure with  $S_L$  and  $S_U$  stories, respectively. For an upper or lower structure with S stories and constant story mass and stiffness (m and k), the normalized first mode natural frequencies were computed with the equation  $\overline{\omega_1} = \omega_1 (m/k)^{0.5}$ , where  $\omega_1$  is the first mode natural frequency [13].

The equation of the minimum story-stiffness ratio equation  $r_{kUI}$  is derived in [13] by using the assumption that the first story of the upper structure has the highest story-drift-ratio in the entire building. This assumption corresponds to the situation of a stiff lower structure and of a relatively soft upper structure, which is frequently met in current practice. Given the above, this would mean that, if the story-drift ratio for the first story of the upper structure complies with the prescribed limits, all the other story-drift ratios will comply as well. Additional details are given in the cited article.

After incorporating a procedure to scale the design spectral acceleration for a target non-exceedance probability of a story-drift larger than the limit prescribed in ASCE 7, the procedure proposed for the evaluation of feasible story stiffnesses  $k_U$  and  $k_L$  will consist of the following steps [13].

1. Estimation of the effective seismic mass distribution ( $m_L$  and  $m_U$ ), computation of  $r_m = m_L/m_U$  and evaluation of  $R_m$  - as given by Eq. (15), and  $R_k$  - as given by Eq. (16):

$$R_m = \frac{M_L}{M_U} = \frac{r_m S_L}{S_U} \tag{15}$$

$$R_k = \frac{K_L}{K_U} = r_k \left(\frac{S_L}{S_U}\right) \left(\frac{\overline{\omega_{1L}}}{\overline{\omega_{1U}}}\right)^2 \tag{16}$$

The story stiffnesses  $k_U$  and  $k_L$  must follow a specific relationship, to ensure that Eq. (17) is satisfied

$$a_U \le \frac{R}{C_d} \frac{k_U \, \Delta_{U \text{lim}}}{m_U S_U S_a(T_U)} \tag{17}$$

In Equation (17):

 $\Delta_{\text{Ulim}}$  is the code specified story-drift limit for the upper structure [3].

 $\alpha_U$  is the shear-force amplification factor of the upper structure, accounting for the interaction between the lower and upper structures in terms of mass and stiffness;

 $T_U$ , R,  $C_d$  are the first mode period of the upper structure with base fix-connected to the ground, the response reduction factor, and the deflection amplification factor, respectively.

The reason of the introduction of the factor  $\alpha_u$  is to transform an MDOF model with mass and stiffness irregularities into a simple 2DOF model, as shown in Fig. 6. The factor  $\alpha_u$  can be computed using the following empirical formulas [13]:

$$a_{U} = \begin{cases} a_{U1} \left(\frac{R_{k}}{R_{kU1}}\right)^{x_{1}} & R_{kU1} \leq R_{k} < R_{kU2} \quad (a) \\ a_{Umax} & R_{kU2} \leq R_{k} < R_{kU3} \quad (b) \\ a_{Umax} \left(\frac{R_{k}}{R_{kU3}}\right)^{x_{2}} & R_{kU3} \leq R_{k} < R_{kU2stg} \quad (c) \\ a_{U2stg} & R_{k} \geq R_{kU2stg} \quad (d) \end{cases}$$

$$(18)$$

where:

$$x_1 = \frac{\ln\left(\frac{a_{Umax}}{a_{U1}}\right)}{\ln\left(\frac{R_{kU2}}{R_{kU1}}\right)} \tag{19}$$

$$x_2 = \frac{\ln\left(\frac{a_{U2stg}}{a_{Umax}}\right)}{\ln\left(\frac{R_{kU2stg}}{R_{kU2}}\right)} \tag{20}$$

$$R_{kU1} = \frac{R_m(0.12S_L + S_u)}{S_L + S_U} + \frac{0.12S_L + S_U}{0.88S_L}$$
 (21)

$$R_{kU3} = \begin{cases} 4.13R_m + 2 & R_m \le 0.8 & (a) \\ -0.26R_m + 5.52 & 0.8 < R_m < 2 & (b) \\ R_m + 3 & R_m \ge 2 & (c) \end{cases}$$
(22)

$$R_{ku2} = R_m + 1 (23)$$

$$a_{U1} = \begin{cases} a_{U11} & \frac{T_U}{T_s} \ge 1 \\ a_{U12} & \frac{T_U}{T_s} \le \left[ \frac{(S_U + 0.12S_L)}{(S_U + S_L)} \right]^{0.5} \\ a_{U11} \left( \frac{T_U}{T_s} \right)^{x_3} & \left[ \frac{(S_U + 0.12S_L)}{(S_U + S_L)} \right]^{0.5} < T_U / T_s < 1 \end{cases}$$
(24)

$$a_{Umax} = \begin{cases} a_{Umax1} & \frac{T_{u}}{T_{s}} \ge 1\\ a_{Umax2} & \frac{T_{U}}{T_{s}} \le 0.769 [R_{m}]^{0.059} \\ a_{Umax1} \left(\frac{T_{U}}{T_{s}}\right)^{x_{4}} & 0.769 [R_{m}]^{0.059} < T_{U}/T_{s} < 1 \end{cases}$$
(25)

where:

$$a_{Umax1} = \begin{cases} 0.03R_m + 1.0 & R_m \le 0.71\\ 0.17R_m + 0.90 & 0.71 < R_m \le 4.5\\ -0.005R_m^2 + 0.190R_m + 0.91 & 4.5 < R_m \le 16\\ 0.047R_m + 1.918 & R_m > 16 \end{cases}$$
(26)

$$a_{Umax2} = \begin{cases} 1.1 & R_m \le 0.40 \\ 0.35R_m + 0.96 & 0.40 < R_m \le 0.71 \\ 0.209R_m + 1.061 & 0.71 < R_m \le 4.5 \\ -0.0025R_m^2 + 0.145R_m + 1.40 & 4.5 < R_m < 21 \\ 0.0136R_m + 3.5 & R_m \ge 21 \end{cases}$$
(27)

$$a_{U2stg} = \begin{cases} 1.1 & R_m \le 1.4 \\ 0.14R_m + 0.918 & 1.4 < R_m \le 2.3 \\ -0.08R_m + 1.424 & 2.3 < R_m \le 4.1 \\ 1.1 & R_m \ge 4.1 \end{cases}$$
 (28)

2. Estimation of critical story-stiffnesses,  $k_{Umax}$  from Eq. (30) and  $k_{Umin}$  from Eq. (31):

$$k_{Umax} = \max(k_{\alpha U1}, k_{\alpha Umax}, k_{\alpha U2stg})$$

$$k_{Umin} = \min(k_{\alpha U1}, k_{\alpha Umax}, k_{\alpha U2stg})$$
(30)

In Eqs. (30) and (31),

$$k_{\alpha U1} = \begin{cases} m_{U} \left[ \alpha_{U11} S_{U} \frac{\overline{\omega}_{1U}}{2\pi} \frac{C_{d}}{R} \frac{S_{D1}}{\Delta_{Ulim}} \right]^{2} & k_{\alpha U1} \leq k_{US1} \\ \alpha_{U12} m_{U} S_{U} \frac{C_{d}}{R} \frac{S_{DS}}{\Delta_{Ulim}} & k_{\alpha U1} \geq k_{US3} \\ m_{U} \left[ \alpha_{U11} S_{U} \left( \frac{2\pi}{\overline{\omega}_{1U} T_{S}} \right)^{x_{3}} \frac{C_{d}}{R} \frac{S_{D1}}{\Delta_{Ulim}} \right]^{\frac{1}{1 + 0.5 x_{3}}} & k_{US1} < k_{\alpha U1} < k_{US3} \end{cases}$$
(32)

$$k_{\alpha U max} = \begin{cases} m_{U} \left[ \alpha_{U max1} S_{U} \frac{\overline{\omega}_{1U}}{2\pi} \frac{C_{d}}{R} \frac{S_{D1}}{\Delta_{U lim}} \right]^{2} & k_{\alpha U max} \leq k_{US1} \\ \alpha_{U max2} m_{U} S_{U} \frac{C_{d}}{R} \frac{S_{DS}}{\Delta_{U lim}} & k_{\alpha U max} \geq k_{US2} \\ m_{U} \left[ \alpha_{U max1} S_{U} \left( \frac{2\pi}{\overline{\omega}_{1U} T_{S}} \right)^{x_{4}} \frac{C_{d}}{R} \frac{S_{D1}}{\Delta_{U lim}} \right]^{\frac{1}{1+0.5x_{4}}} & k_{US1} < k_{\alpha U max} < k_{US2} \end{cases}$$
(33)

$$k_{\alpha U2stg} = \begin{cases} m_{U} \left[ \alpha_{U2stg} S_{U} \frac{\overline{\omega}_{1U}}{2\pi} \frac{C_{d}}{R} \frac{S_{D1}}{\Delta_{Ulim}} \right]^{2} & k_{\alpha U2stg} \leq k_{US1} \\ \alpha_{U2stg} m_{U} S_{U} \frac{C_{d}}{R} \frac{S_{Ds}}{\Delta_{Ulim}} & k_{\alpha U2stg} > k_{US1} \end{cases}$$
(34)

where:

$$k_{US1} = m_U \left[ \frac{2\pi}{\bar{\omega}_{1U} T_S} \right]^2$$

$$k_{US2} = 1.691 (R_m)^{-0.118} k_{US1}$$

$$k_{US3} = \left[ \frac{S_U + S_L}{S_U + 0.12S_I} \right] k_{US1}$$
(35)
(36)

$$k_{US2} = 1.691(R_m)^{-0.118} k_{US1} (36)$$

$$k_{US3} = \left[\frac{S_U + S_L}{S_U + 0.12S_L}\right] k_{US1} \tag{37}$$

3. Determination of the domain of feasible  $k_U$  in Eq. (17), which should satisfy Eqs. (38) and (39)

$$k_U \ge k_{Umin} \tag{38}$$

$$k_U \le k_{Umax} \tag{39}$$

4. For any given  $k_U$  in the feasible domain, the corresponding  $k_L$  should satisfy Eq. (40). The calculated  $k_L$  should be limited to the domain specified in Eq. (41)

 $R_{kU1} \ge R_{kU2}$ ,  $\alpha_{Umax} > \alpha_{U2stg}$  (The case of investigated structure);

$$k_L \ge \left(\frac{\alpha_{Ulim}}{\alpha_{Umax}}\right)^{\frac{1}{x_2}} R_{kU3} \frac{S_U}{S_L} \left(\frac{\overline{\omega}_{1U}}{\overline{\omega}_{1L}}\right)^2 k_U \tag{40}$$

$$m_{max}[r_{kU1}k_u, k_U] \le k_L \le 20k_U$$
 (41)

In the above equations: 
$$a_{Ulim} = \frac{R}{c_d} \frac{k_U \Delta_{Ulim}}{m_U S_U S_a(T_U)}$$
 (42)

The calculations performed for the application of the simplified method on the studied structures are detailed in Appendix A.

#### Conclusion on the application of the method in [13]

From the results in Section 5.6 of this study it was observed that the first story of the upper structure, for all models, has the highest story-drift-ratio in the entire building, which satisfies the assumption of the equation of the minimum story-stiffness ratio,  $r_{kU1}$  (Equation 14) which is derived in [13]. However, the results also show the drawbacks of the new simplified seismic design approach proposed in [13] for structures that have a flexible upper portion over a rigid lower portion (in this study, setback frames that correspond with this type of structural configuration were investigated) in quantifying the performance of this type of configurations.

# 4 LINEAR ANALYSIS. EQUIVALENT LATERAL FORCES PROCEDURE ACCORDING TO ISC 2016

#### 4.1 General

According to ISC 2016 and ASCE/SEI 7-16, the seismic action considered in the analysis is represented by using the equivalent lateral forces procedure (ELFP) per Section C12.2.3.2, which is based on the seismic parameters of the elastic response spectrum specific for Baghdad to compute the story drift. The analysis was carried out using the ETABS 2017 program [23], by considering the four different three-dimensional models in Fig. 2, for which the response in orthogonal directions is computed. The spectrum is plotted in Fig. 7 for ISC 2016 [4], with the seismic response coefficients shown in Table 2-4 ( $S_a$ ,  $S_I$ ,  $F_a$ ,  $F_v$ ,  $S_{DS}$ ,  $S_{DI}$ , R,  $\Omega_0$ , Cd,  $I_e$ , D) and for 5% damping, with 5% accidental eccentricity amplification factor. The response modification coefficient R, accounting for inelastic behavior for special reinforced concrete moment frames is equal to 8.

#### 4.2 Drift and P-Delta Effects

To compute the design inter-story drifts,  $\Delta_x$ , according to Eq. (12.8-15), Section 12.8.6 of ASCE 7-16, the values  $\Delta_{xe}$  (from the linear analysis) must be multiplied by the quantity ( $C_d/I_e$ ). The design story drifts and the limiting values of story drift according to Table 12.8-2 of ASCE 7-16 are provided in Tables 4-1...4-4. The story drift limit is 0.02 times the story height for this risk category II building, according to Table 12.12-1 of ASCE 7-16. The story drifts showed to be significantly less than the drift limit.

$$\Delta_x = \frac{C_d \Delta_{xe}}{I_e}$$
 Eq. (12.8-15) according to ASCE 7-16

where

 $C_d$ : deflection amplification factor;

 $\Delta_{xe}$ : deflection at the location required by this section determined by an elastic analysis; and  $I_e$ : importance factor.

Table 4-1: Story drifts and drift limits in X and Y directions for M-IR1 for ELFP

		X		
STORY	$\Delta_{xe}$ %	$\Delta_{\rm x} = C_d \Delta / I_e$	Drift limit	Check
		%	$\Delta_{\text{lim}} = 0.02  (\%)$	$\Delta_{\rm x} < \Delta_{\rm ,lim}$
LEVEL 5	0.00066	0.0036	0.02	OK
LEVEL 4	0.00101	0.0056	0.02	OK
LEVEL 3	0.00130	0.0072	0.02	OK
LEVEL 2	0.00118	0.0065	0.02	OK
LEVEL 1	0.00030	0.0017	0.02	OK
GF	0.00028	0.0015	0.02	OK

		Y		
STORY	$\Delta_{xe}$ %	$\Delta_{\rm x} = C_d \Delta / I_e$	Drift limit	Check
		%	$\Delta$ , <sub>lim=</sub> 0.02 (%)	$\Delta_{\rm x} < \Delta_{\rm ,lim}$
LEVEL 5	0.00058	0.0032	0.02	OK
LEVEL 4	0.00093	0.0051	0.02	OK
LEVEL 3	0.00118	0.0065	0.02	OK
LEVEL 2	0.00111	0.0061	0.02	OK
LEVEL 1	0.00026	0.0014	0.02	OK
GF	0.00023	0.0012	0.02	OK

Table 4-2: Story drifts and drift limits in X, Y directions for M-IR2 for ELFP

		X		
STORY	$\Delta_{xe}$ %	$\Delta_{\rm x} = C_d \Delta / I_e$	Drift limit	Check
		%	$\Delta$ , <sub>lim=</sub> 0.02 (%)	$\Delta_{\rm x} < \Delta_{ m ,lim}$
LEVEL 5	0.00064	0.0035	0.02	OK
LEVEL 4	0.00099	0.0055	0.02	OK
LEVEL 3	0.00122	0.0067	0.02	OK
LEVEL 2	0.00108	0.0060	0.02	OK
LEVEL 1	0.00017	0.0009	0.02	OK
GF	0.00012	0.0006	0.02	OK

Y							
STORY	$\Delta_{xe}$ %	$\Delta_{\rm x} = C_d \Delta / I_e$	Drift limit	Check			
		%	$\Delta$ , <sub>lim=</sub> 0.02 (%)	$\Delta_{\rm x} < \Delta_{ m ,lim}$			
LEVEL 5	0.00043	0.0024	0.02	OK			
LEVEL 4	0.00070	0.0039	0.02	OK			
LEVEL 3	0.00089	0.0049	0.02	OK			
LEVEL 2	0.00087	0.0048	0.02	OK			
LEVEL 1	0.00021	0.0012	0.02	OK			
GF	0.00014	0.0008	0.02	OK			

Table 4-3: Story drifts and drift limits in X, Y directions for M-IR3 for ELFP

1 4010 1 3.	ruote 1 3. Story units and unit minus in 11, 1 uncertons for 11 into 101 EET 1					
		X				
STORY	$\Delta_{xe}$ %	$\Delta_{\mathrm{x}} = C_d \Delta / I_e$	Drift limit	Check		
		%	$\Delta$ , <sub>lim=</sub> 0.02 (%)	$\Delta_{\rm x} < \Delta_{ m ,lim}$		
LEVEL 5	0.00061	0.0034	0.02	OK		
LEVEL 4	0.00094	0.0052	0.02	OK		
LEVEL 3	0.00117	0.0064	0.02	OK		
LEVEL 2	0.00094	0.0052	0.02	OK		
LEVEL 1	0.00009	0.0005	0.02	OK		
GF	0.00007	0.0004	0.02	OK		

		Y		
STORY	$\Delta_{xe}$ %	$\Delta_{\mathrm{x}} = C_d \Delta / I_e$	Drift limit	Check
		%	$\Delta_{\text{,lim}} = 0.02  (\%)$	$\Delta_{\rm x} < \Delta_{\rm ,lim}$
LEVEL 5	0.00046	0.0025	0.02	OK
LEVEL 4	0.00072	0.0039	0.02	OK
LEVEL 3	0.00082	0.0045	0.02	OK

LEVEL 2	0.00071	0.0039	0.02	OK
LEVEL 1	0.00016	0.0009	0.02	OK
GF	0.00010	0.0006	0.02	OK

Table 4-4: Story drifts and drift limits in X, Y directions for M-IR4 for

		X		
STORY	$\Delta_{xe}$ %	$\Delta_{\mathrm{x}} = C_d \Delta / I_e$	Drift limit	Check
		%	$\Delta$ , <sub>lim=</sub> 0.02 (%)	$\Delta_{\rm x} < \Delta_{\rm ,lim}$
LEVEL 5	0.00064	0.0034	0.02	OK
LEVEL 4	0.00101	0.0053	0.02	OK
LEVEL 3	0.00120	0.0063	0.02	OK
LEVEL 2	0.00105	0.0055	0.02	OK
LEVEL 1	0.00015	0.0008	0.02	OK
GF	0.00010	0.0003	0.02	OK

		Y		
STORY	$\Delta_{xe}$ %	$\Delta_{\rm x} = C_d \Delta / I_e$	Drift limit	Check
		%	$\Delta_{\text{lim}} = 0.02  (\%)$	$\Delta_{\rm x} < \Delta_{\rm ,lim}$
LEVEL 5	0.00044	0.0023	0.02	OK
LEVEL 4	0.00072	0.0038	0.02	OK
LEVEL 3	0.00089	0.0047	0.02	OK
LEVEL 2	0.00083	0.0043	0.02	OK
LEVEL 1	0.00012	0.0006	0.02	OK
GF	0.00010	0.0004	0.02	OK

The criterion for taking into account the second order effects (P- $\Delta$  check) is based on the interstory drift sensitivity coefficient  $\Theta$  for each story, which is computed in accordance with Section 12.8.7 of ASCE 7-16,

$$\Theta = \frac{P_{\mathcal{X}} \cdot \Delta \cdot l_{e}}{V_{\mathcal{X}} \cdot h_{sx} \cdot C_{d}} \le 0.10 \tag{43}$$

where:

 $P_x$ : the total gravity load at and above the considered story, in the seismic design situation, at level x,

 $\Delta$ : the design interstory drift at level x in m, computed using Eq. (12.8-15) in ASCE 7-16,  $\Delta = \frac{cd \cdot \Delta x}{le}$ , where  $\Delta_x$  is the interstory drift at level x in m, determined by an elastic analysis,

 $I_e$ : the seismic importance factor,

 $V_x$ : the total design shear at level x obtained by modal response spectrum analysis,

 $h_{\rm sx}$ : the story height,

 $C_d$ : the deflection amplification factor in ASCE 7-16, Table 12.2-1.

The sensitivity coefficients along the elevation for both directions are determined in Tables 4-5...4-8. In the case of the investigated structures, the second order effects need not be taken into account, because the inter-story drift sensitivity coefficient  $\Theta$  is smaller than 0.10 in all stories, in both directions.

Table 4-5: Determination the inter-story drift sensitivity coefficient Θ for M-IR1

Story	$P_{x}$	h	$V_{x}$ (	kN)	Δ,	m	(	9
	kN	m	X-Dir	Y-Dir	X-Dir	Y-Dir	kN	m
LEVEL 5	1610.00	3	113.16	126.94	0.009	0.006	0.008	0.005
LEVEL 4	3173.28	3	175.18	210.70	0.015	0.010	0.016	0.009
LEVEL 3	4736.57	3	221.58	269.64	0.019	0.014	0.024	0.015
LEVEL 2	6299.86	3	257.37	313.87	0.017	0.013	0.025	0.016
LEVEL 1	10917.66	3	323.41	382.34	0.002	0.003	0.005	0.006
GF	15535.47	3	391.65	448.07	0.002	0.002	0.004	0.005

Table 4-6: Determination the inter-story drift sensitivity coefficient Θ for M-IR2

Story	Px	h	Vx (	(kN)	$\Delta$ ,	m	(	9
	kN	m	X-Dir	Y-Dir	X-Dir	Y-Dir	X-Dir	Y-Dir
LEVEL 5	1659.48	3	85.28	115.84	0.008	0.008	0.009	0.007
LEVEL 4	3397.66	3	134.44	180.05	0.013	0.014	0.021	0.016
LEVEL 3	5135.84	3	172.08	228.39	0.018	0.019	0.033	0.026
LEVEL 2	6874.02	3	200.65	266.94	0.019	0.020	0.039	0.031
LEVEL 1	11113.04	3	255.65	328.90	0.004	0.005	0.011	0.010
GF	15352.07	3	322.72	405.84	0.004	0.004	0.010	0.010

Table 4-7: Determination the inter-storey drift sensitivity coefficient Θ for M-IR3

Story	Px	h	Vx (	(kN)	$\Delta$ ,	m	(	9
Story	kN	m	X-Dir	Y-Dir	X-Dir	Y-Dir	X-Dir	Y-Dir
LEVEL 5	1829.80	3	154.60	175.16	0.009	0.007	0.007	0.004
LEVEL 4	3738.31	3	258.43	308.77	0.015	0.011	0.014	0.008
LEVEL 3	6053.21	3	347.97	423.52	0.019	0.013	0.020	0.011
LEVEL 2	8793.20	3	413.98	511.97	0.016	0.011	0.021	0.011
LEVEL 1	13435.88	3	478.57	580.46	0.002	0.003	0.004	0.004
GF	18109.47	3	549.91	642.02	0.001	0.002	0.002	0.003

Table 4-8: Determination the inter-storey drift sensitivity coefficient Θ for M-IR4

Story	Рх	h	Vx (	(kN)	Δ,	m	6	9
	kN	m	X-Dir	Y-Dir	X-Dir	Y-Dir	X-Dir	Y-Dir
LEVEL 5	1772.60	3	150.99	158.81	0.009	0.006	0.006	0.004
LEVEL 4	3619.93	3	248.43	275.07	0.014	0.011	0.013	0.009
LEVEL 3	5467.25	3	326.61	363.28	0.018	0.014	0.018	0.013
LEVEL 2	7314.58	3	372.97	420.04	0.014	0.013	0.016	0.013
LEVEL 1	11958.68	3	446.05	486.90	0.001	0.002	0.002	0.003
GF	16603.90	3	537.53	555.44	0.001	0.001	0.002	0.002

#### 5 NON-LINEAR ANALYSIS (STATIC NSP AND DYNAMIC NDP)

#### 5.1 General

The non-linear (static and dynamic) analysis is also performed according to ASCE/SEI 7-16 and ASCE/SEI 41-13 codes, since this approach determines the actual performance level of the structure. The CSI software SAP2000 (2019) [27], is utilized to perform the nonlinear analysis, given that it is more realistic for the simulation of nonlinear behavior of materials and structural components.

#### 5.2 Modeling nonlinearity of members

The same 3-D models utilized before in the linear analysis are again utilized for the nonlinear analysis. The structures must be first designed, using the response spectrum analysis RSA, according to ASCE/ SEI 7-16. The design and detailing of the models for ductility are performed to achieve the goal of ASCE/ SEI 7-16 and also to meet the rules and requirements of ACI 318-19.

According to ACI 318-19 (considered for design in Iraq), for nonlinear analysis the effective stiffness values were introduced in the analysis by adopting the cracked stiffnesses of the columns and beams, as mentioned previously in Table 2-3 and model beam-column joints in Section 2.

According to ASCE/SEI 41-13, beams and columns will be modelled as elastic elements with concentrated plastic hinges at each end, after their effective stiffness has been assigned. The moment—rotation relation, as shown in Figure 8, defines these plastic hinges.

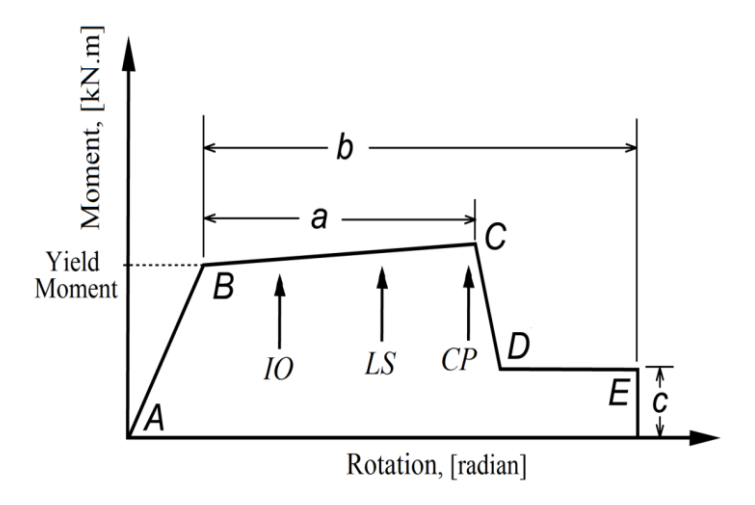


Figure 8: Generalized component load-deformation relation for nonlinear analysis showing performance levels [24]

The numerical acceptance criteria for nonlinear components at different structural performance levels for beams and columns that were determined according to ASCE/SEI 41-13, as well as the updated modeling parameters a, b, and c of Fig. 8. The values in these tables are input in the SAP2000 to model numerically all studied buildings and to determine their components nonlinearity.

For a nonlinear analysis of the frames, plastic hinges are defined at every column and beam endpoint where a plastic hinge may develop. To properly identify the placement of plastic hinges at the ends of each member, the lengths of plastic hinges were estimated according to Park and Paulay (1975) [28],  $L_p = 0.5$  of the member depth, as illustrated in Figure 9. For beams, the moment-rotation relationship is entered to SAP2000 using user-defined hinge property type M3. For columns, the user-defined hinge property type P-M2-M3 is used.

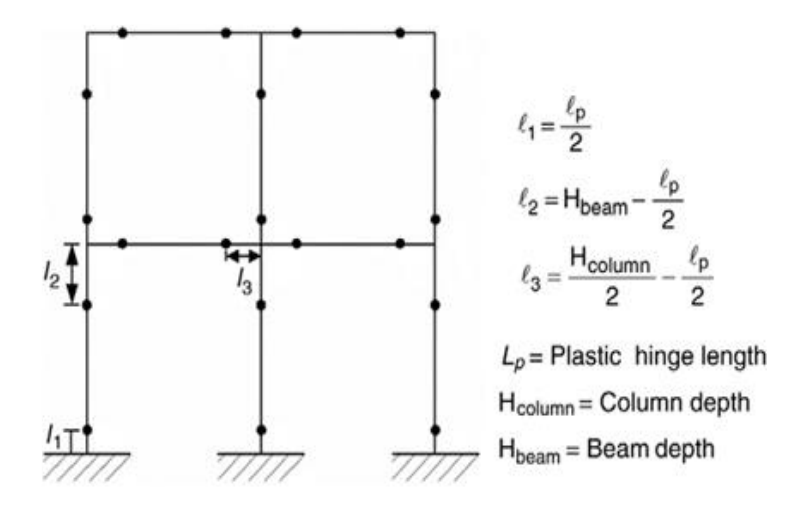


Figure 9: Hinge locations at ends of beams and columns [28]

Referring to Appendix B, for rebars a parametric simple stress-strain curve has been employed in SAP2000, for  $f_y$ = 414 MPa. The Mander confined and unconfined concrete parametric stress-strain models for a rectangular section were utilized in SAP 2000, the stirrups being used to provide confinement.

The Pivot hysteretic model was used to define inelastic cyclic behavior of masonry infill in the nonlinear elastic range in SAP 2000 (Figure 10a). The parameters  $\alpha_1$ ,  $\alpha_2$ ,  $\beta_1$ , and  $\beta_2$  were used to numerically adjust hysteretic rules. The adoption of the Pivot hysteretic model has the advantage of allowing for the application of simpler rules to equivalent diagonal struts (Figure 10b). Because the tensile strength of the masonry infill is not taken into account in this situation, the parameters  $\alpha_1$  and  $\beta_1$  are both null, being set to zero. According to [30], experiment results showed that when the load is reversed on frames with masonry infill, the stiffness does not increase. It was proven that  $\beta_2$  is also zero. Therefore, the hysteretic loop is calibrated through the parameter  $\alpha_2$ . The value of  $\alpha_2$  is selected equal to 0.25, as used in the cited source [30]. Another advantage of the hysteretic model described here is that it always generates positive stiffness. The use of negative or zero tangential stiffness in dynamic analysis can affect the numerical solution's stability [31].

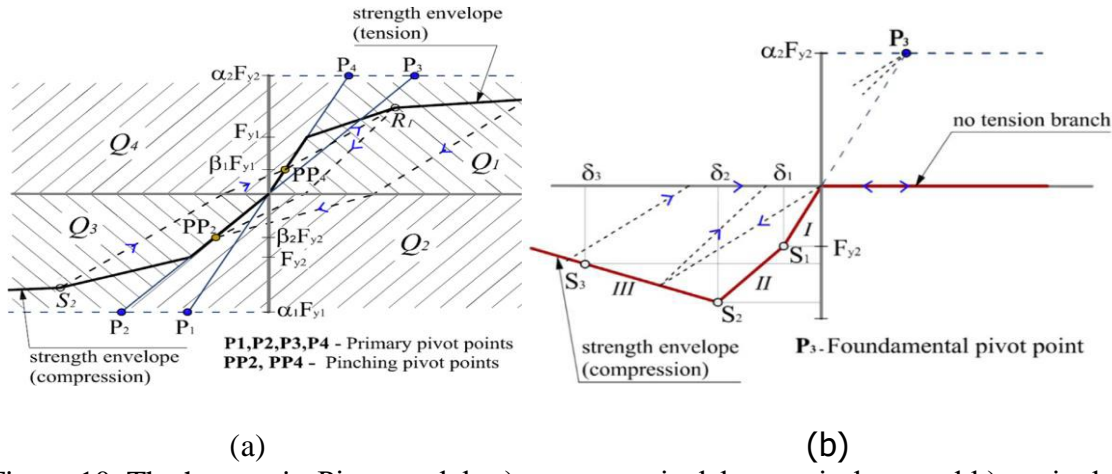


Figure 10. The hysteretic Pivot model: a) unsymmetrical hysteretic loop and b) equivalent compressive diagonal [30]

### 5.3 Seismic performance levels

During the earthquakes, there are three main structural performance levels classifications of RC structures according to ASCE / SEI 41-13 and FEMA 356. These are shown in Table 5-1.

Table 5-1: Structural performance levels and damage of concrete frames [24]

Element type		Structural Performance	Levels
	Collapse	Life Safety	Immediate
	Prevention		Occupancy
Primary	Extensive cracking	Extensive damage to	Minor hairline cracking.
	and hinge formation	beams. Spalling of	Limited yielding
	in ductile elements.	cover and shear	possible at a few
	Limited cracking	cracking (<0.32 mm) for	locations.
	and/or splice failure	ductile columns. Minor	
	in some non-ductile	spalling in non-ductile	No crushing (strains
	columns. Severe	columns. Joint cracks	below 0.003).
	damage in short	<0.32 mm wide.	
Casandany	columns.	Evrtansiva anadzina and	Minor analling in a face
Secondary	Extensive spalling in columns (limited	Extensive cracking and hinge formation in	Minor spalling in a few places in ductile
	shortening) and	ductile elements.	columns and beams.
	beams.	ductife elements.	Flexural cracking in
	ocanis.	Limited cracking and/or	beams and columns.
	Severe joint damage.	splice failure in some	Shear
	Some reinforcing	non- ductile columns.	Z. Z
	buckled	Severe damage in short	Cracking in joints <
		columns	0.16 mm.
Drift	Transient drift	Transient drift sufficient	Transient drift that
	sufficient to cause	to cause nonstructural	causes minor or
	extensive	damage. Noticeable	nonstructural damage.
	nonstructural	permanent drift.	Negligible permanent
	damage. Extensive		drift.
	permanent drift.		
	4% transient or	2% transient; 1 %	1% transient; negligible
	permanent.	permanent	permanent

The performance level is determined by the building's occupancy category. The office buildings, as those in the current study, are classified as occupancy category type II according to ASCE/SEI 7-16 and the Iraqi seismic design code ISC 2016 [4]. Most codes and studies employ the life safety performance level (FEMA P695, ATC- 40 and ASCE/ SEI 7- 16), for which the maximum drift must not be larger than 2%.

#### 5.4 Response limits and acceptability criteria

The main structural response limits that constitute acceptance criteria for the building models are summarized below. Details on the parameters and options adopted in the current study are also given.

- 1. Proportioning of members sections. After determining the preliminary sizing of member for linear analysis based on acceptable cross-sectional aspect ratios and slenderness ratios, the preferred level of axial forces was adopted as proposed in Murty et al. (2012) [55], i.e. that the axial load level in columns,  $P/(A_g f_c')$ , should not exceed or be around 0.3 in order to ensure ductile behavior and, if they fail, failure will be caused by steel yielding. The detailing of the special moment frames according to ACI 318 is illustrated in Appendix A.
- 2. For nonlinear analysis, the minimum ratio of reinforcement requirements required to fulfill the desirable failure mechanism is determined [55, 56] (see Appendix A).
- 3. For nonlinear analysis, according to ASCE/SEI 41-13, the gravity load combination W = D + 0.25L (where D is the dead load and L is the live load) should be applied before the seismic loading.
- 4. According to ASCE/SEI 41-13, for the Life Safety performance level in (Table 5-1), for office buildings (category II), the maximum drift must not more than 2%.
- 5. For pushover analysis, the maximum drift is the maximum inter-story drift at the performance point. The target displacement of the buildings models represents its performance point or its response to the design spectral accelerations (ASCE 41-13).
- 6. According to ASCE/SEI 41-13 and depending on the moment—rotation relation, as shown in Fig. 8, for plastic hinges illustrating the acceptance limit at each performance level, the target displacement on the pushover curve of the nonlinear models needs to be reached before any hinge response exceeds the acceptance limit at life safety performance level.

# 5.5 Methodology for nonlinear analysis

According to ASCE/SEI 41-13, a nonlinear static analysis procedure (NSP) and a nonlinear dynamic analysis procedure (NDP) were applied using SAP2000.

1. Nonlinear static analysis procedure (NSP)

In the nonlinear static analysis procedure (NSP), the building models were subjected to monotonically increasing lateral loads representing inertia forces in an earthquake, until a target displacement ( $\delta_t$ ) at the control node was exceeded. Thus, the capacity curve was established.

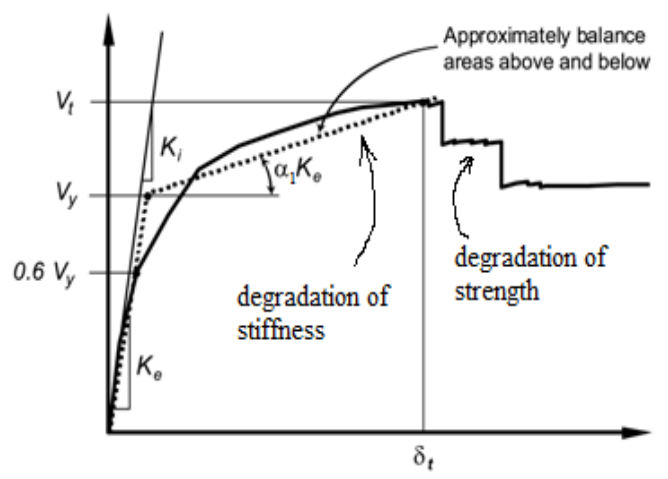


Figure 11. Pushover curves and the idealized force- displacement curves [26, 36]

The target displacement is identified on the pushover curve by utilizing the modified coefficient method of FEMA 440, as adopted in ASCE/ SEI 41-13 (this is illustrated in Appendix B). The established idealized force-displacement curve will be used to obtain the yield point of the models, as shown in Figure 11. The idealized relation's first linear segment starts at the origin point. The second linear segment either ends at a point on the force-displacement curve where was computed target displacement, referred to as "the performance point," or at a maximum base shear point, whichever the smallest displacement. Through the two linear segments intersection the effective lateral stiffness ( $K_e$ ), the effective yield strength ( $V_y$ ), and the effective positive post-yield stiffness ( $K_e$ ) were defined. Two conditions must be met in order that the point of intersection be identified. The first is that the effective stiffness,  $K_e$ , has to be such that the first segment passes through the defined curve at a point where the base shear equals 60% of the effective yield strength. The second requirement is that the areas above and below the specified curve be approximately balanced [26]. These two curves will provide significant data about the nonlinear behavior of models.

According to FEMA 356, "the pushover curve is developed for at least two vertical distributions of lateral loads". The first distribution is the Equivalent Lateral Force (ELF) distribution:  $(S^*_i = m_i \ h_i^k)$  (with i = 1, 2...N being the floor number), where  $S^*_i$  is the lateral force at the  $i^{th}$  floor. The second distribution is the uniform pattern of lateral force distribution:  $(S^*_i = m_i)$ . Nonlinear static analysis is carried out in the both directions ( $\pm X$  and  $\pm Y$ ) of the models. The analyses include P-delta effects and gravity loads.

In addition, and based on ASCE/SEI 41-13 and on the recommendations of FEMA 440, the first mode distribution ( $S^*_i = m_i \phi_{il}$ ) will also be used as a third distribution. According to the response spectra analysis of the building models, the fundamental period of vibration does not exceed 1.0 s, ensuring thus that the first mode of vibration dominates.

#### 2. Nonlinear dynamic analysis procedure (NDP)

Iraq is generally located in a stable continental region, and the majority of its earthquake activity happens in the active tectonic zones between Turkey and Iran. Iraq presently lacks a nationwide strong motion network, making recording strong motion data in Iraq extremely challenging [37]. According to ASCE/SEI 7-16, the site of the models in this study (Baghdad) is not within 10 km of any known fault, so only far-field ground motions are considered.

According to ASCE/SEI 7-16, for ground acceleration histories needed in analysis, eleven pairs of spectrally matched orthogonal components, obtained from eleven artificial accelerograms

pairs, are included in this study (ASCE/SEI 7-16, Section C16.2.2). Because more than seven ground motions have been used, the response parameters will be the mean results obtained from all of the analyses.

For spectral matching, the target response spectrum (design spectrum, specified for Baghdad for Peak Ground Acceleration PGA = 0.125 g) was used as a target spectrum to generate the eleven artificial accelerograms. The target response spectrum, 5%-damped, was developed for single response spectrum. The period range for matching was determined according to ASCE/SEI 7-16, Section 16.2.3.1: "upper [period] bound equal to twice the largest first-mode period in the principal horizontal directions of response. The lower bound period shall not exceed 20% of the smallest first-mode period for the two principal horizontal directions of response".

Two orthogonal seismic actions (in the X and Y directions) were applied independently. The vertical response effects were not included for the studied models, according to ASCE/SEI 7-16, Section 16.1.3. For sources of artificial excitations, the PEER NGA-2022 strong motion database [57] was used to find the best matching (spectral matching with the target response spectrum, design spectrum specified for Baghdad) earthquake records. The two horizontal components were applied for each accelerogram, and then they were scaled (in the time domain) in the SAP2000 program to match the target spectrum. The parameters of the selected record motions are summarized in Appendix B, as well as the target spectrum and the scaled spectra for artificial accelerograms.

#### 5.6 Results and discussion of structural behavior

#### 5.6.1 General

The nonlinear behavior of all models can be tracked by the nonlinear static analysis (pushover curve) until the target displacement is obtained. Also, by the nonlinear dynamic analysis, the average values of the parameters are obtained from all of the matching eleven artificial accelerograms. Figure 12 to 15 represent the plastic hinges assigned for the models before performing nonlinear static and dynamic analysis.

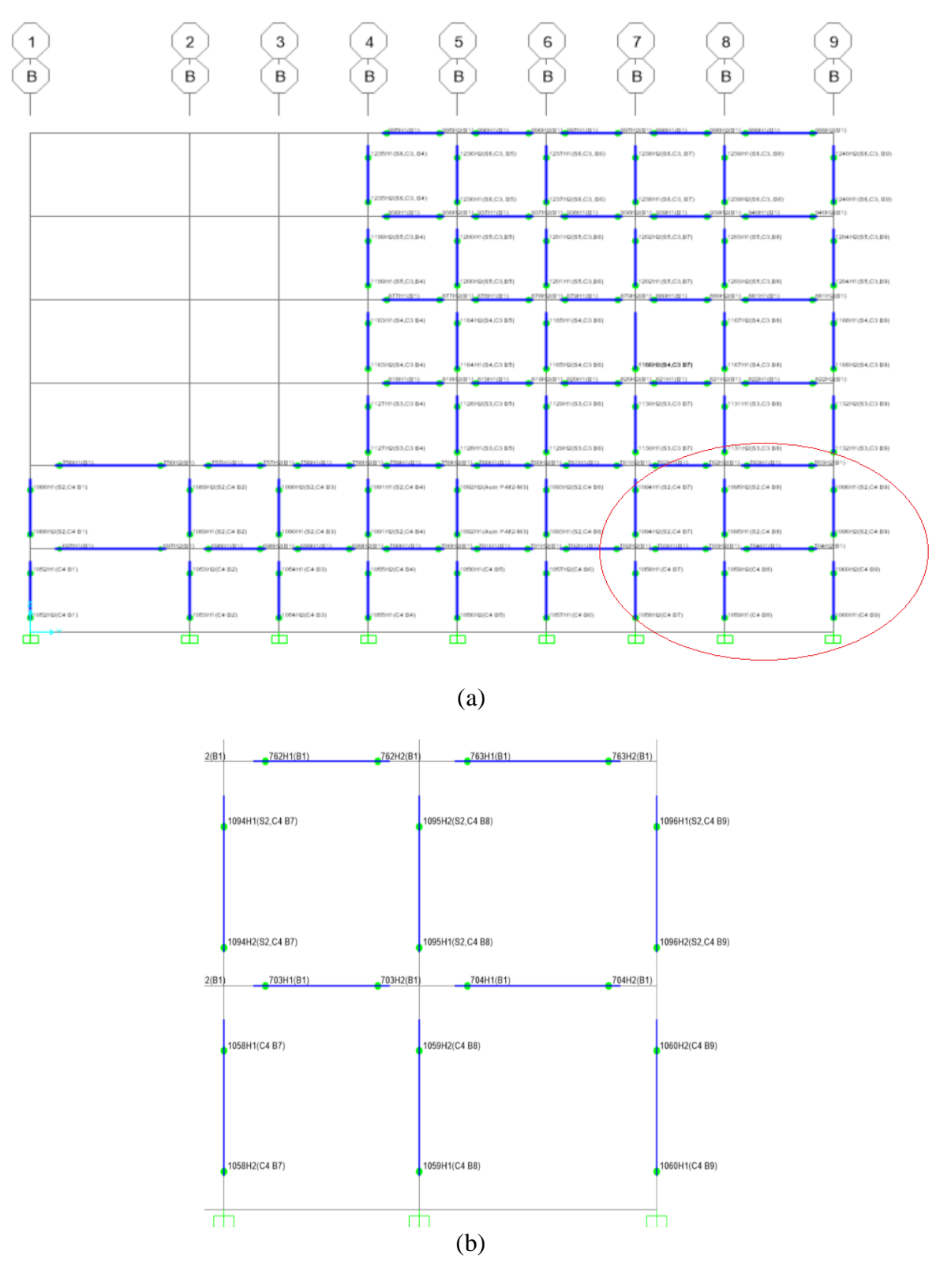


Figure 12. Plastic hinges at the ends of column and beams at ground level and first level for M-IR1

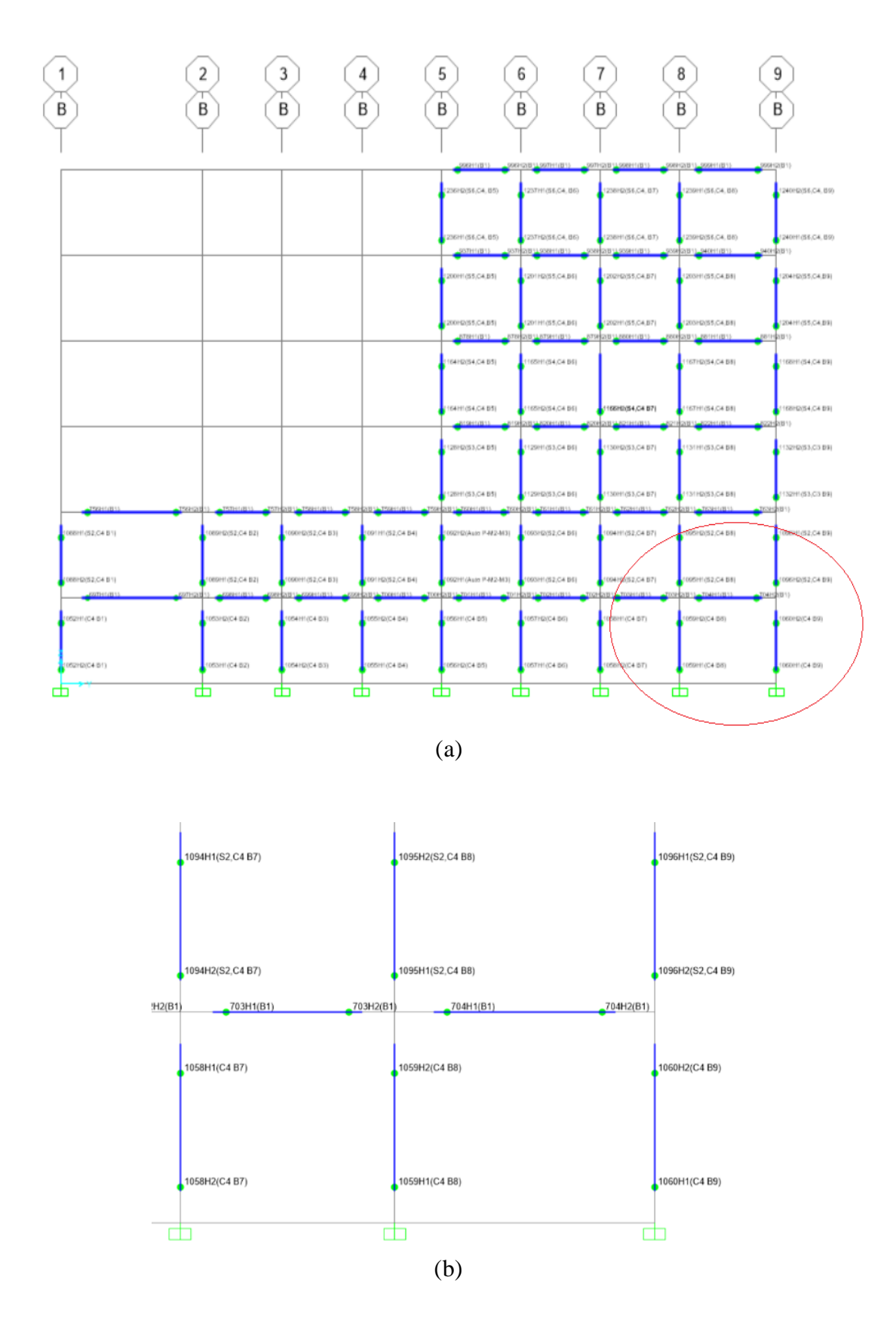


Figure 13. Plastic hinges at the ends of column and beams at ground level and first level for M-IR2

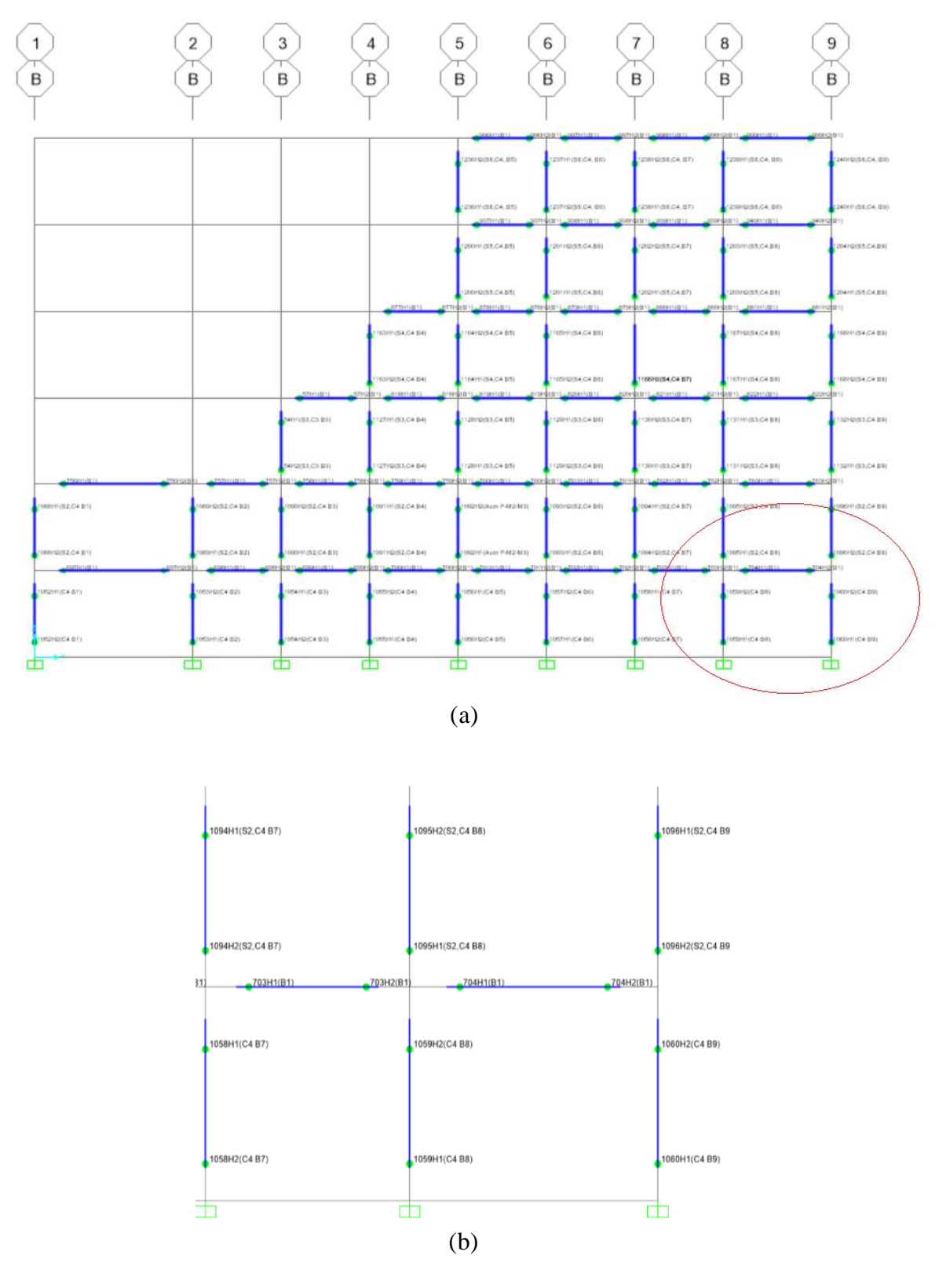


Figure 14. Plastic hinges at the ends of column and beams at ground level and first level for M-IR3.

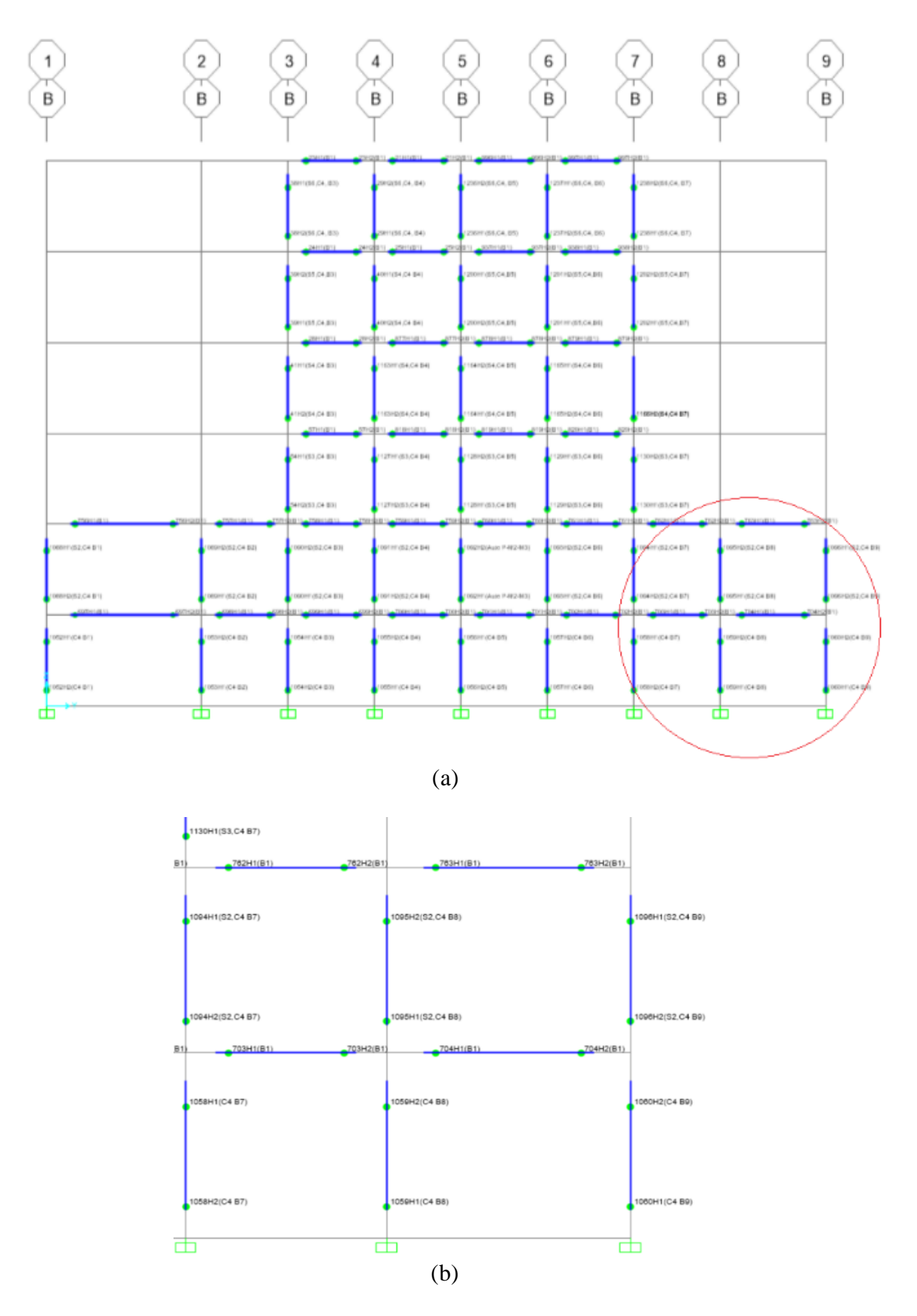


Figure 15. Plastic hinges at the ends of column and beams at ground level and first level for M-IR4

#### 5.6.2 Nonlinear static analysis procedure (NSP)

#### 5.6.2.1 General

The design spectra for Baghdad city, as shown in Figure 7, was defined in SAP2000 to be used in the determination of the performance point of the models. The NSP analysis includes a number of loading steps to establish the pushover curve. To determine the step at which  $\delta_t$  is reached, the models are pushed to reach the values  $\delta_t$  at roof level for each of the three load distribution patterns. After determining the step number to reach  $\delta_t$ , from the story drift distribution along the height at the step of  $\delta_t$ , it can be identified the story and the value at which the maximum difference between the story lateral displacements occurs. In most cases,  $\delta_t$  is not determined at a specific step, but between two steps which are the prior and the next steps. Consequently, for the worst condition, the next step is adopted. For all models (M-IR1, M-IR2, M-IR3 and M-IR4) in all cases (Y+, Y-, X+, X-), under the action of the three load distributions, it was found that all plastic hinges that formed during the model response up to the target displacement were within the life safety performance level. In addition, all plastic hinges that formed in the columns for all models were in the second story at the base of the columns where the setback began. Hence, the models are safe against the soft story failure mechanism.

Table 5-2 represents the values of the target shear (shear capacity  $V_t$ ) and the target displacement ( $\delta_t$ ) for all setback irregular models under the action of the three load distributions. Several aspects can be observed from Table 5-2. First, the increase of the base shear of the models, under the effect of the same load distribution, when irregularity indices decrease due to the mass and stiffness increase. The target shear ( $V_t$ ) values for the second load distribution (uniform) are higher than for the first load distribution (ELF) and the third load distribution (1st mode) for the same frame model. The differences were higher than (ELF) by about 95...113% for M-IR1, 79...86% for M-IR2, 41...67% for M-IR3, and 37...80% for M-IR4. Also, the difference for the uniform pattern is higher than that for the 1st mode distribution by about 132...182% for M-IR1, 104...132% for M-IR2, 31...91% for M-IR3, and 33...106% for M-IR4. In addition, it was noticed that, as the model irregularity indices increased, the target displacement ( $\delta_t$ ) decreased and the target shear (shear capacity,  $V_t$ ) decreased under the effect of the same action of the load distribution.

The larger value of the target displacement demand, conjugating with the smallest value of target shear capacity, was obtained under the action of the 1<sup>st</sup> mode load pattern distribution, which is considered the worst case among the three load pattern distributions. The  $V_t$  and  $\delta_t$  are taken from the pushover curves.

It is obvious that the setback has a large impact on the structure's capacity. The decrease in seismic performance can be illustrated by the fact that the setback has influences on the structure's capacity for inelastic deformation during a seismic action and, as a result, the structure will be less ductile, which will produce a significant energy release that may cause damage to the elements of the structure.

Table 5-2: The target shear values  $(V_t)$  and the target displacement  $(\delta_t)$  for all models, under the action of the three load distributions considered in NSP

M	Modals		Equivalent lateral force (ELF)		uniform pattern of lateral force		1 <sup>st</sup> mode load distribution	
		$V_{t/}[kN]$	$\delta_t$ /mm	$V_{t/}[kN]$	$\delta_t$ /mm	$V_{t/}[kN]$	$\delta_t$ /mm	
	Y-direction	3752	65	7303	71	3144	78	
M-IR1	Y+direction	3915	72	8342	77	3048	72	
IVI-IK 1	X+direction	3297	92	7031	80	2492	94	
	X-direction	3311	91	6443	88	2532	97	
	Y-direction	4921	77	9173	92	4490	94	
M-IR2	Y+direction	4460	101	8010	97	3555	122	
WI-IK2	X+direction	4031	108	7214	98	3104	101	
	X-direction	4507	93	8333	97	4118	100	
	Y-direction	6910	121	11563	110	6066	123	
M ID2	Y+direction	6064	139	8576	128	6535	146	
M-IR3	X+direction	5553	143	7953	139	4858	147	
	X-direction	5961	135	10698	129	4097	154	
_	Y-direction	5928	102	10646	104	5156	112	
M-IR4	Y+direction	6046	106	8256	111	6193	127	
WI-IK4	X+direction	5559	110	7528	114	4165	125	
	X-direction	5116	115	10220	116	4094	116	

# 5.6.2.2 Drift Check

The inter-story inelastic drift ratios ( $IDR_{x,y}$ ) for both directions are computed at the target displacement ( $\delta_t$ ) [38]. The maximum inter-story inelastic drift ratio ( $IDR_{max}$ ) is the maximum IDR of all stories. The story drift limit is 2% for the risk category II building, according to ASCE 7-16 [3]. The inter-story drift ratios should not exceed this limit. The IDR parameter is calculated for the i<sup>th</sup> floor with the following formula:

$$IDRx_i = \frac{\Delta xi}{hi}$$
,  $IDRy_i = \frac{\Delta yi}{hi}$ 

where:

 $\Delta x_i$  is the drift in the X-direction for the i<sup>th</sup> and (i-1)<sup>th</sup> story,  $\Delta y_i$  is the drift in the Y-direction for the i<sup>th</sup> and (i-1)<sup>th</sup> story,  $h_i$  is the story height.

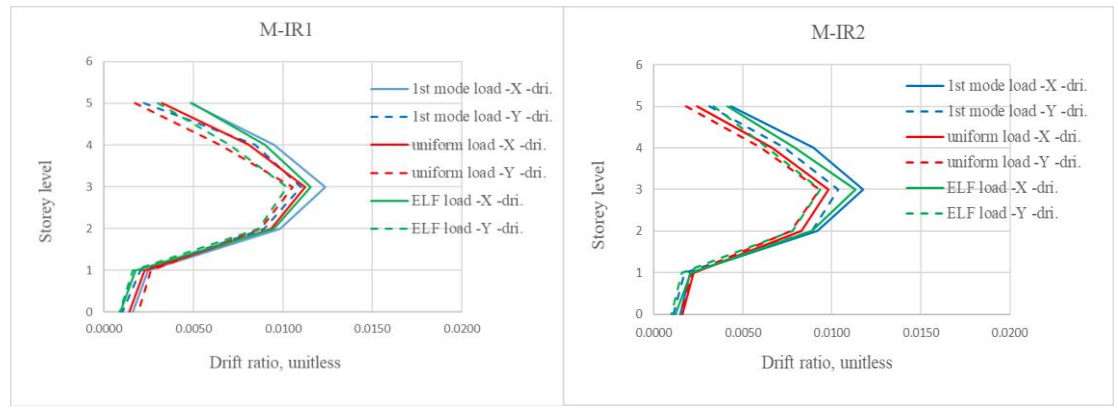


Figure 16: Inter-story drift ratios ( $IDR_{x,y}$ ) along the height of M-IR1 and M-IR2 models for NSP

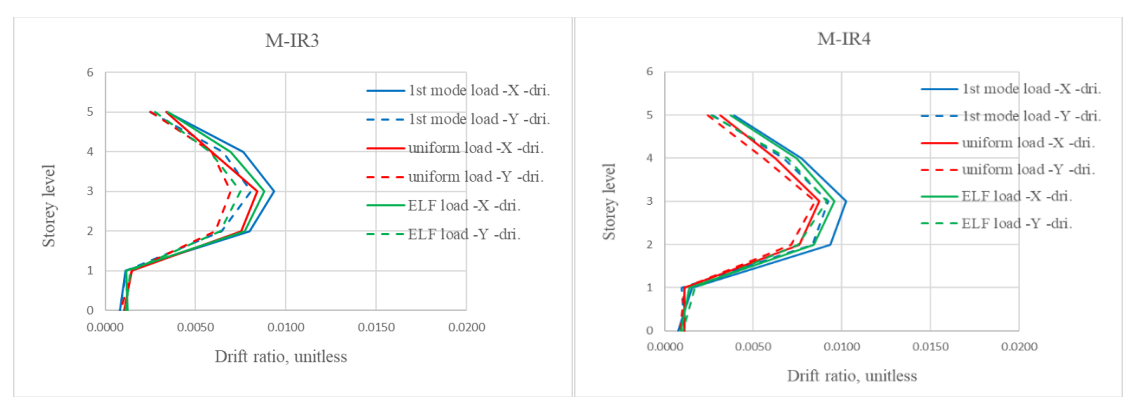


Figure 17: Inter-story drift ratios ( $IDR_{x,y}$ ) along the height of M-IR3 and M-IR4 models for NSP

The story drifts are shown in Figures 16 and 17 for both directions, under effect of the three load distributions considered in the NSP analysis. It can be noticed that the drift of the "1<sup>st</sup> mode" load distribution along the height of the models is larger than the drift of both other two load distributions (Equivalent lateral force, ELF, and Uniform), for the same model. The first story of the upper structure, for all models, has the highest story-drift-ratio in the entire building, which is satisfying the assumption of the equation of the minimum story-stiffness ratio  $r_{kUI}$  (Eq. 14 in this study) which is derived in [13].

Nevertheless, the maximum inter-story drift ratios at  $\delta_t$  ( $IDR_{tmax}$ ) do not exceed the limit of 2%, i.e., the performance of the frames is satisfactory in spite of the existence of the setback. In addition, it can be noted that, as the model irregularity indices increase, the inter-story drift increases under the effect of a particular load distribution, as shown in Figure 18.

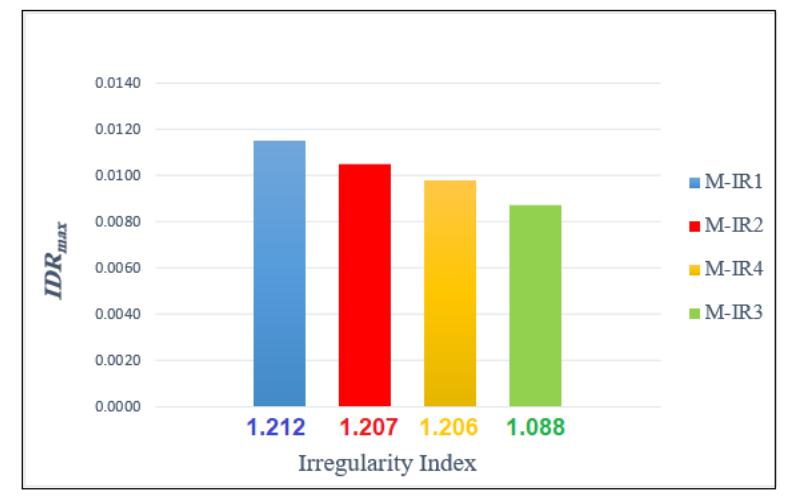


Figure 18: Maximum inter-story inelastic drift ratio ( $IDR_{max}$ ) as a function of the irregularity index of all models for NSP.

#### 5.6.3 Nonlinear dynamic analysis procedure (NDP)

#### 5.6.3.1 General

Table 5-3 and Figures 19...22 show the base shear force for setback irregular models for both directions, resulting from the nonlinear dynamic analysis (NDP). The response parameters were the average values obtained from all of the analyses. From the results, it is noted that the base shear force decreases as the irregularity indices of the models increase.

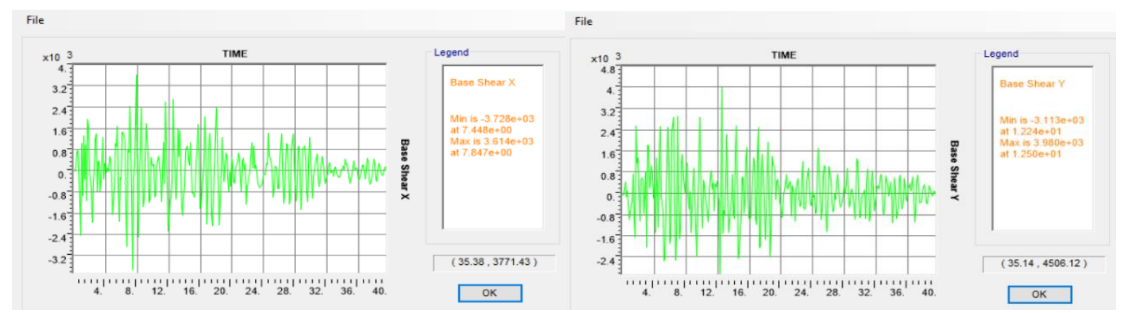


Figure 19. Base shear force for M-IR1 for NDP

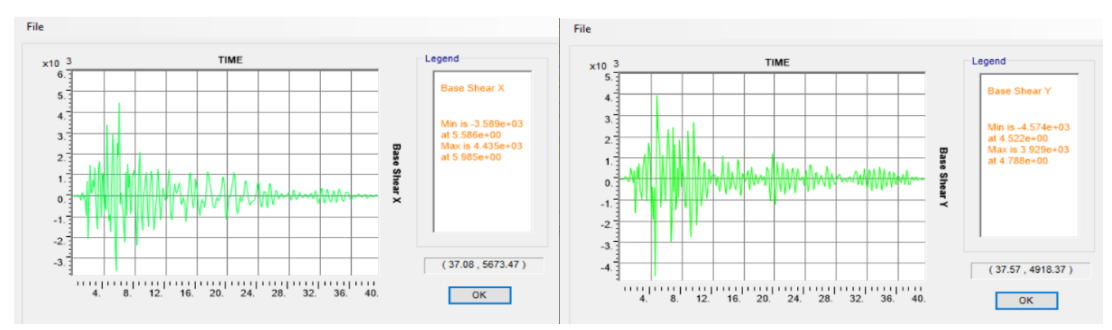


Figure 20. Base shear force for M-IR2 for NDP

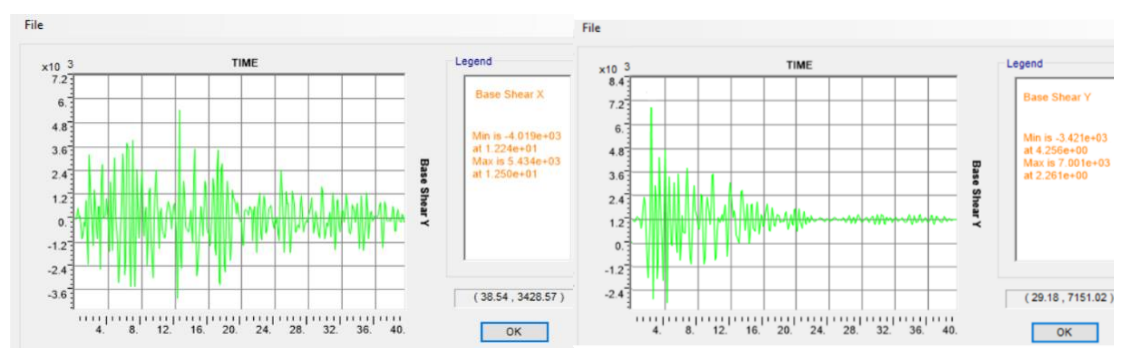


Figure 21. Base shear force for M-IR3 for NDP

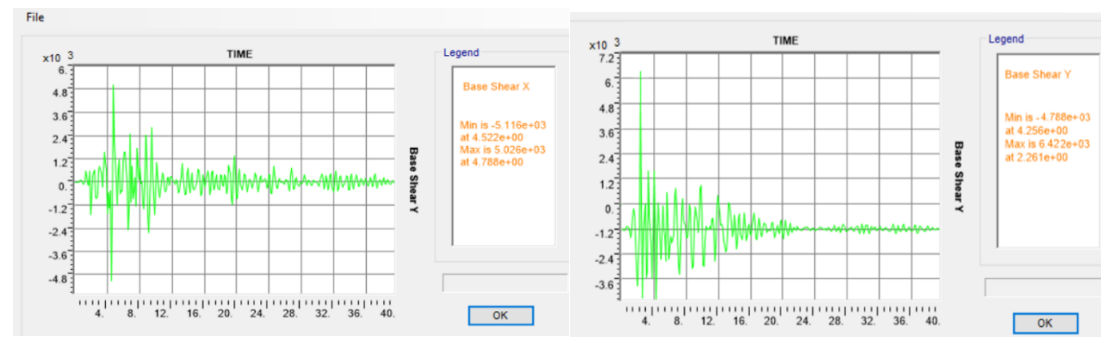


Figure 22. Base shear force for M-IR4 for NDP

Table 5-3: Base shear force for setback irregular models for NDP

Modals	Base shear fo	orce [kN]
Wiodais	X	Y
M-IR1	3728	3980
M-IR2	4435	4574
M-IR3	5434	7001
M-IR4	5026	6422

#### 5.6.3.2 Drift Check

The inter-story drifts ( $IDR_{x,y}$ ) for all models are shown in Figures 23 and 24 for both directions as resulting from the NDP. It can be seen that the maximum inter-storey drift ratios ( $IDR_{max}$ ) do not exceed the limit of 2% according to ASCE 7-16, which means that, in general, the performance of the setback frames are quite satisfactory. In addition, it is noted that the increase of the irregularity indices of the setback models resulted in increased inter-storey drift values.

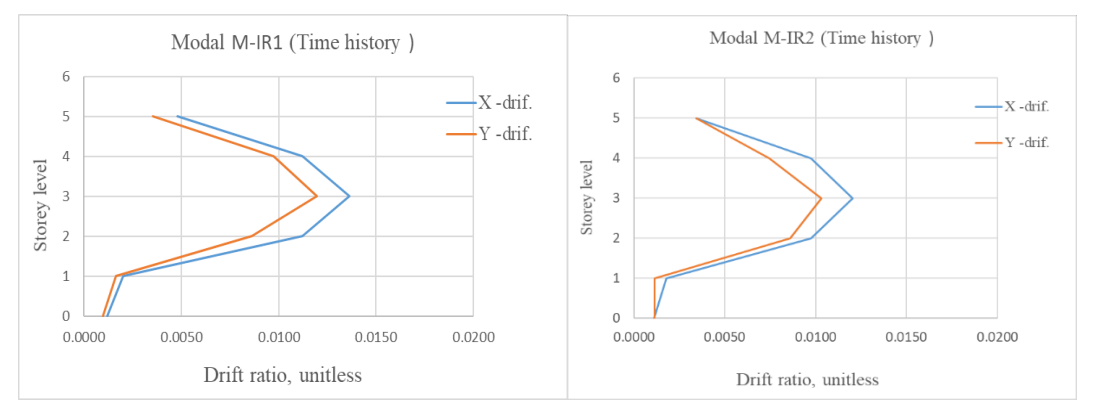


Figure 23. Inter-story drift ratios ( $IDR_{x,y}$ ) along the height of M-IR1 and M-IR2 models for NDP

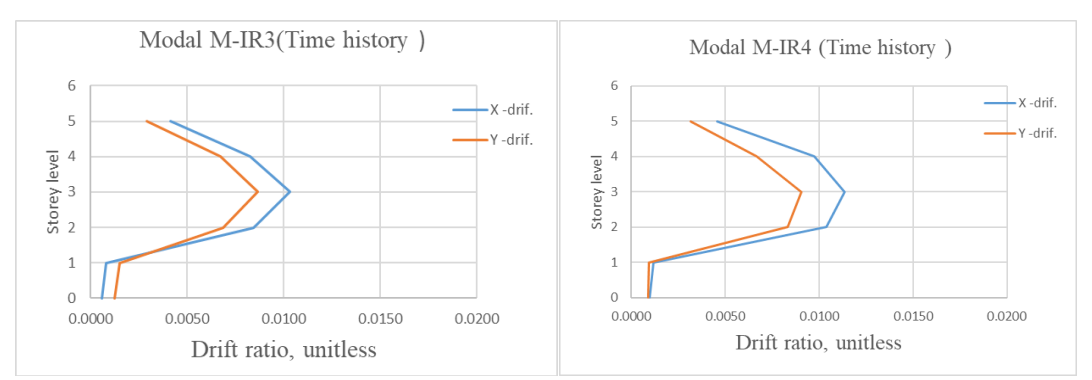


Figure 24. Inter-story drift ratios ( $IDR_{x,y}$ ) along the height of M-IR3 and M-IR4 models for NDP

From the analysis of the NDP results for the setback irregular models and by comparing them with the results of NSP, the "first-mode" load pattern distribution was chosen, being considered the worst case of the three load pattern distributions considered in NSP. First of all, it can be observed that the base shear values obtained from NDP are greater than those obtained from NSP in both main directions, for all models. The differences are of about 47 % in X-direction and 27% in Y-direction for M-IR1, about 43 % in X-direction and 29% in Y-direction for M-IR2, about 12 % in X-direction and 7% in Y-direction for M-IR3, and about 21 % in X-direction and 4% in Y-direction for M-IR2.

In addition, although the inter-story drift ratios for NSP followed the same pattern as the interstory drift ratios for NDP along the height of the models, with very close values in the first story, the differences between the two analyses occurred at the second story, where the average inter-story drift ratios  $(IDR_a)^2$  of the NDP are larger than of the NSP analysis with about 12...27% for M-IR1. This difference decreases for the models whenever model irregularity indices decrease. The differences are of about 7...19% for M-IR2, 2...9% for M-IR3, and 5...18% for M-IR4. Moreover, the inter-story drift ratios  $(IDR_{x,y})$  from the NDP and the NSP are larger than the  $(IDR_{x,y})$  values from the ELF procedure, where the seismic action is represented by the design response spectrum specific for Baghdad. Figure 26 shows, for all models, the comparison between ELF and NDP. The  $(IDR_a)$  from NDP are larger than those from ELF with about 58...111% for M-IR1; this difference decreases for models whenever the model irregularity indices decrease. The differences are of about 39...97% for M-IR2, 4...75% for M-IR3, and 20...92% for M-IR4.

This shows that the equivalent lateral force (ELF) procedure, which is adopted in ISC 2016 is not appropriate for setback structures. Also, this study shows the drawbacks of the new simplified seismic design approach proposed in [13] for structures that have a flexible upper portion over a rigid lower portion (in this study, setback frames of this type were considered) to quantify the performances of this type of configurations. It also reveals an issue in ISC 2016, which includes only two seismic analysis methods: i) Modal Response Spectrum (MRS); ii) Equivalent Lateral Force (ELF), which are the methods applied to analyze and design buildings in Iraq.

The resulting inter-story drift ratios, for all models, are shown comparatively in Figure 25, for NDP and NSP (1<sup>st</sup>-mode). In all models, there is a sudden increase in the drift values where geometry changes, i.e., at the 2<sup>nd</sup> level. The graph shows that, even though the results of the NSP analysis took into account the vertical distribution of lateral forces, this type of analysis is incapable to simulate the impacts of higher modes on the structural response, as these become more important when the structure's irregularity increases.

Although in the past Iraq was rarely exposed to seismic activity, in recent years, seismic activity has begun to increase in parts of Iraq, including the eastern region bordering Iran, which led to its effects reaching Baghdad. Consequently, there is an urgent need to adopt appropriate and more effective methods for designing and evaluating the performance of reinforced concrete buildings, because they are the most used type in Iraq.

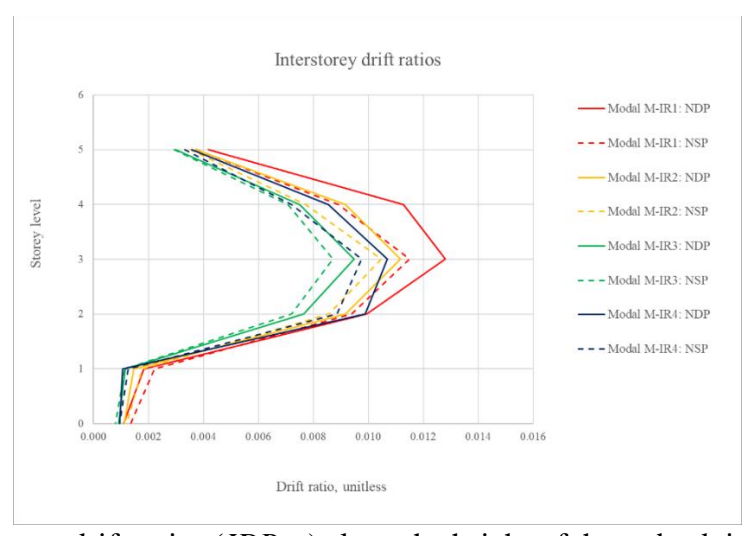


Figure 25. Inter-storey drift ratios ( $IDR_{ave}$ ) along the height of the setback irregular models for NSP and NDP

<sup>&</sup>lt;sup>2</sup> The ( $IDR_a$ ) parameter is calculated as the average value of the  $IDR_{Xx}$  and  $IDR_Y$ .

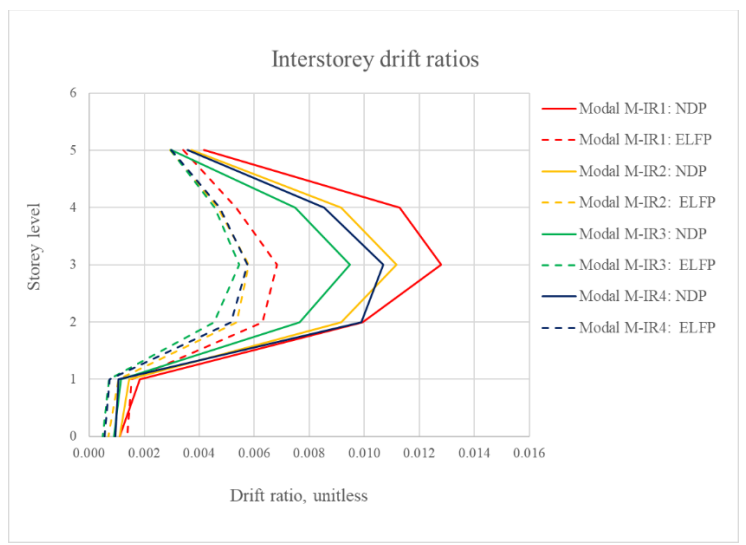


Figure 26: Inter-storey drift ratios ( $IDR_{ave}$ ) along the height of setback irregular models for ELFP and NDP

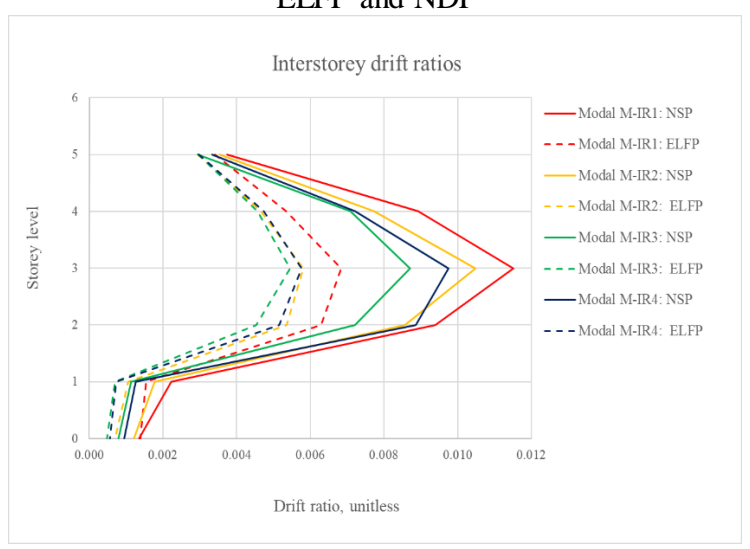


Figure 27: Inter-storey drift ratios ( $IDR_{ave}$ ) along the height of setback irregular models for ELFP and NSP

# 6 DETERMINING PERFORMANCE LEVEL AND VULNERABILITY

The vulnerability index (VI) can be used to assess the damage caused by seismic actions. It is calculated using the weighting factors of the frame elements and based on the number of plastic hinges formed. Because the essential cause for concern about the risk of irregular buildings, according to several analyses of various types of irregularities, is the increased chance of local failure, a vulnerability index can be used to determine the increase or distribution of local damage (Dya [39]).

Dya proposed a modified approach of the original vulnerability index (Lakshmanan [40]), based on an attempt to derive a local vulnerability index for each story frame. The modified formula is the following:

$$VI_{Loci} = \frac{[1.5 \sum N_j^c X_j + 1.0 \sum N_j^b X_j]i}{[\sum N_i^c + \sum N_i^b]i}$$
(44)

where  $N_j^c$  and  $N_j^b$  are the number of plastic hinges created in columns and beams respectively,  $j^{th}$  is the performance level number (j = 1...6) as shown in Table 6-1, and i is the story frame in consideration. The weighting factor  $(X_i)$  is chosen for each performance level as shown in Table 6-1. The importance factor equals 1.5 and 1.0, for the columns and the beams, respectively.

Table 6-1: Performance Level Weighting

Performance level number	Performance Level (j)	Weighting Factor $(X_i)$			
1	< B	0.000			
2	B-IO	0.125			
3	IO-LS	0.375			
4	LS-CP	0.625			
5	CP-C	0.875			
6	C-D,D-E,> E	1.000			

For each irregular model, the score modifier decreases due to the variation in the distribution of the local vulnerability index in comparison with that of the considered regular model.

The local vulnerability index for each story frame of the considered buildings is determined using Equation (44) and the distribution of the local vulnerability relative to the entire building for which the vulnerability is determined. The distribution of the local vulnerability is determined using the formula

$$VI_{Di} = \frac{VI_{Loci}}{Total \, VI_{Loc}} \quad \times 100 \tag{45}$$

where:

 $VI_{Di}$  is the local vulnerability index distribution of the story frame i  $VI_{Loci}$  is the local vulnerability factor of the frame i.

The increase in the distribution of the vulnerability index is calculated as,

$$VI_{Fi} = \frac{VI_{Di} \ of \ irregular \ bulding}{VI_{Di} \ of \ regular \ bulding} \tag{46}$$

where

 $VI_{Fi}$  is the local vulnerability index that represents the increase in  $VI_{Di}$  for frame i.

As described in Section 9 of this study, NSP was performed in two main directions ( $\pm X$  and  $\pm Y$ ) for three load distributions, for regular and setback irregular models. Conservatively, for each load distribution, the pushover curve with the lowest shear capacity (considered as the worst performance of models) was chosen to be represent the respective model capacity.

Tables 6-2, 6-3, and 6-4 show the regular model local vulnerability index for the three load distributions. The damage was distributed evenly throughout the frames of the model, except for the first frame, that had the greatest local vulnerability index due to formation of plastic hinges that developed in both the columns and the beams, not only in the beams as for the other frames. The vulnerability index of the entire regular model for the first mode distribution was the largest, followed by that for the Equivalent lateral force distribution, ELF, and by that for the uniform distribution.

Tables 6-5...6-16 show the values of the local vulnerability index of the studied models, for three load distributions,  $\phi_{avg}$  (1.212, 1.207, 1.088, 1.206) for M-IR1, M-IR2, M-IR3, M-IR4, respectively. Frames are numbered according to the story to which they belong. Taking into

account the configuration in Figure 2, story frames over the dotted line belong to the lower structure, while story frames under the dotted line belong to the upper structure. It can be noticed that the hinges occurred at the third story frame, with the largest VI value, and then at the fourth story frame, for all cases, i.e., where the setback begins and the stiffness of the model changes abruptly.

Tables 6-17 and 6-18 show the local vulnerability factors,  $VI_{Di}$ , distribution, as calculated with Eq. (45). In all cases of setback models, when the  $\phi_{avg}$  values are increasing this will result in the increase of  $VI_{Di}$  for the third and fourth frames comparative to the regular model.

This indicates that there is a vulnerability concentration around of the two first frames where the setback begins and this may be due to for different in stiffness for lower and upper structure. When the factor of local vulnerability index  $VI_{Fi}$  is calculated, this observation becomes clearer. Table 6-19 show  $VI_{Fi}$ , which is calculated through Eq. (46). In all cases of setback models, the index of local vulnerability increased for third and fourth frames comparative to the regular model when the  $\phi_{avg}$  are increasing and with keep close values of the same frame which are less than 1.00 for other levels. Consequently, it was noticed that the local vulnerability was concentrated at the bottom portion of the upper structure of the setback models.

Table 6-2: Plastic hinge count for the regular building and the first mode pattern of lateral force distribution in NSP

First mode		Bea	ams						
Regular model	B-IO	IO-LS	LS-CP	D-E	B-IO	IO-LS	LS-CP	D-E	$VI_{Loci}$
1 <sup>st</sup> Frame	49	10	0	0	4	0	0	0	0.169
2 <sup>nd</sup> Frame	54	0	0	0	0	0	0	0	0.125
3 <sup>rd</sup> Frame	52	0	0	0	0	0	0	0	0.125
4 <sup>th</sup> Frame	32	0	0	0	0	0	0	0	0.125
5 <sup>th</sup> Frame	26	0	0	0	0	0	0	0	0.125
6 <sup>th</sup> Frame	0	0	0	0	0	0	0	0	0.000
								Total	0.669

Table 6-3: Plastic hinge count for the regular building and the Equivalent Lateral Force (ELF) distribution in NSP

ELF		Bea	ams						
Regular model	B-IO	IO-LS	LS-CP	D-E	B-IO	IO-LS	LS-CP	D-E	$VI_{Loci}$
1 <sup>st</sup> Frame	45	4	0	0	4	0	0	0	0.149
2 <sup>nd</sup> Frame	54	0	0	0	0	0	0	0	0.125
3 <sup>rd</sup> Frame	50	0	0	0	0	0	0	0	0.125
4 <sup>th</sup> Frame	48	0	0	0	0	0	0	0	0.125
5 <sup>th</sup> Frame	27	0	0	0	0	0	0	0	0.125
6 <sup>th</sup> Frame	0	0	0	0	0	0	0	0	0.000
								Total	0.649

Table 6-4. Plastic hinge count for the regular building and the uniform pattern of lateral force distribution in NSP

Uniform		Bea	ams		Columns				
Regular model	B-IO	IO-LS	LS-CP	D-E	B-IO	IO-LS	LS-CP	D-E	$VI_{Loci}$
1 <sup>st</sup> Frame	51	4	0	0	0	0	0	0	0.143
2 <sup>nd</sup> Frame	52	0	0	0	0	0	0	0	0.125
3 <sup>rd</sup> Frame	44	0	0	0	0	0	0	0	0.125
4 <sup>th</sup> Frame	29	0	0	0	0	0	0	0	0.125
5 <sup>th</sup> Frame	6	0	0	0	0	0	0	0	0.125
6 <sup>th</sup> Frame	0	0	0	0	0	0	0	0	0.000
								Total	0.643

Table 6-5: Plastic hinge count for M-IR1. First mode pattern of lateral force distribution in NSP

First mode		Bea	ams						
M-IR1	B-IO	IO-LS	LS-CP	D-E	B-IO	IO-LS	LS-CP	D-E	$VI_{Loci}$
1 <sup>st</sup> Frame	3	0	0	0	0	0	0	0	0.125
2 <sup>nd</sup> Frame	16	0	0	0	0	0	0	0	0.125
3 <sup>rd</sup> Frame	14	17	0	0	17	0	0	0	0.236
4 <sup>th</sup> Frame	20	10	0	0	0	0	0	0	0.208
5 <sup>th</sup> Frame	15	0	0	0	0	0	0	0	0.125
6 <sup>th</sup> Frame	0	0	0	0	0	0	0	0	0.000

Table 6-6. Plastic hinge count of M-IR1 for Equivalent Lateral Force (ELF) distribution of NSP

ELF		Bea	ams		Columns				
M-IR1	B-IO	IO-LS	LS-CP	D-E	B-IO	IO-LS	LS-CP	D-E	$VI_{Loci}$
1 <sup>st</sup> Frame	3	0	0	0	0	0	0	0	0.125
2 <sup>nd</sup> Frame	18	0	0	0	0	0	0	0	0.125
3 <sup>rd</sup> Frame	15	11	0	0	16	0	0	0	0.214
4 <sup>th</sup> Frame	26	3	0	0	0	0	0	0	0.151
5 <sup>th</sup> Frame	15	0	0	0	0	0	0	0	0.125
6 <sup>th</sup> Frame	0	0	0	0	0	0	0	0	0.000

Table 6-7. Plastic hinge count of M-IR1 for uniform pattern of lateral force distribution

Uniform		Bea	ams						
M-IR1	B-IO	IO-LS	LS-CP	D-E	B-IO	IO-LS	LS-CP	D-E	$VI_{Loci}$
1 <sup>st</sup> Frame	28	0	0	0	0	0	0	0	0.125
2 <sup>nd</sup> Frame	19	0	0	0	0	0	0	0	0.125
3 <sup>rd</sup> Frame	18	5	0	0	14	0	0	0	0.182
4 <sup>th</sup> Frame	25	2	0	0	0	0	0	0	0.144
5 <sup>th</sup> Frame	15	0	0	0	0	0	0	0	0.125
6 <sup>th</sup> Frame	0	0	0	0	0	0	0	0	0.000

Table 6-8. Plastic hinge count of M-IR2 for first mode pattern of lateral force distribution of NSP

First mode		Bea	ams						
M-IR2	B-IO	IO-LS	LS-CP	D-E	B-IO	IO-LS	LS-CP	D-E	$VI_{Loci}$
1 <sup>st</sup> Frame	3	0	0	0	0	0	0	0	0.125
2 <sup>nd</sup> Frame	8	0	0	0	0	0	0	0	0.125
3 <sup>rd</sup> Frame	20	18	0	0	16	0	0	0	0.227
4 <sup>th</sup> Frame	21	10	0	0	0	0	0	0	0.206
5 <sup>th</sup> Frame	22	0	0	0	0	0	0	0	0.125
6 <sup>th</sup> Frame	0	0	0	0	0	0	0	0	0.000

Table 6-9. Plastic hinge count of M-IR2 for Equivalent lateral force (ELF) distribution of NSP

ELE		Bea	ams		Columns				
M-IR2	B-IO	IO-LS	LS-CP	D-E	B-IO	IO-LS	LS-CP	D-E	$VI_{Loci}$
1 <sup>st</sup> Frame	3	0	0	0	0	0	0	0	0.125
2 <sup>nd</sup> Frame	4	0	0	0	0	0	0	0	0.125
3 <sup>rd</sup> Frame	17	10	0	0	16	0	0	0	0.206
4 <sup>th</sup> Frame	32	3	0	0	0	0	0	0	0.146
5 <sup>th</sup> Frame	16	0	0	0	0	0	0	0	0.125
6 <sup>th</sup> Frame	0	0	0	0	0	0	0	0	0.000

Table 6-10. Plastic hinge count of M-IR2 for uniform pattern of lateral force distribution

Uniform		Bea	ams		Columns				
M-IR2	B-IO	IO-LS	LS-CP	D-E	B-IO	IO-LS	LS-CP	D-E	$VI_{Loci}$
1 <sup>st</sup> Frame	2	0	0	0	0	0	0	0	0.125
2 <sup>nd</sup> Frame	15	0	0	0	0	0	0	0	0.125
3 <sup>rd</sup> Frame	24	6	0	0	0	0	0	0	0.175
4 <sup>th</sup> Frame	28	2	0	0	0	0	0	0	0.142
5 <sup>th</sup> Frame	15	0	0	0	0	0	0	0	0.125
6 <sup>th</sup> Frame	0	0	0	0	0	0	0	0	0.000

Table 6-11. Plastic hinge count of M-IR3 for first mode pattern of lateral force distribution of NSP

First mode		Bea	ams		Columns				
M-IR3	B-IO	IO-LS	LS-CP	D-E	B-IO	IO-LS	LS-CP	D-E	VI <sub>Loci</sub>
1 <sup>st</sup> Frame	2	0	0	0	0	0	0	0	0.125
2 <sup>nd</sup> Frame	12	0	0	0	0	0	0	0	0.125
3 <sup>rd</sup> Frame	11	6	0	0	0	0	0	0	0.213
4 <sup>th</sup> Frame	14	5	0	0	0	0	0	0	0.191
5 <sup>th</sup> Frame	13	0	0	0	0	0	0	0	0.125
6 <sup>th</sup> Frame	0	0	0	0	0	0	0	0	0.000

Table 6-12. Plastic hinge count of M-IR3 for Equivalent lateral force (ELF) distribution of NSP

ELE		Bea	ams		Columns				
M-IR3	B-IO	IO-LS	LS-CP	D-E	B-IO	IO-LS	LS-CP	D-E	$VI_{Loci}$
4	4	0	0	0	0	0	0	0	0.125
2 <sup>nd</sup> Frame	25	0	0	0	0	0	0	0	0.125
3 <sup>rd</sup> Frame	12	4	0	0	0	0	0	0	0.188
4 <sup>th</sup> Frame	40	1	0	0	0	0	0	0	0.131
5 <sup>th</sup> Frame	29	0	0	0	0	0	0	0	0.125
6 <sup>th</sup> Frame	0	0	0	0	0	0	0	0	0.000

Table 6-13. Plastic hinge count of M-IR3 for uniform pattern of lateral force distribution

Uniform		Beams				Colı	umns		
M-IR3	B-IO	IO-LS	LS-CP	D-E	B-IO	IO-LS	LS-CP	D-E	$VI_{Loci}$
1 <sup>st</sup> Frame	3	0	0	0	0	0	0	0	0.125
2 <sup>nd</sup> Frame	27	0	0	0	0	0	0	0	0.125
3 <sup>rd</sup> Frame	21	3	0	0	0	0	0	0	0.156
4 <sup>th</sup> Frame	19	0	0	0	0	0	0	0	0.125
5 <sup>th</sup> Frame	30	0	0	0	0	0	0	0	0.125
6 <sup>th</sup> Frame	0	0	0	0	0	0	0	0	0.000

Table 6-14. Plastic hinge count of M-IR4 for first mode pattern of lateral force distribution of NSP

First mode		Beams				Colı	umns		
M-IR4	B-IO	IO-LS	LS-CP	D-E	B-IO	IO-LS	LS-CP	D-E	$VI_{Loci}$
1 <sup>st</sup> Frame	12	0	0	0	0	0	0	0	0.125
2 <sup>nd</sup> Frame	41	0	0	0	0	0	0	0	0.125
3 <sup>rd</sup> Frame	22	14	0	0	7	0	0	0	0.217
4 <sup>th</sup> Frame	35	15	0	0	0	0	0	0	0.200
5 <sup>th</sup> Frame	32	0	0	0	0	0	0	0	0.125
6 <sup>th</sup> Frame	0	0	0	0	0	0	0	0	0.000

Table 6-15. Plastic hinge count of M-IR4 for Equivalent lateral force (ELF) distribution of NSP

ELE		Bea	ams			Colı	umns		
M-IR4	B-IO	IO-LS	LS-CP	D-E	B-IO	IO-LS	LS-CP	D-E	$VI_{Loci}$
1 <sup>st</sup> Frame	8	0	0	0	0	0	0	0	0.125
2 <sup>nd</sup> Frame	32	0	0	0	0	0	0	0	0.125
3 <sup>rd</sup> Frame	22	8	0	0	0	0	0	0	0.192
4 <sup>th</sup> Frame	25	1	0	0	0	0	0	0	0.135
5 <sup>th</sup> Frame	29	0	0	0	0	0	0	0	0.125
6 <sup>th</sup> Frame	0	0	0	0	0	0	0	0	0.000

Table 6-16. Plastic hinge count of M-IR4 for uniform pattern of lateral force distribution

Uniform		Bea	ams			Colı	ımns		
M-IR4	B-IO	IO-LS	LS-CP	D-E	B-IO	IO-LS	LS-CP	D-E	$VI_{Loci}$
1st Frame	8	0	0	0	0	0	0	0	0.125
2 <sup>nd</sup> Frame	24	0	0	0	0	0	0	0	0.125
3 <sup>rd</sup> Frame	29	4	0	0	4	0	0	0	0.159
4 <sup>th</sup> Frame	24	0	0	0	0	0	0	0	0.125
5 <sup>th</sup> Frame	16	0	0	0	0	0	0	0	0.125
6 <sup>th</sup> Frame	0	0	0	0	0	0	0	0	0.000

Table 6-17. Local vulnerability factors for all models

	Table 0-17. Local vulnerability factors for all models														
	Local Vulnerability factor $VI_{Loci}$														
	First mode						ELF				Uniform				
Models	Reg.	M- IR1	M- IR2	M- IR3	M- IR4	Reg.	M- IR1	M- IR2	M- IR3	M- IR4	Reg.	M- IR1	M- IR2	M- IR3	M- IR4
1 <sup>st</sup> Frame	0.169	0.125	0.125	0.125	0.125	0.149	0.125	0.125	0.125	0.125	0.143	0.125	0.125	0.125	0.125
$2^{nd}$ Frame	0.125	0.125	0.125	0.125	0.125	0.125	0.125	0.125	0.125	0.125	0.125	0.125	0.125	0.125	0.125
3 <sup>rd</sup> Frame	0.125	0.236	0.227	0.203	0.217	0.125	0.214	0.206	0.188	0.192	0.125	0.182	0.175	0.156	0.159
4 <sup>th</sup> Frame	0.125	0.208	0.206	0.178	0.200	0.125	0.151	0.146	0.131	0.135	0.125	0.144	0.142	0.125	0.125
5 <sup>th</sup> Frame	0.125	0.125	0.125	0.125	0.125	0.125	0.125	0.125	0.125	0.125	0.125	0.125	0.125	0.125	0.125
6 <sup>th</sup> Frame	0.000	0.000	0.000	0.000	0.000	0.000	0.000	0.000	0.000	0.000	0.000	0.000	0.000	0.000	0.000
Total	0.669	0.819	0.807	0.788	0.792	0.649	0.740	0.728	0.708	0.713	0.643	0.700	0.692	0.656	0.656

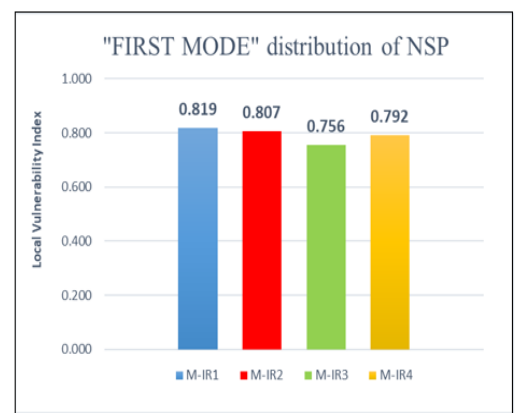
Table 6-18. Local vulnerability distribution for all models

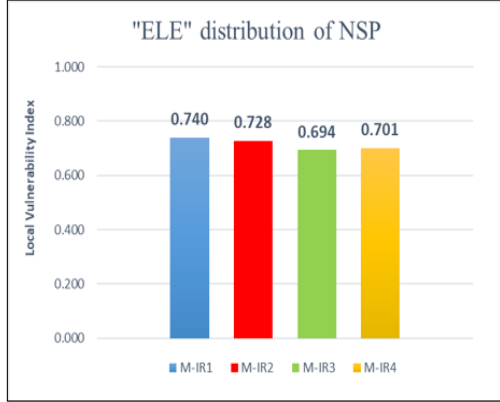
	Local Vulnerability distribution $VI_{Di}$ [%]														
		Fi	rst mod	de			ELF				Uniform				
Models	Reg.	M- IR1	M- IR2	M- IR3	M- IR4	Reg.	M- IR1	M- IR2	M- IR3	M- IR4	Reg.	M- IR1	M- IR2	M- IR3	M- IR4
1st Frame	25.22	15.26	15.48	16.54	15.79	22.91	16.89	17.17	18.02	17.82	22.26	17.83	18.07	19.05	18.97
2 <sup>nd</sup> Frame	18.69	15.26	15.48	16.54	15.79	19.27	16.89	17.17	18.02	17.82	19.43	17.83	18.07	19.05	18.97
3 <sup>rd</sup> Frame	18.69	28.78	28.09	26.88	27.36	19.27	28.95	28.36	27.03	27.33	19.43	26.03	25.30	23.81	24.10
4 <sup>th</sup> Frame	18.69	25.44	25.47	23.28	25.27	19.27	20.38	20.12	18.90	19.20	19.43	20.47	20.47	19.05	18.97
5 <sup>th</sup> Frame	18.69	15.26	15.48	16.54	15.79	19.27	16.89	17.17	18.02	17.82	19.43	17.83	18.07	19.05	18.97
6 <sup>th</sup> Frame	0.00	0.00	0.00	0.00	0.00	0.00	0.00	0.00	0.00	0.00	0.00	0.00	0.00	0.00	0.00

Table 6-19. Local vulnerability index for all models (vulnerability increase as compared with the regular model)

				V		lity ind						
		First mode				E	LF		Uniform			
Models	M-IR1	M-IR2	M-IR3	M-IR4	M-IR1	M-IR2	M-IR3	M-IR4	M-IR1	M-IR2	M-IR3	M-IR4
1 <sup>st</sup> Frame	0.61	0.61	0.66	0.63	0.78	0.75	0.78	0.78	0.80	0.81	0.86	0.85
2 <sup>nd</sup> Frame	0.82	0.83	0.88	0.84	0.92	0.89	0.93	0.92	0.92	0.93	0.98	0.98
3 <sup>rd</sup> Frame	1.54	1.50	1.44	1.46	1.50	1.47	1.39	1.42	1.34	1.30	1.23	1.24
4 <sup>th</sup> Frame	1.36	1.36	1.26	1.35	1.06	1.04	1.00	1.02	1.05	1.05	0.98	0.98
5 <sup>th</sup> Frame	0.82	0.83	0.88	0.84	0.88	0.89	0.92	0.91	0.92	0.93	0.98	0.98
6 <sup>th</sup> Frame	0.00	0.00	0.00	0.00	0.00	0.00	0.00	0.00	0.00	0.00	0.00	0.00

A comparison of the results obtained for all setback models is shown in Table 6-19. The results show that almost all plastic hinges have developed at the 3<sup>rd</sup> and 4<sup>th</sup> stories, which are the base of the upper structure, where there are reductions in stiffness and changes of vertical geometry. It can be noticed that the values of the vulnerability index are larger than unity for the 3<sup>rd</sup> and 4th levels, while the factor is smaller than one at the rest of the levels. In addition, the vulnerability index increased at the 3<sup>rd</sup> and 4<sup>th</sup> levels as the irregularity indices of the models increased under a particular load distribution. The values of the vulnerability index for the "First mode" distribution are larger than those obtained for both the other two distributions (ELF and Uniform), for the same model, at the 3<sup>rd</sup> and 4<sup>th</sup> levels. The analysis of the setback structures results shows that the main reason for setback buildings being more sensitive to seismic action is earthquake forces localization. Despite the fact that the total demand on the structure is lower due to the lower overall mass, disparate demands on various parts of the structure result in a local risk. The severity or degree of structure setback also influences the increase of the risk, thus the setback ratios are studied to take into account its severity. The forces are concentrated on the section of the structure where the abrupt stiffness decrease occurs, i.e., at the bottom of the upper structure. This can be noticed from of the development of the plastic hinges and from the story drift at this location. Consequently, the abrupt changes in the stiffness or in the vertical configurations of the structures are considered local vulnerability locations. The summary of comparison results is also shown in Figure 28.





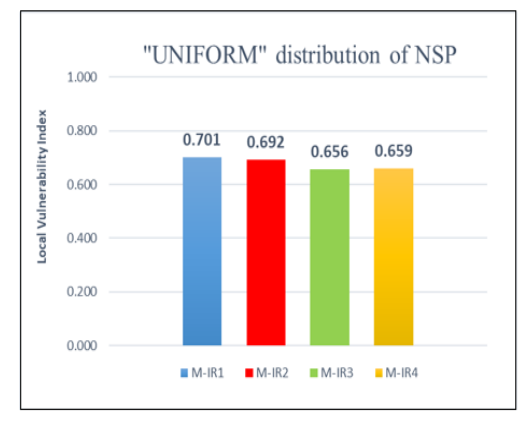


Figure 28: Total values (sum for all stories) of each model of the local vulnerability factor  $VI_{Loci}$ 

# 7 DEVELOPMENT OF FRAGILITY CURVES

The relations seismic action-damage, expressed in the form of fragility curves, are essential for earthquake risk assessments and simulations of earthquake scenarios.

According to HAZUS-MH-MR1, "building fragility curves are lognormal functions that describe the probability of reaching, or exceeding, structural and nonstructural damage states, given median estimates of spectral response, for example spectral displacement. These curves take into account the variability and uncertainty associated with capacity curve properties, damage states and ground shaking. The fragility curves distribute damage among Slight, Moderate, Extensive and Complete damage states."

Seismic motion effects can be expressed in the form of fragility curves, to evaluate the vulnerability of setback irregular structures depending on their probability of damage. The fragility curves of the models under consideration in this study represent the probability of exceedance of a specific damage state  $P(d \ge ds)$ , versus the spectral displacement  $S_d$ , considered as a function to quantify the intensity of the seismic action, as shown in Figure 29. The mean displacement  $S_{ds}$  and the standard deviation  $\beta d_s$  characterize the fragility curves. So, for a specific state of damage  $d_{si}$ , the fragility curves are described by the lognormal functions shown in formula (47) [41, 42]:

$$P [d_s \mid Sd] = \phi \left( \frac{1}{gd_s} \ln \left( \frac{Sd}{\overline{Sd}_{ds}} \right) \right)$$
where:

 $\overline{S}d_{ds}$  - is the median value of spectral displacement at which the building reaches the threshold of the damage state, ds,

 $\beta d_s$ - is the standard deviation of the natural logarithm of spectral displacement of damage state, ds, an

 $\phi$  -the standard normal cumulative distribution function.

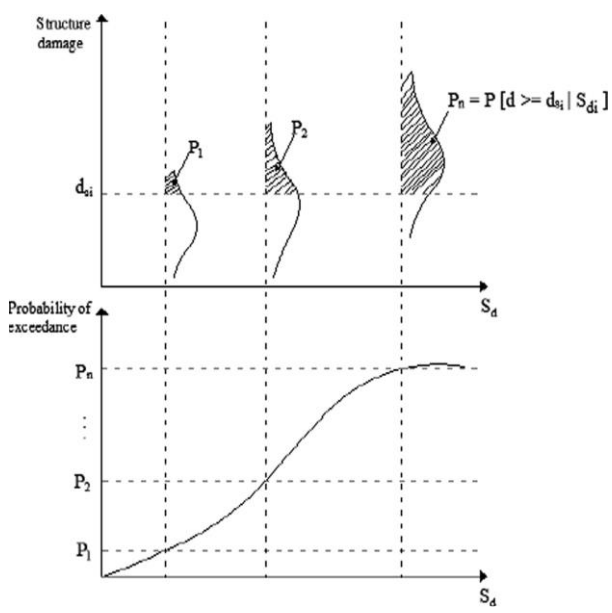


Figure 29. Concept of fragility curve (Park et al. 2009) [44]

The thresholds  $Sd_{dsi}$  represent the yield and the ultimate spectral displacement of the models which are obtained from the bilinear representation of the capacity spectra, as illustrated by the following formulas, which were adopted to calculate the damage state thresholds according to [43]. Table 1-36 shows the results of the yield and ultimate spectral displacement.

Slight 
$$Sd_{dsl} = 0.70 \text{ x D}_y$$
  
Moderate  $Sd_{ds2} = D_y$   
Severe  $Sd_{ds3} = D_y + 0.75(D_u - D_y)$   
Complete  $Sd_{ds4} = D_u$  (48)

where:

D<sub>y</sub>: yield spectral displacement, D<sub>u</sub>: ultimate spectral displacement.

To assess the variability of fragility curves for the above damage states, the values of the standard deviation ( $\Re d_{si}$ ) were established from values provided in HAZUS-MH-MR1, Tables 6.6, for mid-rise buildings. The following assumptions were made to achieve this aim:

- 1) the models under consideration display moderate capacity curves variability, that is  $\beta c = 0.3$ ;
- 2) for slight damage, the damage variability is small (0.2),  $\beta_{T,ds} = 0.65$ ;
- 3) for moderate damage, the damage variability is moderate (0.4),  $\beta_{T,ds} = 0.75$ ;
- 4) for severe and complete damage, the damage variability is large (0.6),  $\beta_{T,ds} = 0.9$  (interpolation value between 0.85 and 0.95 for  $\kappa$ =0.7);

5) the degradation factor of post-yield model response ( $\kappa$ ) is determined in accordance to Table 5.2 [41] as follows:

At  $\frac{1}{2}$  yield = 1.0, at yield = 1.0, and for post-yield shaking duration (moderate) = 0.7.

These values were considered based on the assumptions that the models were designed according to high-code (HC) for seismic design level, and ordinary (O) for construction quality.

6) Consequently, the lognormal standard deviation (β ds) values were computed from formula (49), because the response spectrum is known accurately.

$$\beta_{ds} = \sqrt{(\beta_c)^2 + (\beta_{T,ds})^2}$$
(49)

where:

 $\beta$  ds is the lognormal standard deviation that represents the total variability of damage state, ds,

 $\beta_c$  is the lognormal standard deviation that represents the variability of the capacity curve,

 $\beta_{T,ds}$  is the lognormal standard deviation that represents the variability of the threshold of damage state, ds.

The descriptions for Slight, Moderate, Extensive, and Complete structural damage states for reinforced concrete moment resisting frames are shown in Table 12-1 as definition in HAZUS MR4.

Table 7-1. Descriptions of structural damage according to in HAZUS MR4 [42]

Damage State	Description
Slight	Flexural or shear type hairline cracks in some beams and columns near joints or within joints
Moderate	Most beams and columns exhibit hairline cracks. In ductile frames, some of the frame elements have reached yield capacity indicated by larger flexural cracks and some concrete spalling. Non-ductile frames may exhibit larger shear cracks and spalling.
Extensive	Some of the frame elements have reached their ultimate capacity indicated in ductile frames by large flexural cracks, spalled concrete and buckled main reinforcement; non-ductile frame elements may have suffered shear failures or bond failures at reinforcement splices, or broken ties or buckled main reinforcement in columns, which may result in partial collapse.
Complete	Structure is collapsed or in imminent danger of collapse due to brittle failure of non-ductile frame elements or loss of frame stability. Approximately 13%(low-rise), 10% (mid-rise) or 5% (high-rise) of the total area of buildings with Complete damage is expected to be collapsed

As mentioned previously, the NSP analysis was performed in both main directions (X and Y) for all models. In addition, the third load distribution (1<sup>st</sup> mode) was considered. Conservatively,

the base shear - top displacement capacity curve in X-direction was considered, this having the smallest shear capacity of the two main directions.

The pushover curves of the considered models, are converted automatically by SAP2000 into spectral acceleration-spectral displacement format. An idealized bilinear capacity curve was considered. The yield and ultimate spectral accelerations ( $A_y$  and  $A_u$ ) and the spectral displacements ( $D_y$  and  $D_u$ ) of the spectral bilinear capacity curve are shown in Table 12-2. The thresholds of damage states are illustrated in Table 12-3.

It is worth noting from Table 12-2 that the increase of irregularity indices due to the setback has a significant impact on the ultimate capacities of the models. A significant decrease is observed for model M-IR1 (about 15.69%, 61.73%, and 27.45%), as compared with M-IR2, M-IR3 and M-IR4, respectively. Figures 30 and 31 display the A-D spectrum bilinear capacity. Moreover, they illustrate the effect of setback level on the performance of structures with vertical configuration irregularities. It can be noticed also the decrease of the yielding displacement values as the setback level increases; as mentioned previously, the structure capacity is affected by the increase of setback levels.

Table 7-2. Characteristic accelerations and displacements

Building model	Yield	capacity	Ultimate	capacity
Dunding model	D <sub>y</sub> (mm)	A <sub>y</sub> (g)	D <sub>u</sub> (mm)	A <sub>u</sub> (g)
M-IR1, "First mode"- x	50.69	0.36	140.67	0.51
M-IR2, "First mode"- x	51.38	0.36	151.05	0.59
M-IR3, "First mode"- x	61.56	0.57	227.52	0.74
M-IR4, "First mode"- x	59.81	0.49	164.8	0.65

Table 7-3. Damage state thresholds and beta values

Building model	Dama	ge state t	hresholds	(mm)	Standard deviation				
Duriding moder	$S\overline{d}_{ds_1}$	$S\overline{d}_{ds2}$	$S\overline{d}_{ds3}$	$S\overline{d}_{ds4}$	$\beta_{ds_1}$	$\beta_{ds_1}$	ß ds1	ß ds1	
M-IR1, "First mode"- x	35.50	50.69	73.20	140.67	0.72	0.81	0.95	0.95	
M-IR2, "First mode"- x	35.97	51.38	76.30	151.05	0.72	0.81	0.95	0.95	
M-IR3, "First mode"- x	43.10	61.56	103.10	227.52	0.72	0.81	0.95	0.95	
M-IR4, "First mode"- x	41.90	59.81	86.10	164.80	0.72	0.81	0.95	0.95	

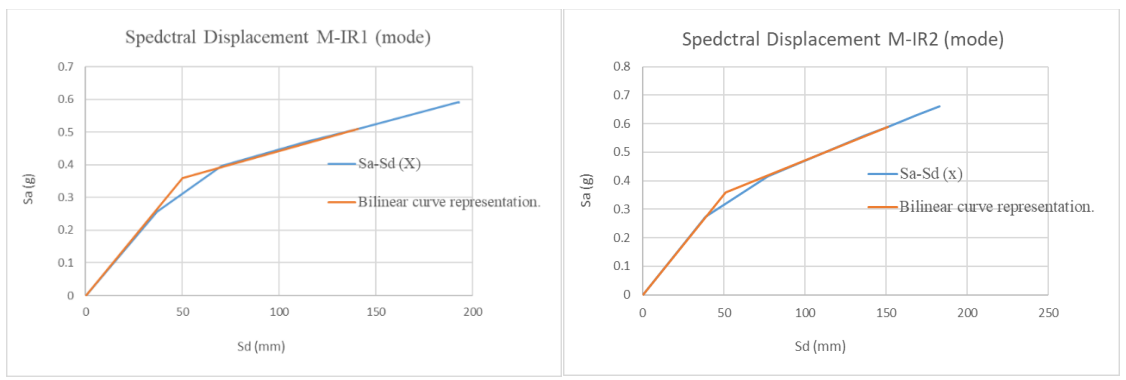


Figure 30. Capacity spectra of M-IR1 and M-IR2 with their bilinear representation

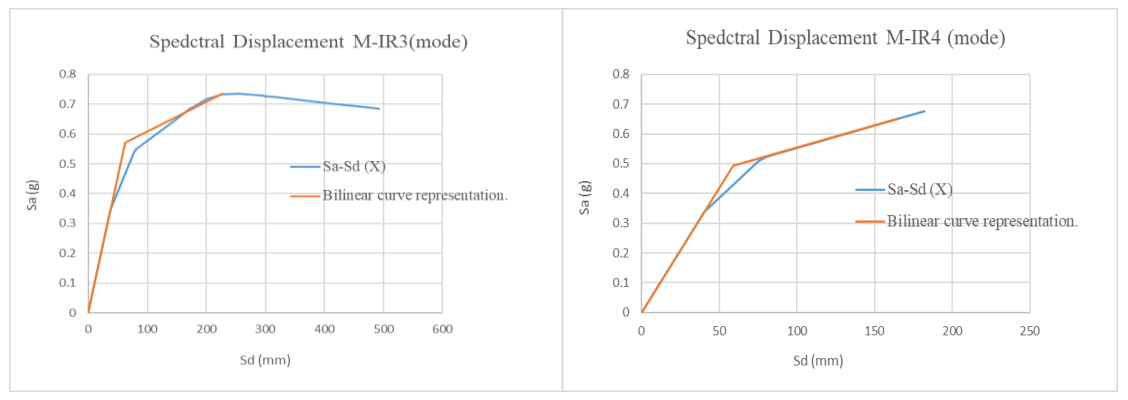


Figure 31. Capacity spectra of M-IR3 and M-IR4 with their bilinear representation

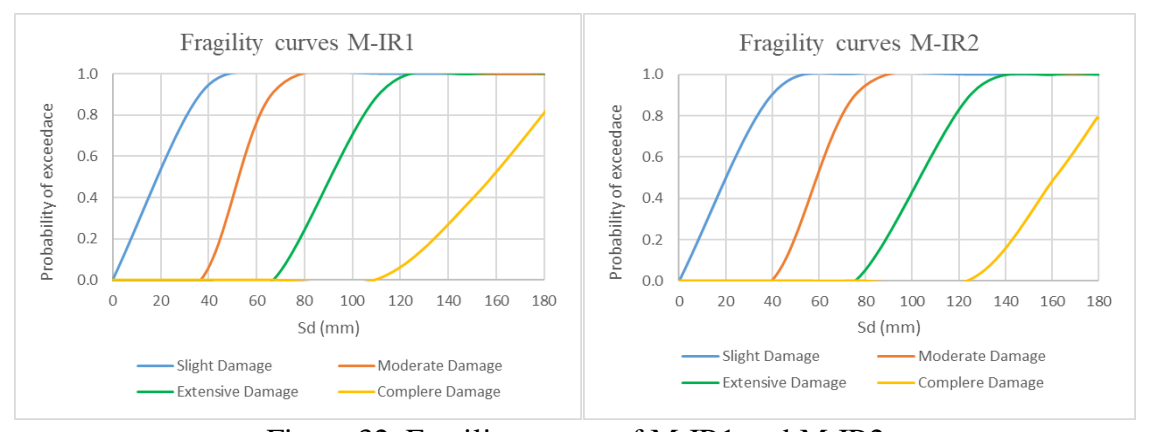


Figure 32. Fragility curves of M-IR1 and M-IR2

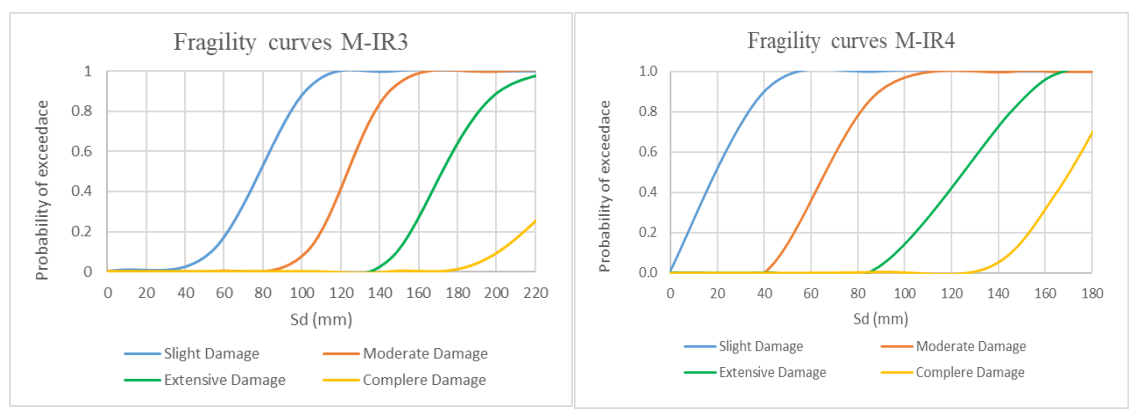


Figure 33. Fragility curves of M-IR3 and M-IR4

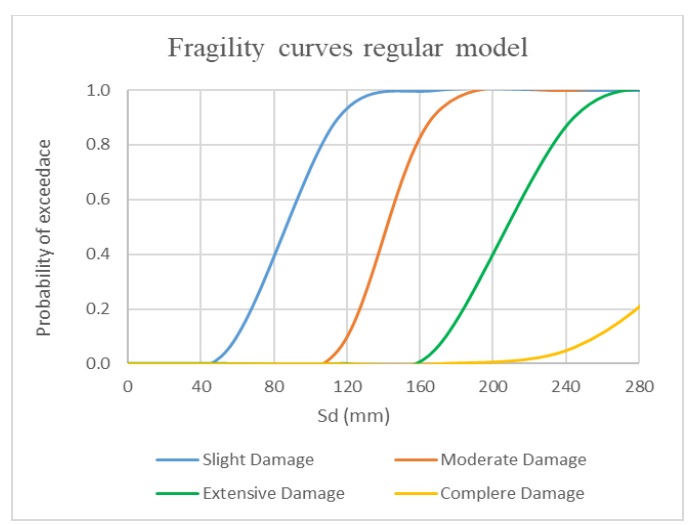


Figure 34. Fragility curves of regular model

The fragility curves of the setback irregular models under consideration and regular model are shown in Figures 32 ... 34. These curves were developed to investigate of the impact of vertical irregularity location (setback) on the vulnerability of frame models. The displacement corresponding to the Slight, Moderate and Extensive states for 50% and 90% probability and to the Complete damage for 20% and 70% probability are shown in Table below:

Table 7-4. Displacement (mm) corresponding of damage state for all models

Building		oility of t state	-	bility of ate state	-	oility of ve state	probability of complete state	
model	At 50%	At 90%	At 50%	At 90%	At 50%	At 90%	At 20%	At 70%
Regular	85	115	140	168	175	244	280	-
M-IR1	20	36	53	67	90	112	135	170
M-IR2	20	40	60	76	103	126	143	175
M-IR3	80	102	123	146	175	203	215	-
M-IR4	20	50	69	89	120	152	170	180

From the comparison of the results for the regular model with the results of the setback models, it is noticeable based on definition in [42] as illustrated in Table 12-1, that the spectral displacement corresponding to the slight damage state for 50% probability increases by 76.47% compared with the M-IR1, M-IR2 and M-IR4 models, respectively, while increases by 5.88% compared with the M-IR3 model. The spectral displacement corresponding to the slight damage state for 90% probability increases by 86.70%, 65.22%, 11.30% and 56.52%, compared with the M-IR1, M-IR2, M-IR3 and M-IR4 models, respectively.

The influence of the setback level on seismic vulnerability is obvious for the moderate damage state where the spectral displacement state for 50% probability increases by 62.14%, 57.14%, 12.14% and 50.71% compared with the M-IR1, M-IR2, M-IR3 and M-IR4 models, respectively. The spectral displacement corresponding to the moderate damage for 90% probability increases by 60.12%, 54.76%, 13.10% and 47.02% compared with the M-IR1, M-IR2, M-IR3 and M-IR4 models, respectively.

In the same way, for the extensive damage state, the spectral displacement corresponding increases by 48.57 % at a probability of 50%, as compared with the M-IR1 model, by 41.14%, 0.0% and 31.43% as compared with the M-IR2, M-IR43 and M-IR4 models, respectively. For a probability of 90%, the spectral displacements probability increases by 54.10%, 48.36%, 16.80% and 37.70% compared with the M-IR1, M-IR2, M-IR3 and M-IR4 models, respectively.

In the same way, for complete damage, the spectral displacement corresponding to this damage state increases by 51.79%, 48.93%, 23.21%, 39.29%, as compared with the M-IR1, M-IR2, M-IR3 and M-IR4 models, respectively, at a probability of 20%.

For the target displacement as shown in Figures 35 and 36, the probability in a moderate damage state are about 40%, 55%, 80%, 60% for M-IR1, M-IR2, M-IR3 and M-IR4 models, respectively, while the probability in an extensive damage state are about 60%, 45%, 20%, 40% for M-IR1, M-IR2, M-IR3 and M-IR4 models, respectively. The probability is 0.0 for the slight damage and complete damage.

It can be noted from the results that, when the irregularity setback level increases, the damage hazard increases, and the models exhibit poorer seismic performance. In addition, it was noticed that at the target displacement the impact of the setback level on seismic vulnerability is higher in the states of moderate damage and extensive damage.

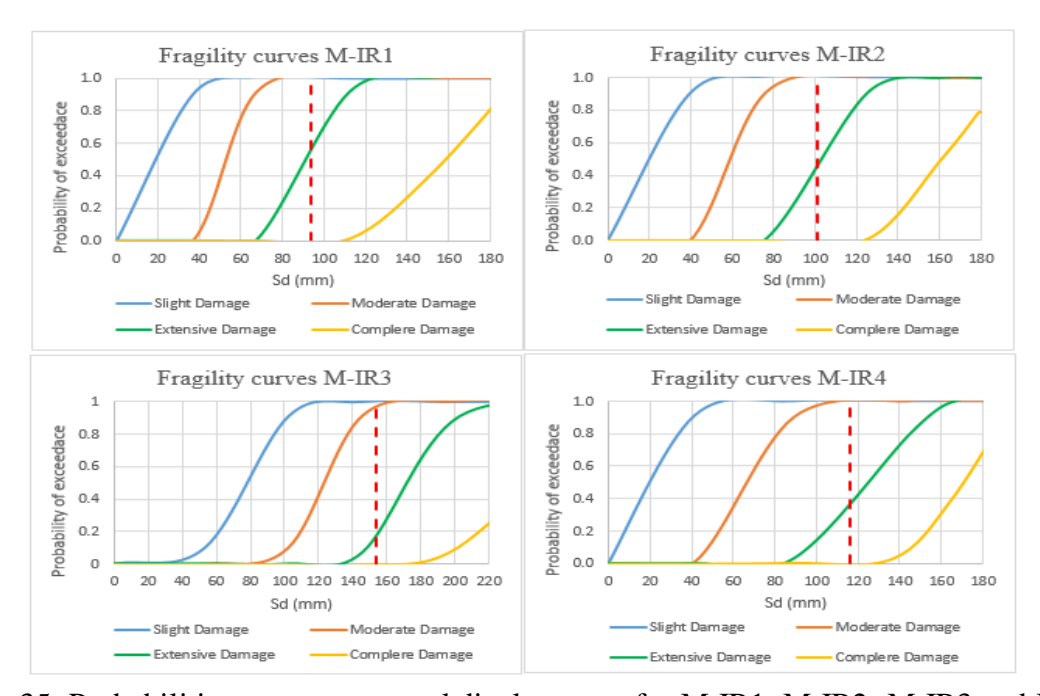
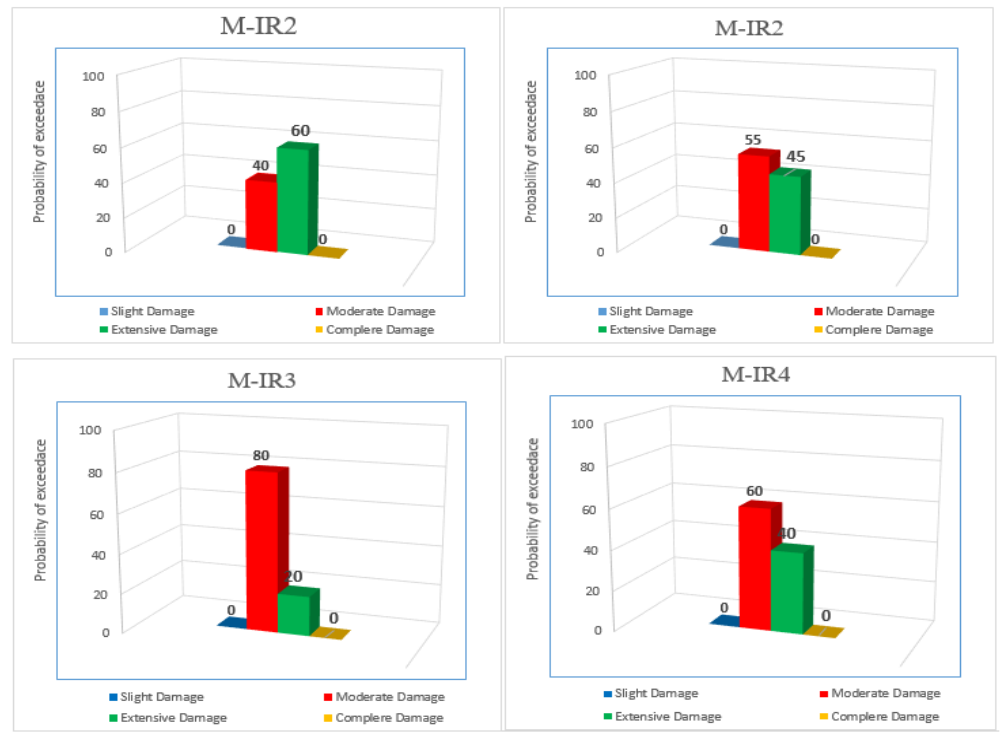


Figure 35: Probabilities at target spectral displacement for M-IR1, M-IR2, M-IR3 and M-IR4



The probabilities of the considered damage states for the target displacements

Figure 36: Summary of the probabilities of the considered damage states for the target displacements. Models M-IR1, M-IR2, M-IR3 and M-IR4

#### 8 PERFORMANCE OF THE STRUCTURAL MEMBERS

Figures 7 and 8 summarize the shear capacity ratio for columns, which represents the ratio of the shear demand on the column V, to the shear strength  $V_n$ . In all cases, the shear demand V is the maximum shear force occurring in columns of the story levels during the nonlinear static and nonlinear dynamic analysis. The shear strength  $V_n$  is calculated from the following equation according to ACI 318-14, Section 22.5.1.1, and equation (22.5.1.1):

$$V_n = V_c + V_s \tag{50}$$

where:

 $V_n$  = nominal shear strength

 $V_c$  = nominal shear strength provided by concrete, from table 22.5.5.1, =  $\left[2\lambda\sqrt{fc^*} + \frac{Nu}{6Aq}\right]b_w d$ 

 $Vs = \text{nominal shear strength provided by the shear reinforcement} = \frac{Av.fy.d}{S}$ 

d: is the effective depth of the column (d = 0.8h was assumed);

 $b_w$ ; is the width of the column;

 $A_g$ : is the gross cross-sectional area of the column;

 $N_u$ : is the axial compression force (set to zero for tension force);

 $f_{y}$ : is the yield strength;

 $f_c$ :is the compressive strength of concrete;

 $A_{v}$ : is the area of transverse reinforcement within spacing s;

 $\lambda$  = modification factor, 1.0 for normal weight aggregate concrete;

From the results values plotted in Figure 36, it can be noticed that the shear ratios for NDP analysis are larger than the corresponding ones for NSP analysis (1st mode load distribution) for all models. For M-IRI, the difference along the height of model is 19...41%, whereas for M-IR2 the difference is 17...34%; for M-IR3 the difference is 9...28%, and for M-IR4 the difference is 14...33%. From the results, it can be concluded that the relatively higher values of the shear ratio occurred at the second story for all models, with reduction in ratios at upper stories, and this is because the lower structure is stiffer than the upper one. It is noteworthy that the shear capacity ratios remain lower than 1.0 (do not exceed 0.4), thus the seismic performance of the columns under consideration (choosing the most critical columns in each frame) is quite satisfactory.

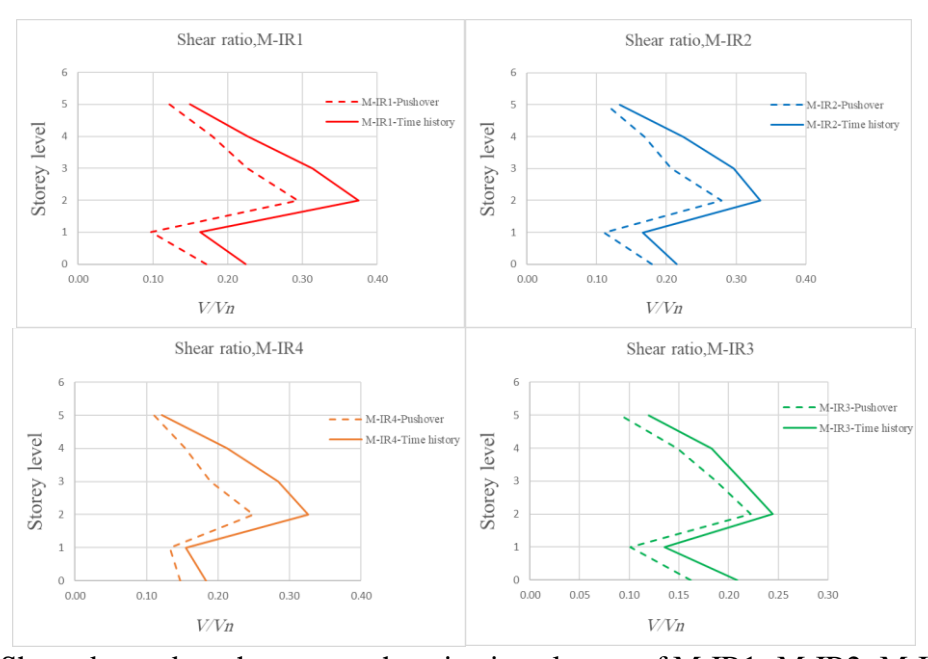


Figure 37. Shear demand to shear strength ratios in columns of M-IR1, M-IR2, M-IR3 and M-IR4 models for NDP and NSP

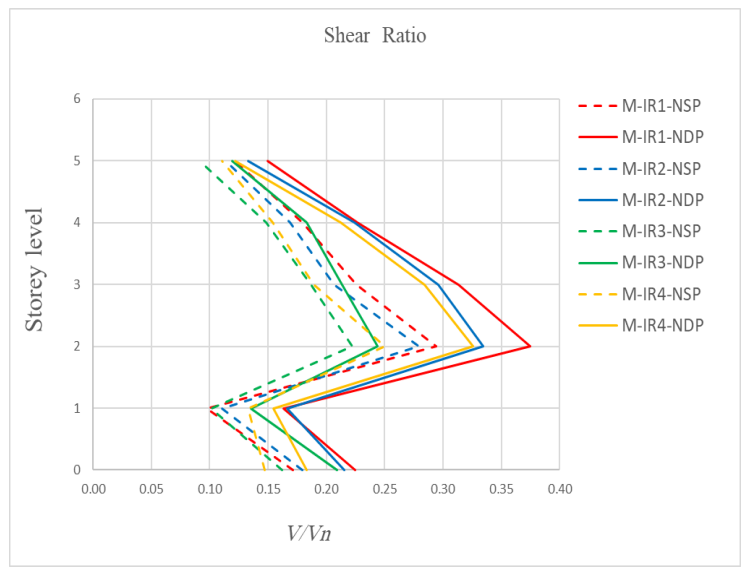


Figure 38. Shear demand to shear strength ratios in columns comparison of M-IR1, M-IR2, M-IR3 and M-IR4 models for NDP and NSP

# 9 **CONCLUSIONS**

In this study, the seismic response of multi-story RC frames with different irregular setbacks, designed for Baghdad locations, were studied and analyzed by three different methods: equivalent lateral force procedure, ELFP, nonlinear static procedure, NSP (with three load pattern distributions), and nonlinear dynamic procedure NDP. Several parameters were investigated (i.e., the inter-story drift, the local vulnerability index (VI), the seismic performance of the structural members through shear capacity ratio (the shear demand on the column, V, to the shear strength  $V_n$ ). Furthermore, the vulnerability was evaluated by fragility curves. The following conclusions were obtained.

- 1- The applicability of a two-stage equivalent lateral force analysis (ELFP) was investigated for structures that have a flexible upper portion over a rigid lower portion, according to the simplified method proposed in [13], by the verification of the inter-story drift (*IDR<sub>a</sub>*) parameter obtained from this approach and by its comparison with the results of the nonlinear static analysis, NSP, and of the nonlinear dynamic analysis, NDP. From the results, it can be concluded that the (ELFP), which is adopted in ISC 2014 to analyze and design the buildings in Iraq, is not appropriate for the analysis of setback structures. Consequently, there is an urgent need to adopt appropriate and more effective methods for designing and evaluating the performance of reinforced concrete buildings in particular, because they are the most used type in Iraq.
- 2- The results of "first mode" load distribution for NSP showed the smallest target shear capacity and the greatest target displacement demand among the three load distribution patterns considered in analysis. Consequently, this was considered the critical pattern.
- 3- The comparison of the results obtained for all models for NDP and NSP ("first mode" load distribution pattern) of the inter-story drift and shear capacity ratio for columns shows that NSP is unable to simulate the impacts of higher modes on the structural response, which become important when the irregularity of the structure increases. Therefore, NDP is the accurate method for this type of building.
- 4- It is worth noting that the shear capacity ratio for columns, which represents the ratio of the shear demand on the column V, to the shear strength  $V_n$ , remains lower than 1.0 (actually does not exceed 0.4), thus the seismic performance of the columns under consideration (choosing the most critical columns in each frame) is quite satisfactory.
- 5- The fragility curves were developed based on NSP, although NDP is more reliable and accurate. The preliminary evaluation of the case can allow the use of a simple method as NSP. It can be observed that, when the irregularity setback level increases, the damage hazard increases, and the models exhibit poor seismic performance. The NSP has also been used in many studies to analyze irregular buildings [i.e., 42-50]. However, given the lack of earthquake damage information required to calibrate the levels of damage proposed by vulnerability functions, the reliability of these functions remains a critical matter.
- 6- The fragility curves developed in this study could be used as preliminary investigation in seismic risk scenarios in Iraq (Baghdad) for irregular setback buildings. Further processing of these curves is considered necessary to account for the potential contrast in input parameters, which are selected for the nonlinear analysis, the damage state thresholds determination, and the hypotheses that have been used for fragility curves for each of the considered damage states.
- 7- As the model setback levels / irregularity indices increase, the target shear capacities and the target displacements decrease under the effect of the three load pattern distributions used for NSP. This due to the decrease of the structure capacity.

8- The severity (or degree) of model setbacks also influences the increase in damage, so setback ratios were studied to take into account their severity. The forces are concentrated on the section of the structure where the abrupt decrease in stiffness occurs, i.e., at the bottom of the upper structure. This can be noticed from of the development of the plastic hinges at this location. Consequently, the abrupt change in stiffness or the irregular vertical configurations of the structures are considered local vulnerability locations.

# 10 **BIBLIOGRAPHY**

- [1] Stefano D. and Pintucchi B. (2008), "A review of research on seismic behaviour of irregular building structures since 2002". Bulletin of Earthquake Engineering. 6, pp285–308.
- [2] EN 1998-1: Eurocode 8 (2004), Eurocode 8: Design of structures for earthquake resistance Part 1: General rules, seismic actions and rules for buildings. EC8 (EN1998 -1: 2004), European Union (CEN): European Committee for Standardization, 2004, December.
- [3] ASCE 7-16. (2016), "Minimum Design Loads and Associated Criteria for Buildings and Other Structures", Reston, Virginia. American Society of Civil Engineers, 2016.
- [4] ISC 2016, Iraqi Seismic Code Requirements for Buildings, 1<sup>st</sup> edition, C.O.S.Q.C., Baghdad, Iraq, 2016.
- [5] IBC 2012, International Building Code, International Code Council, USA, 2011.
- [6] Sumit G., Lovish P. (2017), "Seismic Behaviour of Building Having Vertical irregularities", International Journal of Engineering Science Invention Research & Development, 3(6), pp 620-625.
- [7] Wood, S.L. (1992), "Seismic Response of R/C Frames with Irregular Profiles", Jl. of Struct. Eng., ASCE, 118(2), pp 545–566.
- [8] Wong, C.M. and Tso, W.K. (1994), "Seismic Loading for Buildings with Setbacks", Canadian Jl. of Civil Eng., 21(5), pp 863–871.
- [9] Duan, X.N. and Chandler (1991), A.M., "Seismic torsional response and design procedures for a class of setback frame buildings", Earthquake Engg. and Struct. Dynamics, 24, pp 761–777.
- [10] Kappos, A.J. and Scott, S.G. (1998), "Seismic assessment of an R/C building with setbacks using nonlinear static and dynamic analysis procedures", In: Booth E. (ed) Seismic design practice into the next century. Balkema, Rotterdam.
- [11] UBC 1997, "Uniform Building Code," International Conference of Building Officials, California, USA, 1997.
- [12] Liu HY, van de Lindt JW, Pryor S (2008), "Seismic performance assessment of a seven-story wood-steel hybrid buildings", In: 14<sup>th</sup> World Conference on Earthquake Engineering; Beijing, China.
- [13] L. Xu, and X. L. Yuan (2015), "A simplified seismic design approach for mid-rise buildings with vertical combination of framing systems", Engineering Structures, 99, pp 568–581.
- [14] ACI 318-19 (2019), Building Code Requirments for Reinforced Concrete (ACI 318-19) and Commentary, American Concrete Institute, Farmington Hills, Detroit, 2019.
- [15] Mainstone, R.J. and Weeks, G.A. (1970), "The influences of bounding frame on the racking stiffness and strength of brick walls", Proceedings of the 2<sup>nd</sup> international brick masonry conference.

- [16] Mainstone, R.J. (1971), "On the stiffness and strength of infilled frames", ProcInst Civil Eng Sup; 57-90. National University of Mexico (1990), Design manual for earthquake engineering to the construction regulations for the Federal District of Mexico City.
- [17] Rana Roy and Somen Mahato (2013), "Equivalent lateral force method for buildings with setback: adequacy in elastic range Earthquakes and Structures", 4(6), pp 685-710.
- [18] ASCE/SEI 41, (2006) "Seismic Rehabilitation of Existing Buildings, American Society of Civil Engineers, Reston, Virginia.
- [19] Mazzolani, F.M and Piluso, V. (1996), "Theory and design of seismic resistant steel frames", FN & SPON an Imprint of Chapman & Hall, London, New York.
- [20] Karavasilis, T.L. Bazeos, N. and Beskos, D.E. (2008), "Seismic response of plane steel MRF with setbacks: estimation of inelastic deformation demands", Construct. Steel Struct., 64, pp 644 654.
- [21] Mahato, S. (2012), "Applicability of codal provisions to regulate seismic torsion: multistory buildings with setback", M.E. thesis, Department of Civil Engineering, Bengal Engineering and Science University, Shibpur.
- [22] Pang WC, Rosowsky DV, Pei SL, van de Lindt JW (2011), "Simplified direct displacement design of six-storey woodframe building and pretest seismic performance assessment". J Struct Eng.,136(7), pp 813–25.
- [23] ETABS, Structural and Earthquake Engineering Software, Computers and Structures, Inc., Release 2017.
- [24] ASCE 7-10. (2010), "Minimum Design Loads and Associated Criteria for Buildings and Other Structures", Reston, Virginia.: American Society of Civil Engineers.
- [25] MDLPA (2013). P100-1/2013-Seismic Design Code Part 1: Design rules for buildings. Bucharest (in Romanian).
- [26] ASCE/SEI 41-13 (2014), "Seismic evaluation and retrofit of existing buildings", American Society of Civil Engineers, Reston, Virginia.
- [27] SAP2000, Structural and Earthquake Engineering Software, Computers and Structures, Inc., Release 2019.
- [28] Park R, Paulay T. (1975), "Reinforced concrete structures", New York: John Wiley & Sons; 769 pages.
- [29] Mehmet Inel, Hayri Baytan Ozmen (2006), "Effects of plastic hinge properties in nonlinear analysis of reinforced concrete buildings", Engineering Structures, 28, pp 1494–1502.
- [30] Cavaleri, L. & F. Trapani (2017), "Cyclic response of masonry infilled RC frames: Experimental results and simplified modelling, "Soil Dyn. Earthq. Eng., 65, pp224–242.

- [31] Emin MAHMUD, Zdravko BONEV, Emad ABDULAHAD (2019), "Nonlinear seismic analysis of masonry infilled RC frame structures building materials and structures building materials and structures", 62(1), pp 17-25.
- [32] FEMA 356 (2000), "Prestandard and Commentary for Seismic Rehabilitation of Buildings", Prepared by the American Society of Civil Engineers for the Federal Emergency Management Agency, Washington, D.C.
- [33] FEMA P-695 (2009b), "Quantification of building seismic performance factors", prepared by the Applied Technology Council (ATC) for the Federal Emergency Management Agency, Washington, DC.
- [34] ATC-40 (1996), "Seismic evaluation and retrofit of concrete buildings", Prepared by the Applied Technology Council, Rep. No. ATC-40, Redwood City, CA, for the California Seismic Safety Commission (Rep. No. SSC 96-01)
- [35] ASCE 7-5 (2005), "Minimum Design Loads for Buildings and Other Structures", American Society of Civil Engineers, Reston, Virginia.
- [36] FEMA 440 (2005), "Improvement of Nonlinear Static Seismic Analysis Procedures", prepared by the Applied Technology Council (ATC-55 Project) for the Federal Emergency Management Agency, Washington, D.C.
- [37] Onur, T., Gök, R., Abdulnaby, W., Shakir, A.M., Mahdi, H., Numan, N.M.S., Al-Shukri, H., Chlaib, H.K., Ameen, T.H., Abd, N.A. (2016), "Probabilistic Seismic Hazard Assessment for Iraq", LLNL-691152,
- [38] ATC-40 (1996), "Seismic evaluation and retrofit of concrete buildings", Prepared by the Applied Technology Council, Rep. No. ATC-40, Redwood City, CA, for the California Seismic Safety Commission (Rep. No. SSC 96-01).
- [39] Adrian Fredrick C. Dya, Andres Winston C. Oretaa (2015). "Seismic vulnerability assessment of soft story irregular buildings using pushover analysis". Procedia Engineering 125, pp 925 932.
- [40] N. Lakshmanan, (2006), "Seismic Evaluation and Retrofitting of Buildings and Structures", ISET Journal of Earthquake Technology, 43(1-2), pp 31-48.
- [41] HAZUS MR1, Multi-Hazard Loss Estimation Methodology: Earthquake Model. Department of Homeland Security, Emergency Preparedness and Response Directorate, FEMA, Washington D.C; 2003.
- [42] HAZUS MR4, Multi-Hazard Loss Estimation Methodology: Earthquake Model. Department of Homeland Security, Emergency Preparedness and Response Directorate, FEMA, Washington D.C; 2003.
- [43] Milutinovic ZV, Trendafiloski GS. Risk-UE project (2003), "An advanced approach to earthquake risk scenarios with applications to different European towns". Contract: EVK4-CT-2000-00014, WP4: Vulnerability of Current Buildings, Brussels, Belgium; 2003.
- [44] Park J, Towashiraporn P, Craig JI, Goodno BJ (2009), "Seismic fragility analysis of lowrise unreinforced masonry structures". Eng Struct, 31(1), pp 125–37.

- [45] S. Ahamed and J. G. Kori (2013), "Performance Based Seismic Analysis of an Unsymmetrical Building Using Pushover Analysis," International Journal of Engineering Research, 1(2), pp. 100-110.
- [46] C. Athanassiadou (2008), "Seismic Performance of R/C Plane Frames Irregular in Elevation, "Engineering Structures, 30, pp. 1250-1261.
- [47] O. Merter and T. Ucar (2013), "A Comparative Study on Nonlinear Static and Dynamic Analysis of RC Frame Structures, "Journal of Civil Engineering and Science, 2(3), pp155-162.
- [48] C. M. Ravikumar, K. S. Babu Narayan, B. V. Sujith and D. Venkat Reddy (2012), "Effect of Irregular Configurations on Seismic Vulnerability of RC Buildings," Architecture Research, pp 20-26.
- [49] E. V. Valmundsson and J. M. Nau (1997), "Seismic Response of Building Frames with Vertical Structural Irregularities," Journal of Structural Engineering, 123(1), pp 30-41.
- [50] Adrian Fredrick C. Dya, Andres Winston C. Oretaa. Procedia Engineering (2015), "Seismic vulnerability assessment of soft story irregular buildings using pushover analysis", 125, pp 925 932
- [51] Mohamed Mouhine, Elmokhtar Hilali (2022), "Seismic vulnerability assessment of RC buildings with setback irregularity". Ain Shams Engineering Journal 13(1):101486
- [52] Hanan Al-Nimry (2019), "Development of Seismic Fragility Curves of RC Infilled Frame Buildings in Jordan", MATEC Web of Conferences 281, 01012.
- [53] M. S. Azad, M. M. Sazzad, N. Samadder, M. F. Rahman (2019), "Effect of Setback Percentages in Vertically Irregular Concrete Buildings on Response to Earthquake", Proceedings of International Conference on Planning, Architecture and Civil Engineering, 07-09 February 2019.
- [54] Caltrans (2010), "Seismic Design Criteria", Version 1.6, November 2010, California Department of Transportation, Sacramento, California.
- [55] Murty, C.V.R., Rupen Goswami, Vijayanarayanan, A. R., Vipul V. Mehta, (2012), "Some Concepts in Earthquake Behaviour of Buildings". Gujarat State Disaster Management Authority, Gandhinagar.
- [56] NIST (2016), "Seismic Design of Reinforced Concrete Special Moment Frames: A guide for practicing engineers, NEHRP Seismic Design Technical Brief No. 1, Second Edition, NIST GCR 16-917-40, produced by the Applied Technology Council and the Consortium of Universities for Research in Earthquake Engineering for the National Institute of Standards and Technology, Gaithersburg, MD.
- [57] California earthquake authority, Caltrans department of transportation & Pacific gas and electric company. (2013, April). Pacific Earthquake Engineering Research Center (PEER). <a href="https://ngawest2">https://ngawest2</a>.

# APPENDIX -A

# A-1 Sections of columns and beams for the studied structures

# 1- Columns

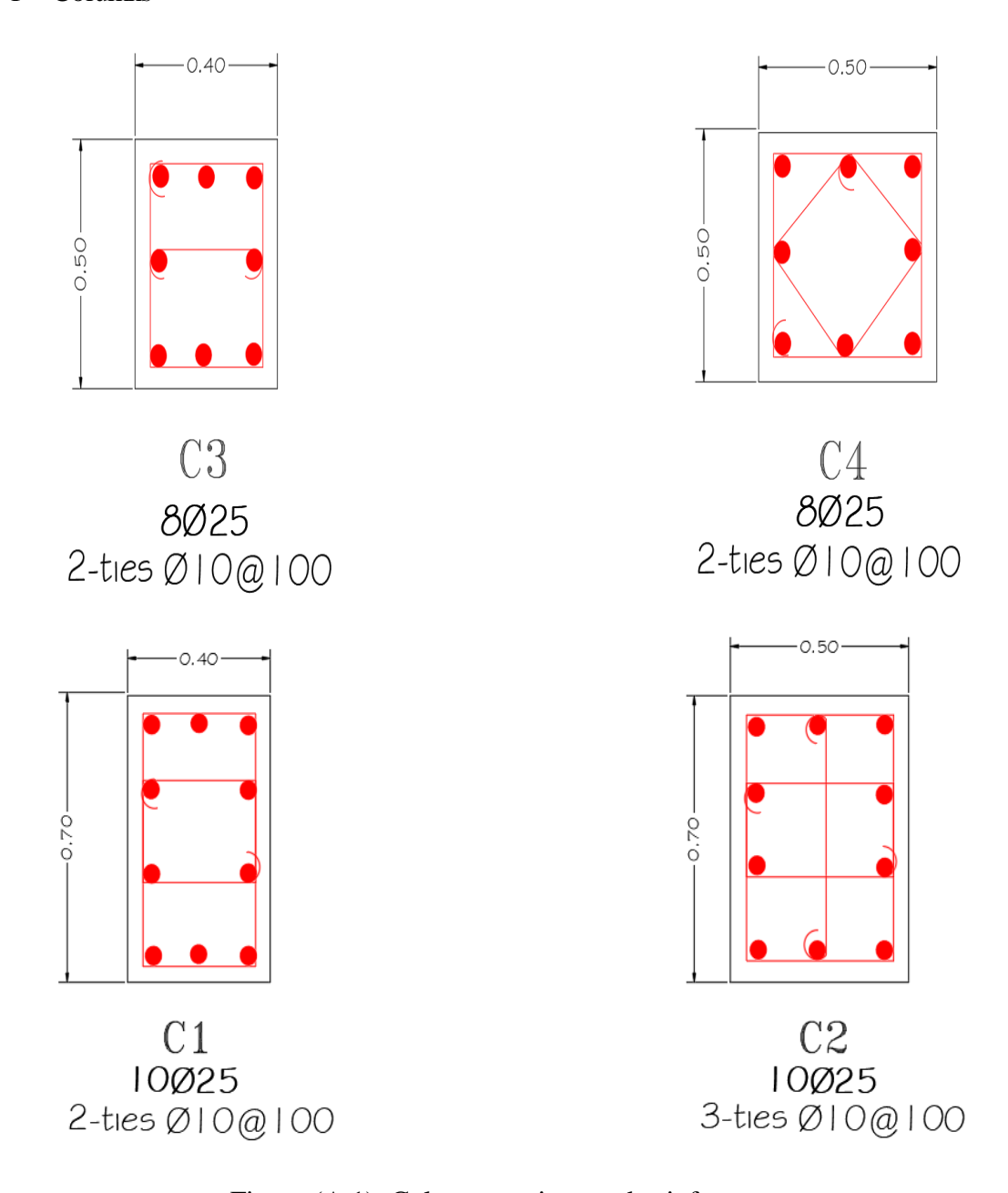


Figure (A.1): Column sections and reinforcement

# 2- Beams

For the preliminary proportioning of beam sections according to ACI 318-19 (Section 6.3.2.1), the effective flange width of beams is as shown in Fig. A.3a, b. The depth of the beams was considered as ten percent of the large bay size (0.6 m). Taking into account the limits of beams dimensions in ACI 318-19, summarized in Fig. A.2, the web width of the beams was selected to be 0.3 m. The sections of the beams are shown in Fig. A.3a, b.

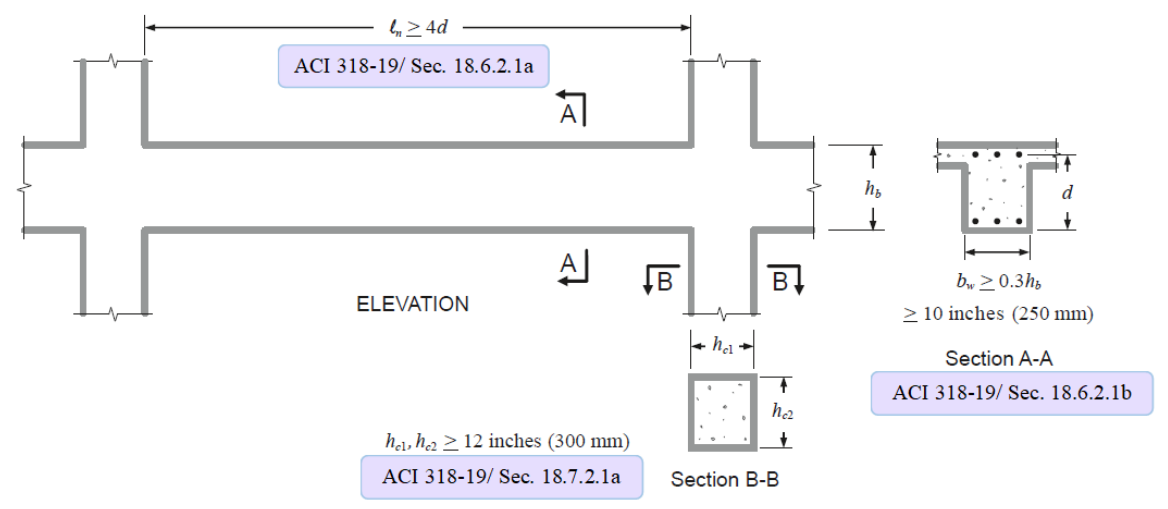


Figure (A.2): Limits of columns and beams dimensions of special moment frames based on ACI 318-19

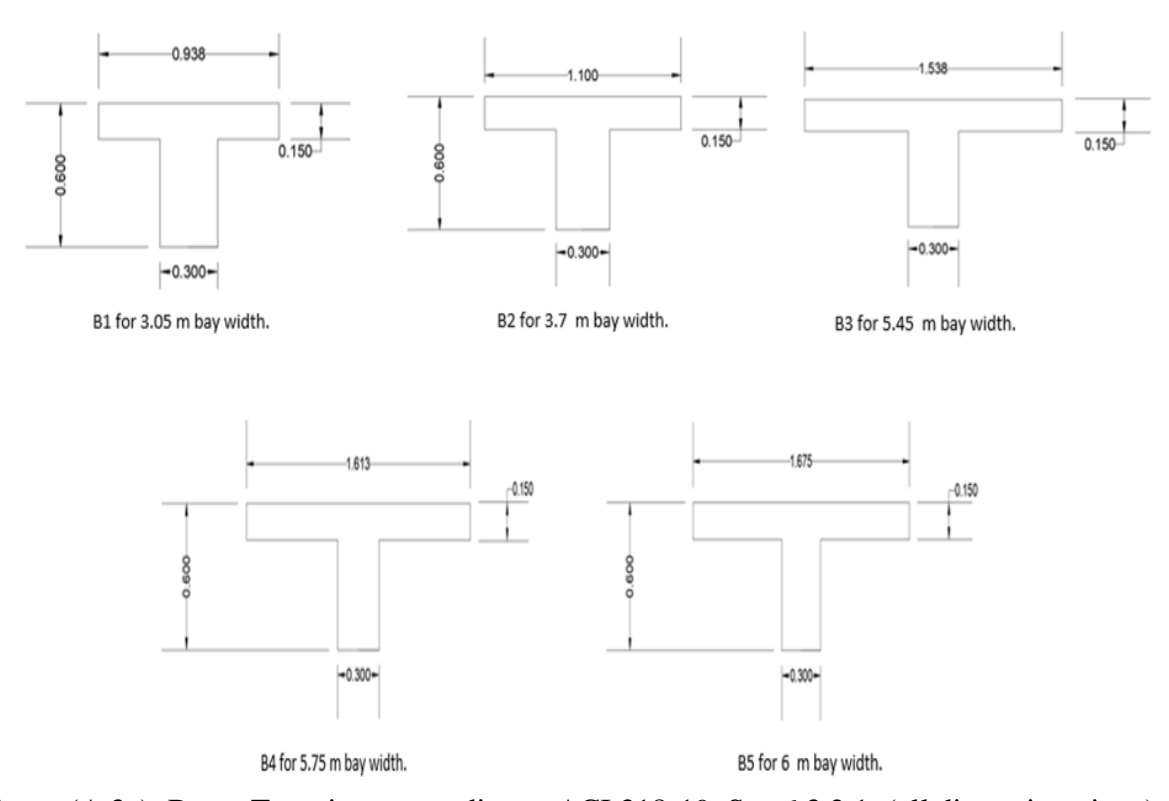


Figure (A.3a): Beam T sections according to ACI 318-19, Sec.6.3.2.1. (all dimensions in m)

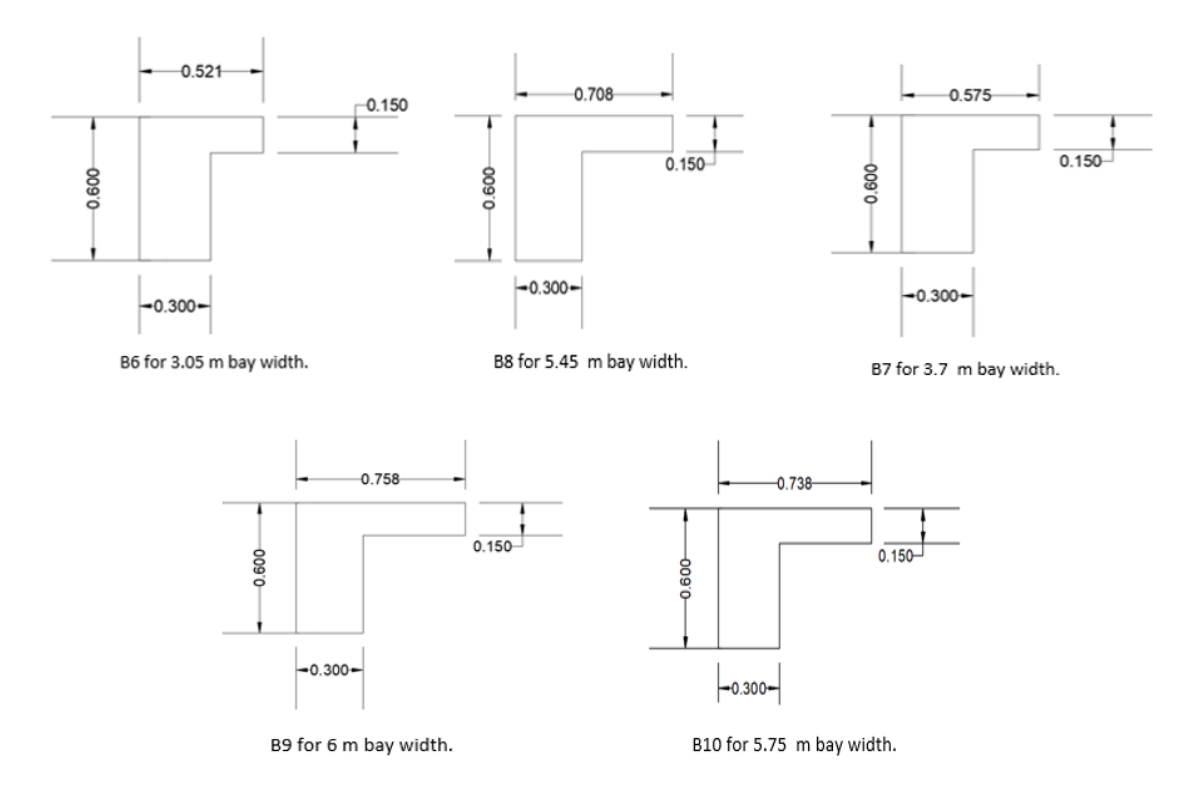


Figure (A.3b): Beam L sections according to ACI 318-19, Sec.6.3.2.1 (all dimensions in m)

# A-2 Reinforcement details according to the seismic provisions of ACI 318-19

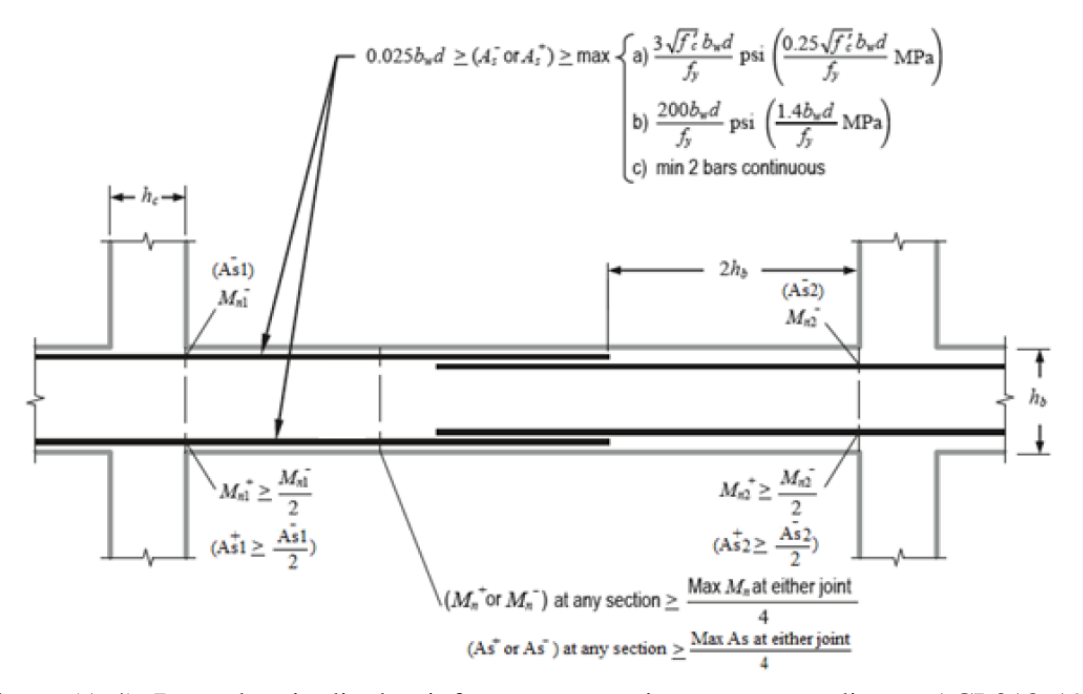


Figure (A.4): Beam longitudinal reinforcement requirements according to ACI 318-19, Sec.18.6.3

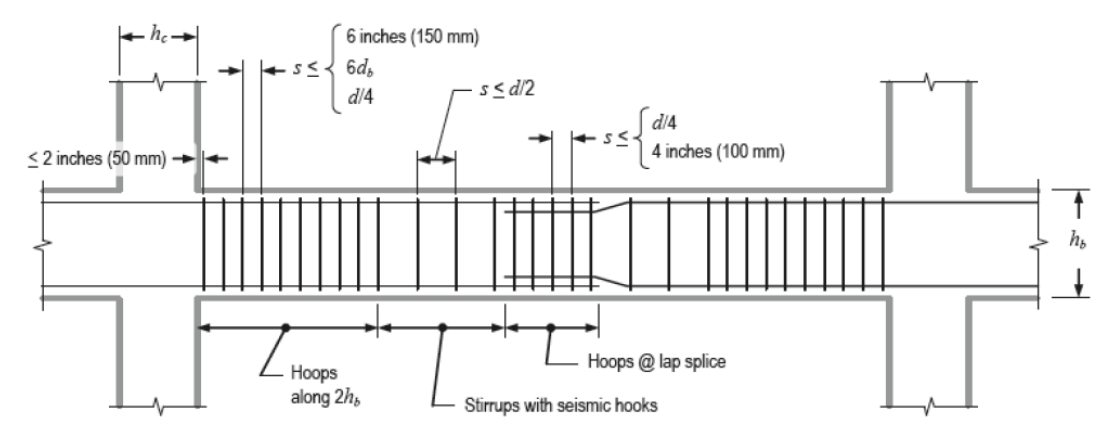
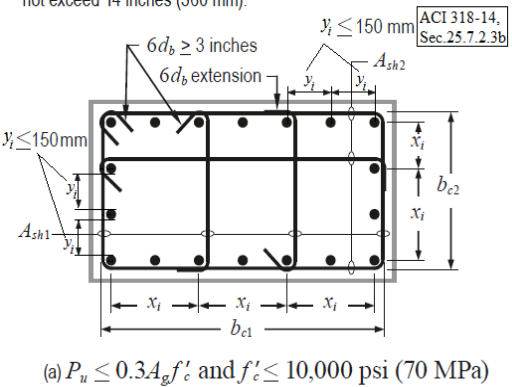


Figure (A.5): Hoops and stirrups locations and spacing requirements according to ACI 318-19, Sec.18.6.3.3

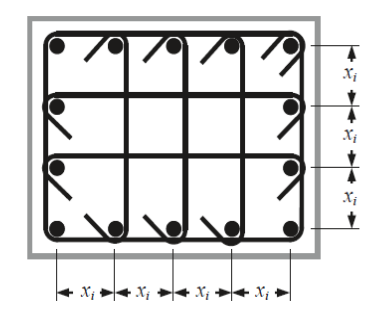
"The longitudinal reinforcement must satisfy the requirements showed in Fig. A-4. Although ACI 318 (Section 18.6.3) allows a reinforcement ratio up to 0.025, 0.01 is more practical for constructability and for keeping joint shear forces within reasonable limits. The designer also needs to specify requirements for reinforcement splicing and bar cutoffs. Where lap splices are used, these should be located at least  $2h_b$  away from critical sections where flexural yielding is likely to occur (Fig. A-4). Although ACI 318 (Section 18.6.3.4) permits these at any location, it is better to locate them at least  $2h_b$  away from critical sections where flexural yielding is likely to occur" [NIST GCR 16-917-40]."

According to ACI 318-19 (Section 18.6.3.3), lap splices of deformed longitudinal reinforcement shall be permitted if hoop or spiral reinforcement is provided over the lap length. Spacing of the transverse reinforcement enclosing the lap-spliced bars shall not exceed the lesser of d/4 and 4 in (100 mm) (Fig. A-5).

- Every corner and alternate longitudinal bar shall have lateral support, and no bar shall be farther than 6 inches (150 mm) clear from a laterally supported bar.
- Consecutive crossties around the perimeter and along the length have their 90° hooks on opposite sides of column.
- The dimension x<sub>i</sub> from centerline to centerline of supported bars shall not exceed 14 inches (360 mm).



- Every longitudinal bar around the perimeter of the column core shall have lateral support, provided by the corner of a hoop or by a seismic hook.
- The dimension x<sub>i</sub> from centerline to centerline of supported bars shall not exceed 8 inches (200 mm).



(b)  $P_u > 0.3 A_g f'_c$  or  $f'_c > 10,000$  psi (70 MPa)

Figure (A.6): Column transverse reinforcement detail according to ACI 318-19, Sec. 18.7.5.2

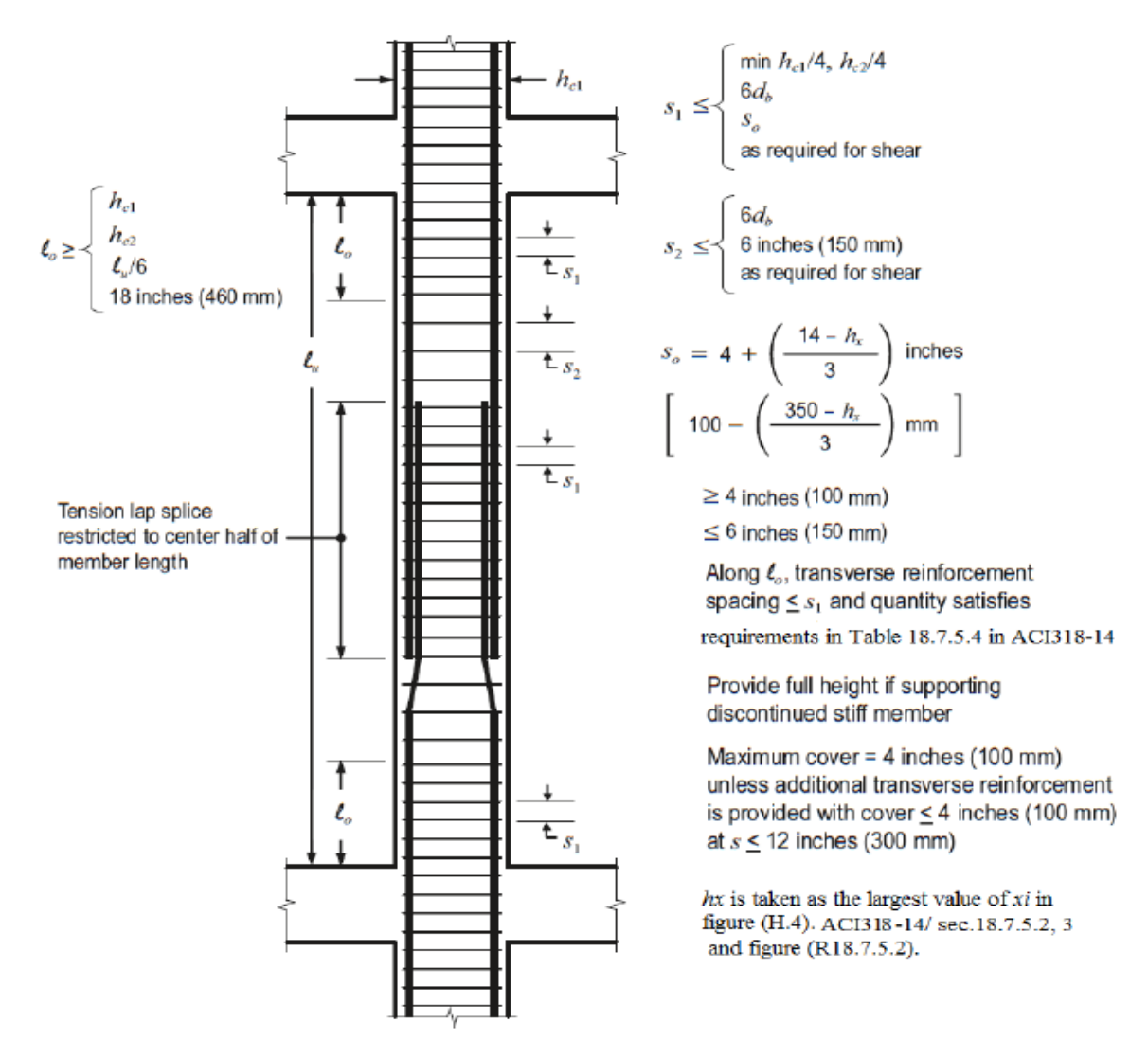


Figure (A.7): Column transverse reinforcement spacing requirements according to ACI 318-19.

# A-3 Verification of vertical irregularity in terms of mass and stiffness according to ASCE 7-16 Table (A-1): Verification for vertical irregularity in terms of stiffness for M-IR1

STORY	stiffness kN/m	K <sub>i</sub> K <sub>i+1</sub>	CHECK	= avg(K <sub>i</sub> . 1,i-2,i-3)	K <sub>i</sub>	CHECK
	X- DIRECTION	0.7		$ m K_{mi} = 1.1$	0.8	
LEVEL 5	85319.64	-	-			
LEVEL 4	85754.67	1.01	R			
LEVEL 3	88433.79	1.03	R			
LEVEL 2	119912.76	1.36	R	86502.70	1.39	R
LEVEL 1	817870.43	6.82	R	98033.74	8.34	R
GF	1484494.87	1.82	R	342072.33	4.34	R

Table (A-2): Verification for vertical irregularity in term of stiffness for M-IR1

	stiffness	Ki		) )	Ki	
STORY	kN/m	$K_{i+1}$	CHECK	= avg( 1,i-2,i-3)	$\mathbf{K}_{mi}$	CHECK
	Y- DIRECTION	0.7		$K_{ m mi}$ :	0.8	
LEVEL 5	142068.04	-	-			
LEVEL 4	143742.80	1.01	R			
LEVEL 3	144726.61	1.01	R			
LEVEL 2	151719.75	1.05	R	143512.48	1.06	R
LEVEL 1	899377.75	5.93	R	146729.72	6.13	R
GF	1441849.32	1.60	R	398608.04	3.62	R

Table (A-3): Verification for vertical irregularity in term of mass for M-IR1

amonii		m <sub>i</sub>		m <sub>i</sub>	a	
STORY	$m_{x,y}$	$m_{i+1}$	CHECK	m <sub>i-1</sub>	CHECK	
LEVEL 5	162835.55	-	-	0.96	-	
LEVEL 4	169411.09	1.04	R	1	R	
LEVEL 3	169411.09	1	R	1	R	
LEVEL 2	169411.09	1	R	0.36	R	
LEVEL 1	473902.80	2.80	IR	0.96	R	
GF	494997.61	1.04	R	-	-	

Table (A-4): Verification for vertical irregularity in term of stiffness for M-IR2

STORY	stiffness kN/m	K <sub>i</sub>	СНЕСК	= avg(K <sub>i</sub> . 1,i-2,i-3)	K <sub>i</sub> K <sub>mi</sub>	CHECK
	X- DIRECTION	0.7		K <sub>mi</sub> :	0.8	
LEVEL 5	71332.22	-	-			
LEVEL 4	69366.34	0.97	R			
LEVEL 3	69673.03	1.00	R			
LEVEL 2	81541.70	1.17	R	70123.86	1.16	R
LEVEL 1	700355.52	8.59	R	73527.02	9.53	R
GF	993414.40	1.42	R	283856.75	3.50	R

Table (A-5): Verification for vertical irregularity in terms of stiffness for M-IR2

STORY	stiffness kN/m	$K_{i}$ $K_{i+1}$	CHECK	= avg(K <sub>i</sub> - 1,i-2,i-3)	K <sub>i</sub>	CHECK
	Y- DIRECTION	0.7		$\mathbf{K}_{mi} = 1, i \cdot j$	0.8	
LEVEL 5	85564.92	-				
LEVEL 4	85464.73	1.00				
LEVEL 3	85890.05	1.00				
LEVEL 2	96031.04	1.12	R	85639.90	1.12	R
LEVEL 1	707581.66	7.37	R	89128.60	7.94	R
GF	929894.52	1.31	R	296500.91	3.14	R

Table (A-6): Verification for vertical irregularity in terms of mass for M-IR2

OTODN/		$m_{\rm i}$	CHECK	m <sub>i</sub>	СНЕСК	
STORY	$m_{x,y}$	m <sub>i+1</sub>	CHECK	m <sub>i-1</sub>		
LEVEL 5	169850.71	-	-	0.96	-	
LEVEL 4	177245.16	1.04	R	1	R	
LEVEL 3	177245.16	1	R	1	R	
LEVEL 2	177245.16	1	R	0.37	R	
LEVEL 1	473902.80	2.67	IR	0.96	R	
GF	494997.61	1.04	R	-	-	

Table (A-7): Verification for vertical irregularity in terms of stiffness for M-IR3

	stiffness	$K_{i}$		$(K_{i-}$	$K_{i}$	
STORY	kN/m	$K_{i+1}$	CHECK	= avg( 1,i-2,i-3)	K <sub>mi</sub>	CHECK
	X- DIRECTION	0.7		$ m K_{mi} = 1, i = 1,$	0.8	
LEVEL 5	116538.97	-	-			
LEVEL 4	126866.58	1.09	R			
LEVEL 3	153191.45	1.21	R			
LEVEL 2	231172.30	1.51	R	132199.00	1.75	R
LEVEL 1	1520025.82	6.58	R	170410.11	8.92	R
GF	2665786.16	1.75	R	634796.52	4.20	R

Table (A-8): Verification for vertical irregularity in terms of stiffness for M-IR3

	stiffness	$K_{i}$		) )	Ki	
STORY	kN/m	$K_{i+1}$	CHECK	= avg(K <sub>i</sub> . 1,i-2,i-3)	K <sub>mi</sub>	CHECK
	Y- DIRECTION	0.7		$K_{ m mi}$	0.8	
LEVEL 5	178214.64	-	-			
LEVEL 4	202210.15	1.13	R			
LEVEL 3	250638.26	1.24	R			
LEVEL 2	346978.10	1.38	R	210354.35	1.65	R
LEVEL 1	1533131.03	4.42	R	266608.83	5.75	R
GF	2277398.38	1.49	R	710249.13	3.21	R

Table (A-9): Verification for vertical irregularity in terms of mass for M-IR3

атори		m <sub>i</sub>	CITE CIT	m <sub>i</sub>	CHECK	
STORY	$m_{x,y}$	m <sub>i+1</sub>	CHECK	m <sub>i-1</sub>		
LEVEL 5	164468.03	-	-	0.94	-	
LEVEL 4	174613.50	1.06	R	0.86344	R	
LEVEL 3	202230.80	1.15816	R	0.82349	R	
LEVEL 2	245577.01	1.21434	R	0.52	R	
LEVEL 1	473902.80	1.93	IR	0.96	R	
GF	494997.61	1.04	R	-	-	

Table (A-10): Verification for vertical irregularity in terms of stiffness for M-IR4

	stiffness	K <sub>i</sub>		Ki-1	K <sub>i</sub>		
STORY	kN/m	$K_{i+1}$	CHECK	avg(K <sub>i</sub> . 2,i-3)	K <sub>mi</sub>	CHECK	
	X- DIRECTION	0.7		$ m K_{mi} =$	0.8		
LEVEL 5	130282.42	-	-				
LEVEL 4	135149.63	1.04	R				
LEVEL 3	145591.37	1.08	R				
LEVEL 2	184437.60	1.27	R	137007.81	1.35	R	
LEVEL 1	1792478.51	9.72	R	155059.54	11.56	R	
GF	2818106.11	1.57	R	707502.50	3.98	R	

Table (A-11): Verification for vertical irregularity in terms of stiffness for M-IR4

STORY	stiffness kN/m	K <sub>i</sub>	CHECK	= avg(K <sub>i</sub> . 1,i-2,i-3)	K <sub>i</sub>	CHECK	
STORT	Y- DIRECTION	0.7	CILCK	$\mathbf{K}_{\mathrm{mi}}=\mathbf{i}_{1,\mathrm{i-2}}$	0.8	CHECK	
LEVEL 5	173757.37	-	-				
LEVEL 4	182038.49	1.05	R				
LEVEL 3	187386.83	1.03	R				
LEVEL 2	240011.82	1.28	R	181060.90	1.33	R	
LEVEL 1	1561539.46	6.51	R	203145.71	7.69	R	
GF	2602904.02	1.67	R	662979.37	3.93	R	

Table (A-12): Verification for vertical irregularity in terms of mass for M-IR4

		m <sub>i</sub>	urity in terms of ma	m <sub>i</sub>	
STORY	$m_{x,y}$	$m_{i+1}$	CHECK	m <sub>i-1</sub>	CHECK
LEVEL 5	171635.21	-	-	0.91	-
LEVEL 4	188374.72	1.10	R	1	R
LEVEL 3	188374.72	1	R	1	R
LEVEL 2	188374.72	1	R	0.40	R
LEVEL 1	473902.80	2.52	IR	0.96	R
GF	494997.61	1.04	R	-	-

# A-4 Infill wall modeling

Calculation of the equivalent width of a diagonal compressive strut

Table (A-13): Equivalent width a (mm) of an outer diagonal compressive strut for all models

BAY	h/l	Ө	sin O	2* Ө	sin 20	<i>λ1</i>	r, inf	а
3.7	0.727	36.03	0.588	72.055	0.951	0.001	4080.4	479
3.05	0.906	42.17	0.671	84.332	0.995	0.001	3575.3	418
5.45	0.490	26.10	0.440	52.191	0.790	0.001	5456.2	653
6	0.436	23.57	0.400	47.149	0.733	0.001	6000.8	724
5.75	0.457	24.57	0.416	49.134	0.756	0.001	5772.6	694

Table (A-14): Equivalent width a (mm) of an inner diagonal compressive strut for all models

BAY	h/l	θ	sin O	2* Ө	sin 20	<i>λ1</i>	r, $inf$	а
5.75	0.457	24.57	0.416	49.134	0.756	0.0007	5772.6	744

# A-5 Application of simplified design approach on the models as in [13]

Table (A-15): checked for  $r_m$  for M-IR1

STORY	Mass	$1 <= r_m <= 3$
STORT	kg	$r_m = m_u/m_L$
LEVEL 5	162835.5	3.0
LEVEL 4	169411.1	2.9
LEVEL 3	169411.1	2.9
LEVEL 2	169411.1	2.9
LEVEL 1	473902.8	
GF	494997.6	

Table (A-16): checked for  $r_k$  for M-IR1

STORY	Stiffness	$1 <= r_k <= 20$
STORT	kN/m	$r_k$
LEVEL 5	142068	10
LEVEL 4	143743	10
LEVEL 3	144727	10
LEVEL 2	151720	10
LEVEL 1	899378	
GF	1441849	

Table (A-17): first natural frequencies for M-IR1

first natural frequencies *	
$\omega_{I,st}$	1.370
$\omega_{IU}$	1.489
$\omega_{IL}$	5.635

<sup>\*</sup> $\omega_{I,st}$ ,  $\omega_{IU}$ ,  $\omega_{IL}$ : the first natural frequencies of the corresponding MDOF model for entire structure, lower, and upper structures with fixed bases, respectively.

Table (A-18): design parameter for M-IR1

	<u>U</u> 1	_
$K_L$	30765712.09	$K_L = (\acute{\omega}_{IL})^2$ . $M_L$
$K_U$	1487840.77	$K_U = (\acute{\omega}_{IU})^2$ . $M_U$

$T_u$	0.672	
$T_s$	0.513	
$R_m$	1.444	<=1.4
$R_k$	20.68	$> R_{Ku2stg}$

$T_u/_{TS}$	1.31	>=1
$R_{ku1}$	3.4	
$R_{ku2}$	2.44	
$R_{ku3}$	5.14	$0.8 < R_m < 2$
$R_{ku2stg}$	13.42	
$X_2$	-0.04	

$R_m$	1.444		
$\alpha_u =$	$\alpha_{u(d)}$	$R_k > R_{ku2stg}$	
$\alpha_u =$	$\alpha_{u2stg}$	1.10	
	$T_{u}/T_{S}$	1.31	>1
$\alpha_{u, max} =$	$\alpha_{u, max1}$	1.15	$0.71 < R_m < 4.5$

	1.10	一
$\alpha_u =$	1.10	
R	8	
$C_d$	5.5	
$\Delta_{ m U~limt}$	0.33	m
$m_{u,5}$	162835	kg
$m_{u,4}$	169411	kg
$m_{u,3}$	169411	kg
$m_{u,2}$	169411	kg
$S_u$	4	g
$S_a(T_u)$	0.24	g
$C_{NE}$	2.6	
$\dot{S}_a = C_{NE} S_a$	0.621	m/s2
$S_{DI}=2/3 S_{MI}$	0.160	m/s2
$S_{Ds}$	0.312	
$\alpha_u <$	$(R* K_u*\Delta_{\text{U limt}})/(C_d*m_u*S_u*S_a(T_u)$	
$k_{u,5}=$	142068	kN/m
$k_{u,4}=$	143743	kN/m
$k_{u,3}=$	144727	kN/m
$k_{u,2}=$	151720	kN/m

$\alpha_u =$	$\alpha_{u2stg}$	1.10
	$\alpha_{u, max1}$	1.15
	$\alpha_{u, lim} =$	1.1

For checked Eq. (40), 
$$k_L \ge X$$

$$k_L \ge \left(\frac{\alpha_{Ulim}}{\alpha_{Umax}}\right)^{\frac{1}{x_2}} R_{kU3} \frac{s_u}{s_L} \left(\frac{\overline{\omega}_{1v}}{\overline{\omega}_{1L}}\right)^2 k_U$$

STORY	$k_u$	X	$K_{L,stl} = 899378$	K <sub>L,GF</sub> =1441849
LEVEL 5	142068	266321	$K_L > X$	$K_L > X$
LEVEL 4	143743	269460	$K_L > X$	$K_L > X$
LEVEL 3	144727	271305	$K_L > X$	$K_L > X$
LEVEL 2	151720	284414	$K_L > X$	$K_L > X$

STORY	$k_{Us1}$	$k_{Us2}$	$k_{Us3}$
LEVEL 5	1704262	2771801	4123215
LEVEL 4	2871266	4669810	6946612
LEVEL 3	2890918	4701771	6994156
LEVEL 2	3030606	4928959	7332112

STORY	$lpha_{I}$	$m_u$	$klpha_{\mathit{Umax}} \ k_{\mathit{Umin}}$	$klpha_{U2\;stg} \ k_{Umax}$	$K_u$	$K_u > min$	$K_u < max$
LEVEL 5	1.89	162835.55	34498	313685	142068	ok	ok
LEVEL 4	1.49	169411.09	22164	201531	143743	ok	ok
LEVEL 3	1.48	169411.09	22013	200161	144727	ok	ok
LEVEL 2	1.45	169411.09	20999	190935	151720	ok	ok

Table (A-19): checked for  $r_m$  for M-IR2

` ,		
STORY	Mass	$1 <= r_m <= 3$
STORT	kg	$r_m = m_u/m_L$
LEVEL 5	169850.7	2.9
LEVEL 4	177245.2	2.8
LEVEL 3	177245.2	2.8
LEVEL 2	177245.2	2.8
LEVEL 1	473902.8	
GE	101007.6	

Table (A-20): checked for  $r_k$  for M-IR2

STORY	Stiffness	$1 <= r_k <= 20$
STORT	kN/m	$r_k$
LEVEL 5	85565	11
LEVEL 4	85465	11
LEVEL 3	85890	11
LEVEL 2	96031	10
LEVEL 1	707582	
GF	929895	

Table (A-21): first natural frequencies for M-IR2

first natural frequencies *	
$\omega_{I,st}$	1.127
$\omega_{IU}$	1.216
$\omega_{IL}$	4.769

Table (A-22): design parameter for M-IR2

	,	_
$K_L$	22036051.34	$KL = (\acute{\omega}_{IL})^2$ . $M_L$
$K_U$	1037404.63	$KU = (\acute{\omega}_{IU})^2$ . $M_U$

$T_u$	0.822	
$T_s$	0.513	
$R_m$	1.381	<=1.4
$R_k$	21.24	$> R_{Ku2stg}$

$T_u/T_S$	1.60	>=1
$R_{ku1}$	3.4	
$R_{ku2}$	2.38	
$R_{ku3}$	5.16	$0.8 < R_m < 2$
$R_{ku2stg}$	12.73	
$X_2$	-0.03	

$R_m$	1.381		_
$\alpha_u =$	$\alpha_{u(d)}$	$R_k > R_{ku2stg}$	
$\alpha_u =$	$\alpha u_{2stg}$	1.10	
	$T_{u}/T_{S}$	1.60	>1
$\alpha_{u, max} =$	$\alpha_{u, max1}$	1.13	$0.71 < R_m < 4.5$

$\alpha_u =$	1.10	
R	8	
$C_d$	5.5	
$\Delta_{U\ limt}$	0.33	m
$m_{u,5}$	169850	kg
$m_{u,4}$	177245	kg
$m_{u,3}$	177245	kg
$m_{u,2}$	177245	kg
$S_u$	4	g
$S_a(T_u)$	0.195	g
$C_{NE}$	2.61	
$\dot{S}_a = C_{NE} S_a$	0.508	m/s2
$S_{DI}=2/3_{SMI}$	0.160	m/s2
$S_{Ds}$	0.312	
$\alpha_u <$	$\frac{(R*K_u*\Delta_{\text{U limt}})/(C_d*m_u*S_u*S_a(T_u))}{}$	
$k_{u,5}=$	85565	kN/m
$k_{u,4}=$	85465	kN/m
$k_{u,3}=$	85890	kN/m
$k_{u,2}=$	96031	kN/m

$\alpha_u =$	$\alpha_{u2stg}$	1.10
	$\alpha_{u, maxI}$	1.13
	$\alpha_{u, lim} =$	1.10

For checked Eq. (40),  $k_L \ge X$ 

STORY	$k_u$	X	$K_{L,st1} = 707582$	$K_{L,GF} = 929895$
LEVEL 5	85565	141647	$K_L > X$	$K_L > X$
LEVEL 4	85465	141481	$K_L > X$	$K_L > X$
LEVEL 3	85890	142185	$K_L > X$	$K_L > X$
LEVEL 2	96031	158973	$K_L > X$	$K_L > X$

STORY	$k_{UsI}$	$k_{Us2}$	$k_{Us3}$
LEVEL 5	2105554	3427415	5094083
LEVEL 4	2522712	4106462	6103335
LEVEL 3	2535266	4126898	6133708
LEVEL 2	2834603	4614159	6857912

STORY	$\dot{\omega}_{I}$	$m_u$	$klpha_{Umax} \ kU_{min}$	$klpha_{U2\;stg} \ kU_{max}$	$K_u$	$K_u > min$	$K_u < max$
LEVEL 5	1.74	169850.71	29818	276248	85565	OK	OK
LEVEL 4	1.62	177245.16	27101	251080	85465	OK	OK
LEVEL 3	1.62	177245.16	26967	249837	85890	OK	OK
LEVEL 2	1.53	177245.16	24119	223454	96031	OK	OK

Table (A-23): Check for  $r_m$  for M-IR3

STORY	Mass	$1 <= r_m <= 3$
SIORI	kg	$r_m = m_u/m_L$
LEVEL 5	164468.0	3.0
LEVEL 4	174613.5	2.8
LEVEL 3	202230.8	2.4
LEVEL 2	245577.0	2.0
LEVEL 1	473902.8	
GF	494997.6	

Table (A-24): Check for  $r_k$  for M-IR3

STORY	Stiffness	$1 <= r_k <= 20$
STORT	kN/m	$r_k$
LEVEL 5	178215	12.78
LEVEL 4	202210	11.26
LEVEL 3	250638	9.09
LEVEL 2	346978	6.56
LEVEL 1	1533131	
GF	2277398	

Table (A-25): First natural frequencies for M-IR3

First natural frequencies *	
$\omega_{I,st}$	1.585
$\omega_{IU}$	1.742
$\omega_{IL}$	6.293

Table (A.26): Design parameter for M-IR3

$K_L$	38370246.94	$K_L = (\acute{\omega}_{IL})^2$ . $M_L$
$K_U$	2387865.91	$K_U = (\acute{\omega}_{IU})^2$ . $M_U$

$T_u$	0.574	
$T_s$	0.513	
$R_m$	1.231	<=1.4
$R_k$	16.07	$> R_{Ku2stg}$

$T_u/T_S$	1.12	>=1
$R_{kul}$	3.3	
$R_{ku2}$	2.23	
$R_{ku3}$	5.20	$0.8 < R_m < 2$
$R_{ku2stg}$	11.08	
$X_2$	-0.011	

$R_m$	1.231		
$\alpha_u =$	$\alpha_{u(d)}$	$R_k > R_{ku2stg}$	
$\alpha_u =$	$\alpha_{u2stg}$	1.10	
	$T_{u}/T_{S}$	1.12	>1
$\alpha_{u, max} =$	$\alpha_{u, maxl}$	1.11	$0.71 < R_m < 4.5$

$\alpha_u =$	1.10	
R	8	
$C_d$	5.5	
$\Delta_{U\ limt}$	0.33	m
$m_{u,5}$	164468	kg
$m_{u,4}$	174613	kg
$m_{u,3}$	202230	kg
$m_{u,2}$	245577	kg
$S_u$	4	g
$S_a(T_u)$	0.279	g
$C_{NE}$	2.61	
$\dot{S}_a = C_{NE} S_a$	0.728	m/s2
$S_{DI}=2/3 S_{MI}$	0.160	m/s2
$S_{Ds}$	0.312	
$\alpha_u <$	$(R* K_u*\Delta_{\text{U limt}})/(C_d*m_u*S_u*S_a(T_u)$	
$k_{u,5}=$	178215	kN/m
$k_{u,4}=$	202210	kN/m
$k_{u,3}=$	250638	kN/m
$k_{u,2}=$	346978	kN/m

$\alpha_u$ =	$\alpha_{u2stg}$	1.10
	$\alpha_{u, maxl}$	1.11
	$\alpha_{u, lim}=$	1.10

# For checked Eq. (40), $k_L \ge X$

STORY	$k_u$	X	$K_{L,st1} = 2277398$	$K_{L,GF}=1533131$
LEVEL 5	178215	95421	$K_L > X$	$K_L > X$
LEVEL 4	202210	108269	$K_L > X$	$K_L > X$
LEVEL 3	250638	134199	$K_L > X$	$K_L > X$
LEVEL 2	346978	185782	$K_L > X$	$K_L > X$

STORY	$k_{Us1}$	$k_{Us2}$	$k_{Us3}$
LEVEL 5	2659582	4388275	6434472
LEVEL 4	3017678	4979129	7300834
LEVEL 3	3740394	6171601	9049340
LEVEL 2	5178119	8543829	12527708

STORY	$lphi_{l}$	$m_u$	$klpha_{Umax} \ kU_{min}$	$klpha_{U2\;stg} \ kU_{max}$	$K_u$	$K_u > min$	$K_u < max$
LEVEL 5	1.54	164468.0	20108	353789	178215	ok	ok
LEVEL 4	1.55	174613.5	19975	375613	202210	ok	ok
LEVEL 3	1.53	202230.8	21617	435021	250638	ok	ok
LEVEL 2	1.41	245577.0	23026	528263	346978	ok	ok

Table (A-27): checked for  $r_m$  for M-IR4

STORY	Mass	1<=r <sub>m</sub> <=3
SIOKI	kg	$r_m = m_u/m_L$
LEVEL 5	171635.2	2.9
LEVEL 4	188374.7	2.6
LEVEL 3	188374.7	2.6
LEVEL 2	188374.7	2.6
LEVEL 1	473902.8	
GF	494997.6	

Table (A.28): checked for  $r_k$  for M-IR4

STORY	Output Case	Stiff y	$1 <= r_k <= 20$
STORY		kN/m	$r_k$
LEVEL 5	Y	173757	14.98
LEVEL 4	Y	182038	14.30
LEVEL 3	Y	187387	13.89
LEVEL 2	Y	240012	10.84
LEVEL 1	Y	1561539	
GF	Y	2602904	

Table (A.29): first natural frequencies for M-IR4

first natural frequencies *	
$\omega_{I,st}$	1.555
$\omega_{IU}$	1.668
$\omega_{IL}$	6.335

Table (A.29): design parameter for M-IR4

$K_L$	38884128.45	$K_L = (\acute{\omega}_{IL})^2$ . $M_L$
$K_U$	2049829.60	$K_U = (\acute{\omega}_{IU})^2. M_U$

$T_u$	0.6	
$T_s$	0.513	
$R_m$	1.315	<=1.4
$R_k$	18.97	$> R_{Ku2stg}$

$T_u/T_S$	1.17	>=1
$R_{ku1}$	3.3	
$R_{ku2}$	2.32	
$R_{ku3}$	5.18	$0.8 < R_m < 2$
$R_{ku2stg}$	12.00	
$X_2$	-0.025	

$R_m$	1.315		_
$\alpha_u$ =	$\alpha_{u(d)}$	$R_k > R_{ku2stg}$	
$\alpha_u$ =	$a_{u2stg}$	1.10	
	$T_u/T_S$	1.17	>1
$\alpha_{u, max} =$	$\alpha_{u, maxl}$	1.12	$0.71 < R_m < 4.5$

Г	T	
$a_u =$	1.10	
R	8	
$C_d$	5.5	
$\it \Delta_{U limt}$	0.33	m
$m_{u,5}$	171635	kg
$m_{u,4}$	188374	kg
$m_{u,3}$	188374	kg
$m_{u,2}$	188374	kg
$S_u$	4	g
$S_a(T_u)$	0.267	g
$C_{NE}$	2.61	
$\dot{S}_a = C_{NE} S_a$	0.696	m/s2
$S_{DI}=2/3 S_{MI}$	0.160	m/s2
$S_{Ds}$	0.312	
$\alpha_u <$	$(R^* K_u * \Delta_{\text{U limt}}) / (C_d * m_u * S_u * S_a(T_u)$	
$k_{u,5}=$	173757	kN/m
$k_{u,4}=$	182038	kN/m
$k_{u,3}=$	187387	kN/m
$k_{u,2}=$	240012	kN/m

$\alpha_u$ =	$\alpha_{u2stg}$	1.10
	$\alpha_{u, max1}$	1.12
	$\alpha_{\text{u. lim}}=$	1.1

For checked eq. (40),  $k_L \ge X$ 

	1 \ //			
STORY	ku	X	$K_{L,st1} = 2602904$	$K_{L,GF} = 1561539$
LEVEL 5	173757	93227	$K_L > X$	$K_L > X$
LEVEL 4	182038	97670	$K_L > X$	$K_L > X$
LEVEL 3	187387	100540	$K_L > X$	$K_L > X$
LEVEL 2	240012	128775	$K_L > X$	$K_L > X$

STORY	$k_{UsI}$	$k_{Us2}$	$k_{Us3}$
LEVEL 5	2694083	4410807	6517943
LEVEL 4	2822480	4621022	6828582
LEVEL 3	2905406	4756789	7029208
LEVEL 2	3721349	6092667	9003263

STORY	$lpha_{I}$	$m_u$	$klpha_{Umax} \ k_{Umin}$	$klpha_{U2\;stg} \ k_{Umax}$	$K_u$	$K_u > min$	$K_u < max$
LEVEL 5	1.55	171635.2	22177	369206	173757	ok	ok
LEVEL 4	1.58	188374.7	25498	405215	182038	ok	ok
LEVEL 3	1.56	188374.7	24770	405215	187387	ok	ok
LEVEL 2	1.38	188374.7	19339	405215	240012	ok	ok

Table (A-30): Criteria for irregularity in plan (torsional irregularity,  $\delta_{max} > 1.2 \ \delta_{avg}$ ) for M-IR1

		Spec x					
STORY	$D_{X,m}$	Displacement, mm		ratio	check		
		$\delta_{max}$	$\delta_{\mathrm{avg}}$	Tauo	CHECK		
LEVEL 5	17.5	11.495	10.686	1.076	R		
LEVEL 4	17.5	9.890	9.186	1.077	R		
LEVEL 3	17.5	7.224	6.690	1.080	R		
LEVEL 2	17.5	3.816	3.497	1.091	R		
LEVEL 1	17.5	0.771	0.679	1.135	R		
GF	17.5	0.332	0.285	1.167	R		

		Spec y				
STORY	$D_{Y,m}$	Displacement, mm		ratio	check	
		$\delta_{max}$	$\delta_{\mathrm{avg}}$	Tano	CHECK	
LEVEL 5	12.85	8.868	8.42	1.053	R	
LEVEL 4	12.85	7.783	7.392	1.053	R	
LEVEL 3	12.85	5.899	5.606	1.052	R	
LEVEL 2	12.85	3.42	3.251	1.052	R	
LEVEL 1	27.45	1.006	0.909	1.107	R	
GF	27.45	0.4	0.369	1.083	R	

Table (A-31): Criteria for irregularity in plan (torsional irregularity,  $\delta_{max} > 1.2~\delta_{avg})$  for M-IR2

			<u> </u>		4,8/		
STORY		Spec x					
	$D_{X,m}$	Displace					
	D <sub>X,m</sub>	$\delta_{max}$	$\delta_{ m avg}$	ratio	check		
LEVEL 5	17.5	11.8780	11.1600	1.0640	R		
LEVEL 4	17.5	10.4970	9.8320	1.0680	R		
LEVEL 3	17.5	8.0480	7.4940	1.0740	R		
LEVEL 2	17.5	4.7620	4.3450	1.0960	R		
LEVEL 1	17.5	1.3870	1.1860	1.1690	R		
GF	17.5	0.6430	0.5710	1.1260	R		

		Spec y					
STORY	$D_{Y,m}$	Displace					
	D <sub>Y,m</sub>	$\delta_{\text{max}}$	$\delta_{ m avg}$	ratio	check		
LEVEL 5	12.85	12.886	12.359	1.043	R		
LEVEL 4	12.85	11.359	10.9	1.042	R		
LEVEL 3	12.85	8.742	8.392	1.042	R		
LEVEL 2	12.85	5.262	5.049	1.042	R		
LEVEL 1	27.45	1.644	1.576	1.043	R		
GF	27.45	0.789	0.754	1.046	R		

Table (A-32): Criteria for irregularity in plan (torsional irregularity,  $\delta_{max} > 1.2 \ \delta_{avg}$ ) for M-IR3

CTODY	<b>D</b>	Spec x					
STORY	$D_{X, m}$	Displacement, mm		<b>,</b> •	1 1		
		$\delta_{ m max}$	$\delta_{ m avg}$	ratio	check		
LEVEL 5	17.5	11.55	9.97	1.16	R		
LEVEL 4	17.5	9.85	8.37	1.18	R		
LEVEL 3	17.5	7.05	5.69	1.24	IR		
LEVEL 2	17.5	3.58	2.72	1.32	IR		
LEVEL 1	17.5	0.62	0.47	1.32	IR		
GF	17.5	0.19	0.15	1.24	IR		

		Spec y			
STORY	$D_{Y,\ m}$	Displacement, mm		ratio	check
		$\delta_{max}$	$\delta_{\mathrm{avg}}$		
LEVEL 5	12.85	8.19	7.86	1.04	R
LEVEL 4	12.85	6.98	6.71	1.04	R
LEVEL 3	15.9	5.03	4.83	1.04	R
LEVEL 2	18.95	2.75	2.63	1.04	R
LEVEL 1	27.45	0.76	0.72	1.06	R
GF	27.45	0.30	0.28	1.07	R

Table (A-33): Criteria for irregularity in plan (torsional irregularity,  $\delta_{max} > 1.2 \ \delta_{avg}$ ) for M-IR4

			Spec x			
STORY	$D_X$	Displacem	nent, mm	ratio	-11-	
		$\delta_{max}$	$\delta_{ m avg}$	Tauo	check	
LEVEL 5	17.5	10.453	10.146	1.030	R	
LEVEL 4	17.5	8.88	8.621	1.030	R	
LEVEL 3	17.5	6.271	6.085	1.031	R	
LEVEL 2	17.5	2.977	2.884	1.032	R	
LEVEL 1	17.5	0.464	0.392	1.185	R	
GF	17.5	0.21	0.162	1.293	IR	

		Spec y				
STORY	$D_{Y}$	Displacement, mm		ratio	check	
		$\delta_{max}$	$\delta_{avg}$	Tauo	CHECK	
LEVEL 5	12.2	8.514	8.141	1.046	R	
LEVEL 4	12.2	7.384	7.066	1.045	R	
LEVEL 3	12.2	5.421	5.19	1.044	R	
LEVEL 2	12.2	2.832	2.716	1.043	R	
LEVEL 1	27.45	0.533	0.511	1.043	R	
GF	27.45	0.208	0.191	1.089	R	

# 11 APPENDIX -B

# B-1 Stress- strain model of rebars for concrete used in SAP2000



Figure (B-1): Rebar parametric simple stress-strain curve used in SAP 2000.

The program uses the Caltrans default strains, where  $\varepsilon_u$  and  $\varepsilon_{sh}$  are modified according to the size of the used bar [27 and 54].

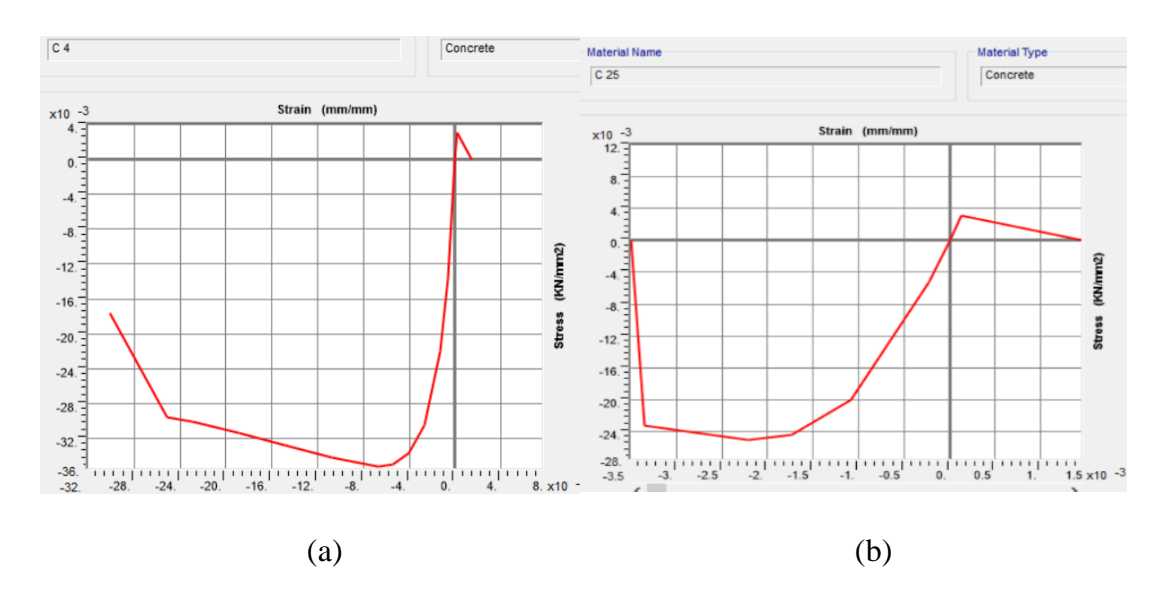


Figure (B-2): Mander concrete parametric stress-strain curves for M4 used in Figure (B-2): SAP 2000 (a) confined (b) unconfined concrete

#### B-2 The modified coefficient method

The ASCE/ SEI 41- 13 adopted the modified coefficient method of FEMA 440 to compute the target displacement ( $\delta_t$ ) which is also used in SAP 2000 program; as follows (extract from the document):

$$\delta_t = C_o. C_1. C_2. S_a \frac{T_e^2}{4\pi^2}. g$$

where  $T_e$  is the effective fundamental period and calculated according to the following equation:

$$T_e = T_i \cdot \sqrt{\frac{K_i}{K_e}}$$

where:

 $T_i$ : is the elastic fundamental period in the considered direction and calculated by elastic dynamic analysis, (in seconds), it can also be calculated from the first increment of lateral load;  $K_i$ : is the elastic lateral stiffness of the building structure in the considered direction and calculated using the modeling requirements of linear analysis, it can also be calculated as the slope of the first increment of lateral load;

 $K_e$ : is the effective lateral stiffness of the building structure in the considered direction;

 $C_o$ : is calculated as following;

$$C_o = \emptyset_{r,1} \cdot \frac{\sum_{i=1}^{N} m_i \cdot \emptyset_{i,1}}{\sum_{i=1}^{N} m_i \cdot \emptyset_{i,1}^2}$$

where:

 $\Phi_{r,1}$ : is the ordinate of first mode shape at control point, (roof level);

N: is the total number of storeys above the base; and

 $C_1$ ,  $C_2$  : are coefficients each of them equals 1 for periods greater than 1.0 second,

As shown in (Figure 11), the established relationship between base shear and roof displacement is substituted with an idealized relationship to determine the nonlinear building model's effective yield strength  $(V_y)$ , effective lateral stiffness  $(K_e)$ , and effective positive post yield stiffness  $(\alpha \mid K_e)$ . The idealized relation's first linear segment starts at the origin point. The second linear segment finishes at a point on the established force-displacement curve where the estimated target displacement is, referred to as "the performance point," or at point of maximum base shear, whichever of least displacement. The intersection of the two linear segments determines the effective yield strength  $(V_y)$ , effective lateral stiffness  $(K_e)$ , and effective positive post-yield stiffness  $(\alpha \mid K_e)$ . Two conditions must be met in order for the point of intersection to be identified. The first one is that the effective stiffness,  $K_e$ , should be such that the first segment passes through the established curve at a point where the base shear equals 60% of the effective yield strength. The second requirement is that the areas above and below the specified curve be approximately equal.

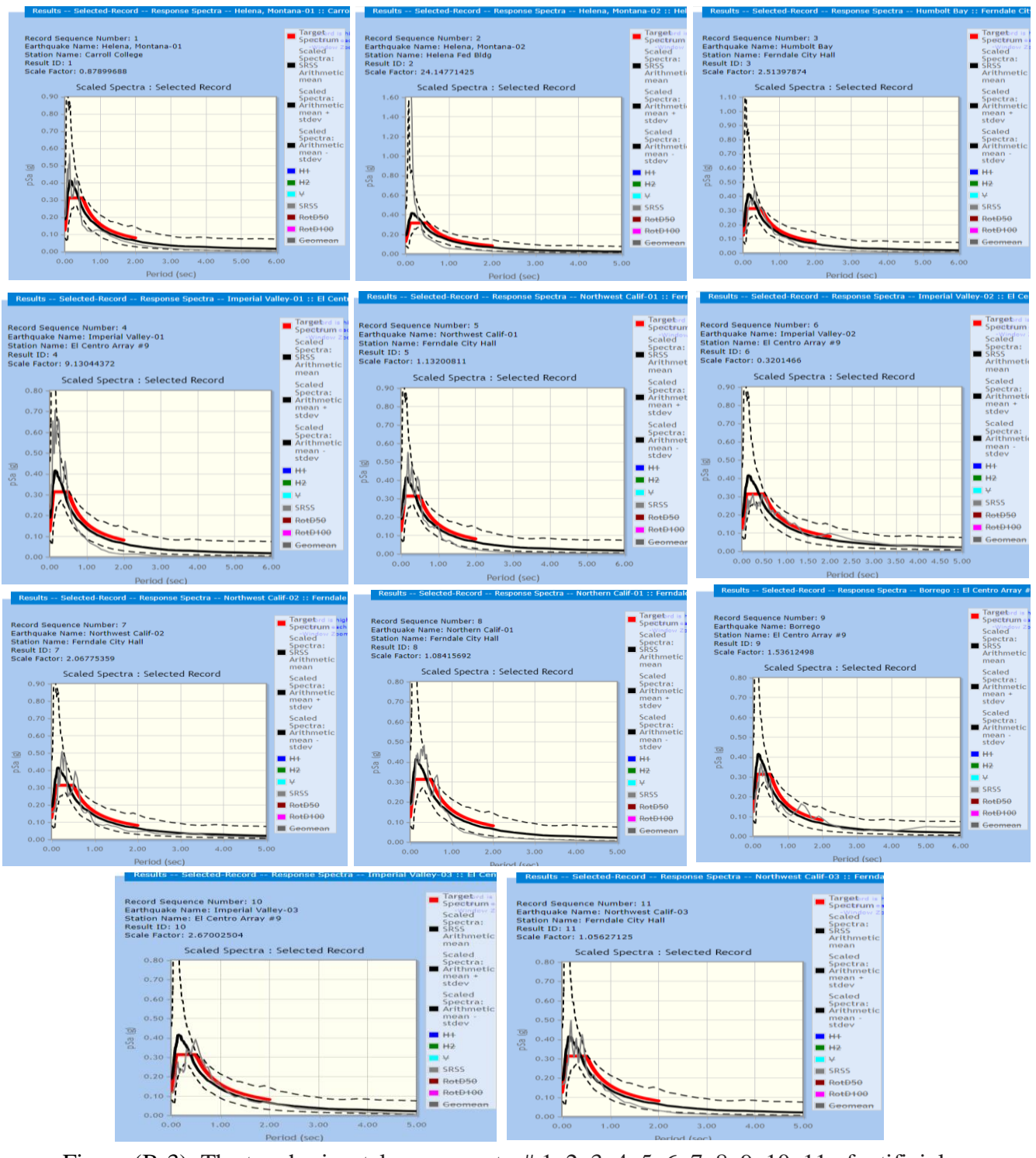


Figure (B-3): The two horizontal components # 1, 2, 3, 4, 5, 6, 7, 8, 9, 10, 11 of artificial strong motion records (acceleration in mm/s²) used in NDP and corresponding spectra

Table B-1: The parameters of the selected ground motion records

	Table B-1: The parameters of the selected ground motion records							
I D	Earthqua ke Name	Yea r	Station Name	Magnitude	Horizontal-1 Acc. Filename	Horizontal-2 Acc. Filename		
1	"Helena_ Montana -01"	193 5	"Carrol l College	6	RSN1_HELENA.A_A- HMC180.AT2	RSN1_HELENA.A_A- HMC270.AT2		
2	"Helena_ Montana -02"	193 5	"Helen a Fed Bldg"	6	RSN2_HELENA.B_B- FEB000.AT2	RSN2_HELENA.B_B- FEB090.AT2		
3	"Humbol t Bay"	193 7	"Fernda le City Hall"	5.8	RSN3_HUMBOLT_FRN22 5.AT2	RSN3_HUMBOLT_FRN31 5.AT2		
4	"Imperia 1 Valley- 01"	193 8	"El Centro Array #9"	5	RSN4_IMPVALL.BG_B- ELC000.AT2	RSN4_IMPVALL.BG_B- ELC090.AT2		
5	"Northw est Calif- 01"	193 8	"Fernda le City Hall"	5.5	RSN5_NWCALIF.AB_A- FRN045.AT2	RSN5_NWCALIF.AB_A- FRN135.AT2		
6	"Imperia 1 Valley- 02"	194 0	"El Centro Array #9"	6.95	RSN6_IMPVALL.I_I- ELC180.AT2	RSN6_IMPVALL.I_I- ELC270.AT2		
7	"Northw est Calif- 02"	194 1	"Fernda le City Hall"	6.6	RSN7_NWCALIF.C_C- FRN045.AT2	RSN7_NWCALIF.C_C- FRN135.AT2		
8	"Norther n Calif- 01"	194 1	"Fernda le City Hall"	6.4	RSN8_NCALIF.FH_F- FRN225.AT2	RSN8_NCALIF.FH_F- FRN315.AT2		
9	"Borrego	194 2	"El Centro Array #9"	6.5	RSN9_BORREGO_B- ELC000.AT2	RSN9_BORREGO_B- ELC090.AT2		
1 0	"Imperia 1 Valley- 03"	195 1	"El Centro Array #9"	5.6	RSN10_IMPVALL.BG_C- ELC000.AT2	RSN10_IMPVALL.BG_C- ELC090.AT2		
1	"Northw est Calif- 03"	195 1	"Fernda le City Hall"	5.8	RSN11_NWCALIF.AB_B- FRN224.AT2	RSN11_NWCALIF.AB_B- FRN314.AT2		